The influence of waterlogging on agricultural monitoring from space
Observations from an irrigated sugarcane plantation

den Besten, N.I.

DOI
10.4233/uuid:c6c41634-87b8-45e9-8ead-2288596a6aa2

Publication date
2023

Document Version
Final published version

Citation (APA)
den Besten, N. I. (2023). *The influence of waterlogging on agricultural monitoring from space: Observations from an irrigated sugarcane plantation*. [Dissertation (TU Delft), Delft University of Technology]. https://doi.org/10.4233/uuid:c6c41634-87b8-45e9-8ead-2288596a6aa2

Important note
To cite this publication, please use the final published version (if applicable).
Please check the document version above.

THE INFLUENCE OF WATERLOGGING IN AGRICULTURAL MONITORING FROM SPACE

OBSERVATIONS FROM AN IRRIGATED SUGARCANE PLANTATION

Nadja den Besten

THE INFLUENCE OF WATERLOGGING IN AGRICULTURAL MONITORING FROM SPACE

OBSERVATIONS FROM AN IRRIGATED SUGARCANE PLANTATION

THE INFLUENCE OF WATERLOGGING IN AGRICULTURAL MONITORING FROM SPACE

OBSERVATIONS FROM AN IRRIGATED SUGARCANE PLANTATION

Dissertation

for the purpose of obtaining the degree of doctor
at Delft University of Technology,
by the authority of Rector Magnificus Prof. dr. ir. T.H.J.J. van der Hagen,
chair of the Board for Doctorates,
to be defended publicly on Wednesday 10 May 2023 om 12:30 uur

by

Nadja Ingrid DEN BESTEN

Master of Science in Civil Engineering,
Delft University of technology, Delft, the Netherlands,
born in Tiel, the Netherlands.

This dissertation is approved by the promotors

Composition of doctoral committee:

Rector Magnificus	chairperson
Prof. dr. ir. S. Steele-Dunne	Delft University of Technology, Promotor
Prof. dr. ir. p. van der Zaag	IHE Delft and Delft University of Technology, Promotor
Independent members:	
Prof. dr. G. Jewitt	IHE Delft
Prof.dr. B. Basso	Michigan State University
Prof. dr. W. Dorigo	Technische Universiteit Wien
Dr. T. le Toan	Centre d'Etudes Spatiales de la Biosphère - Cesbio
Prof. Dr. ir. Bas van de Wiel	Delft University of Technology, reserve member
Other members:	
Dr. R. de Jeu	Planet Labs Inc.

Keywords: Waterlogging, Agricultural monitoring, Sugarcane, Irrigated agriculture, Sentinel-1 backscatter

Front & Back: Nadja den Besten

I will be a hummingbird

Wangari Maathai

CONTENTS

SUMMARY

Waterlogging is the accumulation of excess water in the rootzone. When soils are waterlogged the rootzone is either saturated or submerged with water. As a result, waterlogging prevents aeration of the rootzone which has adverse effects on crop growth. Waterlogging is an issue in both irrigated and rain-fed agriculture and crop productivity issues related to waterlogging are reported around the globe. As most terrestrial crops are within days susceptible to the negative effects of waterlogging, timely information on waterlogging and its presence spatially is beneficial. In that regard, to understand the impact of waterlogging on agriculture and combat consequential negative effect, satellite remote sensing can play a role.

However, in the field of satellite Remote Sensing of agriculture, waterlogging has so far received little attention. Previous related research focused on remote sensing of inundation or monitoring surface water, but waterlogging in agriculture is an overlooked subject. Little is known about how waterlogging is present in (irrigated) agriculture and what the ability of different remote sensing techniques is to detect and monitor waterlogging. Therefore, this thesis aimed to extend knowledge on how waterlogging influences agricultural monitoring with satellite remote sensing. Ultimately, to set footsteps towards monitoring waterlogging with satellite remote sensing.

The results presented evolve around a sugarcane plantation in Xinavane, Mozambique. The plantation served as a case study to demonstrate different satellite remote sensing observations in the context of waterlogging. First, the case study is presented and a describption is provided on the ground data collected. By providing remote sensing evaporation estimates, the high demand of irrigation water is illustrated. Vast quantities of water is needed to sustain sugarcane crop growth in the semi-arid environment of the plantation.

To continue, with a thorough literature review and the case study it is demonstrated waterlogging is a major issue burdening crop productivity. By assessing different remote sensing evaporation algorithms the results showed currently available evaporation estimates interpret waterlogging stress as a need to irrigate. This implies, before evaporation estimates from satellite data can play a role in optimizing field-scale water use in irrigated areas, evaporation algorithms must be able to identify water stress only in the case of water deficit in the root-zone. Throughout the chapter the presence of waterlogging or crop response to waterlogging is illustrated in different satellite remote sensing observations. In sum, the results imply a need to integrate observations of multiple sensors and potentially ancillary data (e.g. DEMs) to unravel how to monitor waterlogging with satellite remote sensing.

In search for the influence of waterlogging on agricultural monitoring, the research continued by comparing optical vegetation indices, radar vegetation indices, and sugarcane yield over the growing season in the plantation. The analysis gave an interesting and unexpected result. Contrary to the expectation the results showed a negative

correlation between the Cross Ratio (CR) and sugarcane yield over the growing season. A modeling study proved the negative correlation results from a change in the sugarcane's internal composition which affects the dielectric constant of sugarcane canopies observed. The chemical composition of plant water in sugarcane changes over the growing season. As a consequence of sucrose accumulation in the stalk, water is increasingly bound to sucrose and this process lowers the dielectric constant.

To follow up, active and passive microwave observations, optical vegetation indices, and production data are evaluated in different seasons. In addition to a temporal change of sucrose and moisture, the results showed vertically the sucrose-moisture distribution changes as well over the growing season. Therefore, the vertical distribution of sucrose - plant moisture influences the dielectric constant and, hence, the backscattered signal. The results highlight the VV backscatter responds to the stalk biomass, which is also the reservoir of sucrose in the sugarcane crop.

Finally, the influence of waterlogging on Sentinel-1 backscatter was detected through benchmarking with passive microwave observations, optical vegetation indices, and production data in a period where waterlogging was reported. Despite a thick sugarcane canopy, an increase in VH and VV polarizations was observed as a result of waterlogging. The increase was present at all stages during the growing season. The difference in backscatter as a result of waterlogging was highest in the VH backscatter. Also, the effect of waterlogging is translated through to the CR, which proves CR can play a role in the discrimination of waterlogging.

The results presented in this thesis help to further understand the influence of waterlogging in agricultural monitoring. Also, this work shows to correctly interpret irrigation estimates and crop development, waterlogging and sucrose development need to be flagged or otherwise considered during the growing season. Especially radar observations from Sentinel-1 backscatter appeared to be useful in monitoring waterlogging and sucrose development.

SAMENVATTING

Het verzadigen van de bodem is de ophoping van overtollig water in de wortelzone, verder aangeduid als waterlogging. Waterlogging verhindert de beluchting van de wortelzone, wat nadelige effecten heeft op de groei van het gewas. Afname van gewasproduciviteit als gevolg van een verzadigde bodem wordt over de hele wereld gemeld, in zowel geïrrigeerde als door regen gevoede landbouw. Aangezien de meeste terrestrische gewassen binnen enkele dagen vatbaar zijn voor de negatieve effecten van waterlogging, is tijdige en ruimtelijke informatie over waterlogging belangrijk. Satelliet data kan een rol spelen bij het monitoren van waterlogging om de impact op de landbouw te begrijpen en de daaruit voortvloeiende negatieve effecten te bestrijden.

Onderzoek op het gebied van waterlogging in de landbouw en hoe deze te monitoren heeft tot nu toe weinig aandacht gekregen in de wetenschap van satellietwaarnemingen. Er zijn betrekkelijk weinig studies gedaan naar de potentie van verschillende satelliet observatietechnieken om waterlogging te waarnemen en te controleren. Daarom heeft dit proefschrift tot doel de kennis uit te breiden over hoe waterlogging in de landbouw satelliet observatietechnieken beïnvloedt. Om zodoende bij te dragen aan het verder ontwikkelen van methodes om waterlogging waar te nemen met satelliet observatietechnieken.

De resultaten in deze dissertatie worden gepresenteerd rondom een suikerrietplantage in Xinavane, Mozambique. De plantage dient als casus om verschillende satelliet observatietechnieken te onderzoeken in de context van waterlogging. Allereerst zullen de verzamelde veldgegevens gepresenteerd worden en een wordt de suikerrietplantage verder uitgelicht. Met verdampingsschattingen vanuit satellietwaarnemingen wordt de grote vraag naar irrigatiewater geillustreerd, die nodig is om de groei van suikerrietgewassen in de semi-aride omgeving van de plantage te ondersteunen.

Vervolgens, wordt er aangetoond dat waterlogging een groot probleem is voor de productiviteit van de landbouw met een grondig literatuuronderzoek en observaties van de casus. Door verschillende verdampingsalgoritmen op basis van satellietwaarnemingen te beoordelen, laten de resultaten zien dat de momenteel beschikbare verdampingsschattingen gewas-stress door waterlogging interpreteren als noodzaak te irrigeren. Dit houdt in dat, voordat schattingen van verdamping op basis van satellietwaarnemingen een rol kunnen spelen bij het optimaliseren van het watergebruik in geïrrigeerde gebieden, verdampingsalgoritmen alleen in staat moeten zijn om waterstress te identificeren in het geval van een watertekort in de wortelzone. Door het hele hoofdstuk heen wordt de aanwezigheid van waterlogging of de reactie van gewassen op waterlogging geillustreerd aan de hand van verschillende satellietwaarnemingen. Om verder te ontrafelen hoe waterlogging kan worden gedetecteerd met satellietwaarnemingen zullen observaties van meerdere sensoren moeten worden geintegreerd, en mogelijk aanvullende gegevens (bijv. DEM's).

In hoofdstuk 4 wordt verder onderzocht wat de invloed van waterlogging is op landbouwmonitoring met satellietwaarnemingen door optische vegetatie-indexen, radarvegetatie-indexen en suikerrietopbrengst te vergelijken gedurende het groeiseizoen in de plantage. De analyse laat een interessant en onverwacht resultaat zien. In tegenstelling tot de verwachting blijkt de vegetatie index gebaseerd op radarwaarnemingen, negatief te correleren met suikerrietopbrengsten naarmate het groeiseizoen vordert. Een modelleerstudie verklaart de negatieve correlatie, en bewijst dat de verandering in de interne samenstelling van de suikerriet plant, de diëlektrische constante beïnvloedt. Als gevolg van sucrose-ophoping in de steel van de suikerriet plant wordt water in toenemende mate gebonden aan sucrose met als gevolg een verlaging van het waargenome radarsignaal.

Om te vervolgen, in Hoofdstuk 5, worden actieve en passieve microgolfwaarnemingen, optische vegetatie-indices en productiegegevens in verschillende seizoenen geëvalueerd. Naast een temporele verandering van sucrose en vocht in de plant, laten de resultaten ook zien dat de sucrose-vochtverdeling vertikaal ook verandert gedurende het groeiseizoen. Zodoende kan er worden geconcludeerd dat de verticale verdeling van sucrose en plantwater de diëlektrische constante beïnvloedt. De resultaten benadrukken dat de radarwaarnemeningen in de VV-polarisatie reageren op de biomassa van de steel, die tevens het reservoir van sucrose is gedurende de suikerriet groei.

Ten slotte, wordt de invloed van waterlogging op Sentinel-1-waarnemingen gedetecteerd door middel van passieve microgolfwaarnemingen, optische vegetatie-indices en productiegegevens te analyseren in een periode waarin de bodem verzadigde. De resultaten laten zien dat ondanks het dikke bladerdak van suikerriet, waterlogging zorgt voor een toename van radarwaarnemingen in de VH- en VV-polarisaties. De toename is aanwezig in alle stadia van het groeiseizoen. Ook wordt het effect van waterlogging doorvertaald naar de CR, een veel gebruikte radar vegetatieindex.

De resultaten gepresenteerd in dit proefschrift helpen om de invloed van waterlogging in de landbouw op satelliet observatietechnieken verder te begrijpen. Tevens laat dit werk zien dat bij het monitoren van irrigatie en landbouw met satellietwaarnemingen, er rekening moet worden gehouden met het effect van waterlogging en sucroseontwikkeling in de plant. Om irrigatieschattingen en vegetatiesignalen met satellietwaarnemingen juist te intepreteren moeten waterlogging en sucroseontwikkeling in de plant worden gesignaleerd of anderszins worden overwogen. Radarwaarnemingen van Sentinel-1 blijken zeer nuttig te zijn bij het monitoren van waterlogging alsmede het monitoren van het suikergehalte in de suikerriet plant.

PREFACE

Dear reader,

Aside from researching satellite remote sensing observations, this thesis is also a personal quest to find a way to contribute to positive change in our agricultural system. In many ways agriculture impacts our environment a great deal and, therefore, holds tremendous opportunities to improve. To give an example relevant to the context of this thesis, agriculture accounts for approximately seventy percent of the total fresh water withdrawals (FAO, 2016a). With an increasing amount of mouths to feed on this globe, irrigation will increase in the coming decades. Currently, a lot of basins already experience difficulties to meet agricultural water demand. Indisputably the difficulties in meeting water demand for agriculture will continue to increase due to a rising population and climate change. That is, if we sustain our current agricultural system.

Every day we collectively gain more and more knowledge on what we can observe from space. However, we should not get lost in misinterpreting a tool as a solution. The core issue of our current agricultural system is that we are completely and utterly out of balance with our environment. We create sugarcane plantations in places they should not be. To convert them into products we do not need, e.g. Coca-cola. Consequently, the only real way forward in agriculture is fundamental change in human behavior to maximize positive impact.

For example, to produce sugarcane a lot of water is needed and the hydrology of a basin changes when crops like these are planted in manifold. This has consequences to the supply of water to other users. Now, and even more in the long run. Every generation we get more considerate of the consequences of putting monetary value above environmental value, but there is still limited action.

Therefore, hand in hand with the development of technological tools discussions should be held on: are we able to SUSTAIN a certain agricultural practice and produce? and do the negative effects of production outweigh the monetary value? The latter discussion is needed, because we seem to still believe in technocratic solutions for our current climate crisis. As such, SUSTAINability is used, sometimes unintentionally, to disguise a system that is no longer working. A system that should not be sustained.

The results in this thesis contribute to finding ways to monitor waterlogging and sugarcane from space. They are written and researched in the paradigm of sustainability. Therefore they imply that by the use of such technologies within sugarcane production, improvement to agriculture will be inherently made. But, in order to really make improvements to our agricultural system we need to make different choices with regard to our human and natural capital. Which means choices considerate of human and natural capital, resulting from a shift in our consciousness.

Of course, here tools can be very helpful. Now my hope is, and of many others, that we will use these tools to get away from old systems and start using remote sensing tools

to encourage new systems in agriculture. However, this starts with pointing out what goes wrong on the ground, by visualizing negative impact.

What is also fundamental here is that we, you and me, the society that we are part of, starts seeing that our behaviour (in)directly influences the environment and other societies across the globe. For example, we cannot separate us from the sugarcane plantations across the world and at the same time drink coca cola. There will not be a technological breakthrough that will save the climate, or us. It will be very simple: we need to make different choices. And I repeat, choices that respect our ecology and each other, not trying to tame it nor each other. In that regard, remote sensing of agriculture can play a great role in showing how our current practices are not to be sustained, and encourage new ways needed. We can use remote sensing of agriculture to visualize change needed in our behaviour.

(Almost) Everybody I spoke to wants an agricultural system more considerate of its environment. Naturally, people that work in agriculture are nature lovers, they enjoy the outdoors. They do not want to spray their land a few times a year to get rid of some insect or pest and kill all other life along. Nevertheless, we are stuck in our current practices. We know it is not working and yet we continue, because we think this is it.

By writing this down I want to encourage you and myself to think beyond the borders of our current agricultural system. And to point out that it is a system that you and me are very much part of. Therefore, by connecting with your own impact in the agricultural sector (i.e. what you consume), you can help change it every day. Let's re-think our habits and change them, in terms of human behavior as well as existing plantation systems. I hope the knowledge gathered in this thesis will not sustain old plantation systems, but encourage ways to make real improvements in the agricultural sector. Not minimize negative impact, but eliminate them and maximize positive impact[1].

Nadja den Besten
Noja, December 2022

[1] https://www.bodemzicht.nl/

1

INTRODUCTION

1.1. THE IMPORTANCE OF MONITORING WATERLOGGING IN AGRICULTURE

Waterlogging is the accumulation of excess water in the rootzone and inhibits crop development (Houk et al., 2006; Ritzema, 2016). When soils are waterlogged there is a low oxygen availability in the rootzone, a reduction of the availability of nutrients, and a change in microbial activity, which affects plant physiology. Waterlogging issues have been observed in many countries around the world, such as Australia (Christen et al., 2001; Shaw et al., 2013), Pakistan (A. Singh, 2016), Hungary (Van Leeuwen et al., 2020), India, among other countries (Poddar et al., 2011; Valipour, 2014). In Australia, Dennis et al., 2000 estimated a EUR 180 million annual loss in wheat production due to waterlogging.

Waterlogging is an issue in both irrigated and rain-fed agriculture. Academic literature reports on waterlogging in irrigated agriculture as a result from over-irrigation or poor sub-surface drainage (FAO, 2016c). As waterlogging prevents aeration of the rootzone and in some cases may even induce secondary soil salinization, as salts are unable to leave the soil profile (Steduto et al., 2017; Wallender, Tanji, et al., 2011). It is estimated that roughly twenty percent of irrigated land is burdened by waterlogging and secondary soil salinization resulting from over-irrigation or poor sub-surface drainage (FAO, 2016c).

In rain-fed agriculture waterlogging also causes harm to crop productivity. Martinez-Feria and Basso, 2020 found waterlogging is an important driver behind yield instability in the US Midwest. They assessed temporal yield variability in maize, soybean, wheat and cotton and proved that the largest in-field variability can be found in depressional areas, where waterlogging occurs in wet years. In Hungary country-wide waterlogging issues are reported as a consequence of high precipitation events in winter or at the start of the season. This, in combination with the local geomorphology, causes periods with prolonged waterlogging that inhibit optimal crop growth (Van Leeuwen et al., 2020).

In addition, waterlogging as an abiotic stress factor is linked to biotic stress (e.g.

pests, diseases and weeds) (Chaerle et al., 2009). For example, a study on wheat and barley showed the increase of fungal pathogen growth under waterlogged compared to non-waterlogged conditions (Martıénez et al., 2019). In other words, waterlogging increases the vulnerability to pathogen attack (D. Chen et al., 2013). Therefore, information on waterlogging can help in the identification of biotic stress.

Considering the above, spatial and temporal information on waterlogging occurrence touches a wide variety of topics and issues that are key to agricultural monitoring: such as optimizing irrigation, understanding crop development, or chemical input use, amongst others. Satellite remote sensing offers a multitude of techniques to potentially monitor waterlogging. However, so far limited research has been conducted to understand the influence of waterlogging on agricultural monitoring with satellite remote sensing. This is a first step towards understanding how to monitor waterlogging with remote sensing. Remote sensing technologies of particular interest here are: passive microwave, optical and infra-red, and radar (RAdio Detection And Ranging).

1.2. MEASUREMENT TECHNIQUES AND RECENT DEVELOPMENTS IN OBSERVING WATERLOGGING

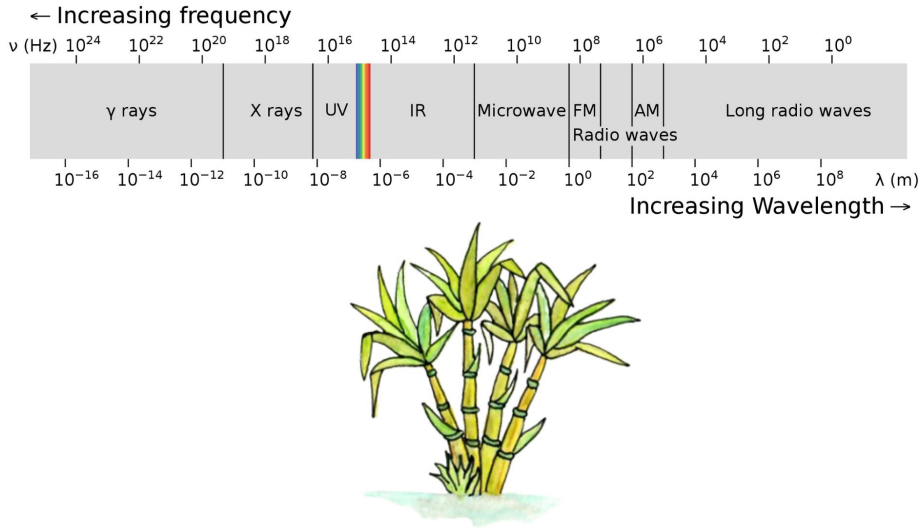

Figure 1.1: The electromagnetic spectrum and observing waterlogging under a sugarcane canopy

Detection of surface water with satellite remote sensing is based on the difference between radiometric properties and temperature of water and other surfaces (Prigent et al., 2016). However, observing waterlogging in agriculture from space is not straightforward. Unlike monitoring water on the surface (e.g. inundation), waterlogging in agriculture focuses predominantly on water underneath a canopy. Therefore, the surface of interest is a mixture of water and growing vegetation, or saturated soil and growing vegetation,

see figure 1.1. As a consequence, the phenomena of interest, waterlogging, is dynamic in space and time. Different observation techniques may contain different information relevant to detection and monitoring of waterlogging.

From a theoretical perspective, the longer the wavelength observed, the better the ability to penetrate the vegetation canopy (Martinis & Rieke, 2015). In general, shorter wavelengths (e.g. optical measurements) sense the skin of the surface, where longer wavelengths (e.g. microwave observations) are able to penetrate the medium. Nevertheless, optical measurements contain information on, for example vegetation health, which reflects what is happening underneath the canopy and should therefore not be disregarded to detect and monitor waterlogging.

1.2.1. PASSIVE MICROWAVE OBSERVATIONS AND WATERLOGGING

Waterlogging or surface water can theoretically be detected by passive microwave observation (Basist et al., 2001; Giddings & Choudhury, 1989; Sippel et al., 1994). By combining data from different wavelengths, polarizations, and/or viewing angles, it is possible to retrieve information about the soil surface. Due to the high contrast in dielectric properties between water and dry soil, microwave observations are particularly suitable for sensing water in the topsoil or on the surface (Ulaby et al., 1981). The difference in dielectric constant (k) is the basis for microwave remote sensing of, for example, inundation and soil moisture, due to a large contrast of the constant in dry soil (k 4) and water (k 80) (Jeu de, 2003).

The presence of water in the soil will lower the brightness temperature, which is measured by microwave radiometers (Philpot & Philipson, 2012). All bodies or surfaces with a non-zero Kelvin temperature emit electromagnetic radiation (Emery & Camps, 2017). The thermal electromagnetic radiation in the microwave spectrum (0.3-300 GHz) is captured with a radiometer (Emery & Camps, 2017). A microwave radiometer is an instrument that can respond to very low levels naturally emitted microwave energy (Lillesand et al., 2015; Sharkov, 2003). The radiometer contains an antenna, a receiver, and a system to store and transmit data to processing points. Observations can be obtained in multiple wavelengths, polarizations, and viewing angles, dependent on the instrument (Sharkov, 2003).

Microwave observations are particularly suitable for measuring land surface properties related to the hydrological cycle. For example, observing large scale inundation under dense canopies using the polarization difference in 37GHz observations (Choudhury, 1989; Sippel et al., 1994), or the retrieval of surface soil moisture using low frequency (<20GHz) (Schmugge et al., 1986).

The difficulty in using passive microwave observations to detect waterlogging is that the spatial resolution is coarse. Observations at lower frequencies have a lower spatial resolution than observations at higher frequencies (e.g., L-band's spatial resolution is in the order of 36 km). There are operational products that downscale brightness temperature observations. For example, NASA provides a downscaled 9 km resolution brightness temperature and soil moisture product (Chaubell et al., 2016). While a 9 km spatial resolution is sufficient for many applications (e.g. drought monitoring), it is relatively coarse for agricultural applications, which require field-scale monitoring.

1

1.2.2. ACTIVE MICROWAVE OBSERVATIONS AND WATERLOGGING

Radar observations also have proven to be useful in the detection of surface water. Just like passive microwave observations, radar observes in the microwave domain of the electromagnetic spectrum, see figure 1.1. However, in radar observations a different technique is used. Active microwave remote sensing operates by emitting a signal (microwave) and measuring the backscattered power of the returning signal (Steele-Dunne et al., 2017). As a result of emitting a microwave signal by itself, higher spatial resolutions are reached with radar satellites in orbit (e.g. Sentinel-1: 20mx5m). Radar observations can be obtained at different incidence angles, polarizations, and frequencies, the choice of which determines which surface information can be retrieved.

Backscatter behavior of agricultural crops is governed by many principles including: the dielectric constant of the crop and its constituents, the size and shape distribution of crop constituents (e.g. fruit, stalk) and their orientation, the roughness and dielectric constant of the underlying surface, and the canopy cover (e.g. row direction, plant height) (Ulaby et al., 1982). The dielectric constant is a material property that governs how a material behaves in an electric field (Ulaby & Jedlicka, 1984). The contribution of all aforementioned governing principles to the total backscatter is controlled by the observation characteristics, such as the polarization, wavelength, and incidence angle (Ulaby et al., 1982).

Different scattering mechanisms can be distinguished that contribute to the backscatter signal, these are: surface scattering (from the soil), volume scattering (from the vegetation), and soil-vegetation interactions inclduing double bounce and multiple scattering (Steele-Dunne et al., 2017). In agricultural canopies the structure of the crops play an important role in the distribution of the different scattering mechanisms to the total backscatter observed (McNairn & Brisco, 2004). The dielectric properties influence the response to backscatter and are driven by the water content in the plant (Ulaby & Jedlicka, 1984). The vegetation water content fluctuates throughout the season. Therefore, the observed by backscatter differs throughout the season. In addition, different layers in the crop canopy contribute to the total backscattered signal (Vermunt et al., 2022). Backscatter is not only influenced by vegetation water content, but also by Surface Canopy Water (SCW) and moisture in the soil under the canopy (Khabbazan et al., 2022; Vermunt et al., 2020). Moreover, backscatter observations are used for soil moisture retrievals (De Roo et al., 2001) and inundation detection (Tsyganskaya et al., 2018b).

Open water is relatively easy to detect with radar, due to the fact that standing water lowers the roughness of the surface creating specular reflection (Pulvirenti et al., 2015). This lowers the observed backscatter, especially in VV polarization, and is ideal for change detection in case of inundation monitoring (Twele et al., 2016). Inundation underneath a canopy is more complex, because it is a mixture of vegetation and water. As a result, most radar-based inundation algorithms underestimate the presence of inundation where vegetation is present. Studies relating to waterlogging in this context observe so-called Temporarily Flood Vegetation (TFV) (Tsyganskaya et al., 2018b). These studies assume that the presence of water underneath the canopy increases the double bounce resulting from backscatter (Pierdicca et al., 2017), which is hard to standardize as this changes per vegetation type and incidence angle (Pulvirenti et al., 2015).

1.2.3. OPTICAL AND NEAR INFRA-RED REMOTE SENSING AND WATERLOGGING

Optical and near-infra-red (NIR) observations measure between 360 and 2500 nm, see figure 1.1. Here we focus on optical and near-infra-red observations which use passive remote sensing technologies. These techniques measure the reflectance of solar illumination of the surface in specific bandwidths. Unfortunately, the observations in these bands can be hindered by cloud formation or shadow effects (Jiang et al., 2006).

Optical vegetation indices are widely used to understand crop or vegetation dynamics (Weiss et al., 2020). This is because vegetation absorbs radiation in the visible part of the spectrum and reflects a large amount of NIR radiation. Therefore, a normalized ratio can be used to identify vegetation activity of which the Normalized Difference Vegetation Index (NDVI) has become the most commonly used index nowadays (Bausch & Neale, 1987). In addition, optical satellite images are capable of detecting surface water because water responds to optical and near infra-red differently (Townsend & Walsh, 1998). In general, water absorbs longer wavelengths (NIR), whereas shorter wavelengths (e.g. red) are more reflected by an inundated surface.

For example, Choubey, 1997 used the infra-red band to delineate waterlogged areas. Normalized Difference Vegetation Index (NDVI) and Normalized Difference Water Index (NDWI) are also common indices used to delineate waterlogged areas (Chowdary et al., 2008; Dwivedi et al., 2007; El Bastawesy et al., 2012; Kaushik et al., 2019; Mandal & Sharma, 2011; S. K. Singh & Pandey, 2014). Ultimately, the results are generally static risk maps delineating perennial and/or permanent waterlogged areas. The analysis of temporal variation in, for example, Enhanced Vegetation Index (EVI) or Land Surface Temperature (LST), can also be useful for identifying waterlogged croplands (Fei et al., 2014). The difficulty in optical and near infra observation are the inability of these techniques to penetrate a crop canopy. The vegetation indices can be useful to benchmark crop growth in waterlogged areas (Pierdicca et al., 2017).

1.3. RESEARCH GAP AND OBJECTIVES

Despite the fact that a lot of research has been done on remote sensing of inundation (G. Schumann & Moller, 2015) and monitoring surface water (Alsdorf et al., 2007), waterlogging in agriculture is an overlooked subject. From a remote sensing perspective, little is known about how waterlogging is present in (irrigated) agriculture and what the ability of different remote sensing techniques is to detect and monitor waterlogging. Moreover, especially in remote sensing studies on irrigated agriculture the focus is generally on drought, not waterlogging (Calera et al., 2017; Veloso et al., 2017; Weiss et al., 2020). This is surprising, as at least twenty percent of the world's irrigated agriculture struggles with productivity issues related to waterlogging (FAO, 2016c). Therefore, *this thesis aimed to understand what the influence of waterlogging is on agricultural monitoring with satellite remote sensing.* Ultimately, the aim is to increase knowledge on how to monitor and prevent waterlogging with satellite remote sensing.

To begin with, it is often assumed that remote sensing-based irrigation estimates will help as a tool to achieve sustainable irrigated agriculture (Bastiaanssen et al., 2000; FAO, 2018). There are many different satellite evaporation algorithms available to monitor

crop water use to calculate irrigation requirements (Bastiaanssen et al., 1998; Calera et al., 2017; Kustas et al., 2003; Miralles et al., 2011). Examples of research conducted with such algorithms are estimating irrigation water use, crop water use, and technical validation and comparative assessments of such algorithms (Bazzi et al., 2020; Blatchford et al., 2020; P. Gowda et al., 2007). Very few research the functionality, benefits, or malfunctions when the algorithms are applied in the field (Barker et al., 2018; Bhatti et al., 2020; O'Shaughnessy et al., 2019). However, in order to achieve increased productivity with the help of satellite remote sensing, research is needed to what is still missing in these algorithms to assist irrigated agriculture.

To continue, the satellite-derived evaporation algorithms interpret vegetation stress directly as a need for water. Nonetheless, there are more abiotic stresses affecting crop growth (Jones, 2016). Examples of these issues are nutrient deficits, diseases, pests, and waterlogging. It is not known how different evaporation algorithms deal with stress resulting from waterlogging. Consequently, *the first objective of this thesis is to understand how waterlogging influences satellite-based evaporation estimates used for irrigation.* This will set guidelines as to what is still needed to further interpret the evaporation estimates driving irrigation estimates from space.

Previous research showed passive microwave remote sensing can capture large-scale surface dynamics underneath a canopy, such as flooding of the Amazon river (Sippel et al., 1994). The foundation of this work is based on a significant relation between passive microwave remote sensing and fraction of area inundated (Prigent et al., 2016). The focus in similar studies are on natural water bodies, so previous work has not yet considered waterlogging in agriculture. In addition to passive microwave remote sensing, radar remote sensing is able to sense flooding underneath a canopy with high spatial resolution (Tsyganskaya et al., 2018b). Nevertheless, waterlogging underneath agricultural canopies is an understudied topic (Pierdicca et al., 2017; Pulvirenti et al., 2015).

So far, research on rice paddies and wheat has demonstrated that radar backscatter increases as a result of double bounce scattering from the interaction crop-water (Le Toan et al., 1997; Pierdicca et al., 2017; Pulvirenti et al., 2015). However, this was, to our knowledge, never studied for a thick canopy like sugarcane. Moreover, Pierdicca et al. (2017) mentions plant density and volume scattering may attenuate the signal resulting from double bounce scattering. Therefore, to better understand the capability of remote sensing to monitor waterlogging, *the second objective of this thesis is to understand how waterlogging influences crop growth monitoring with satellite remote sensing at field-scale.*

In order to reach the aim of the research presented in this dissertation we use a case study. The case study is an irrigated sugarcane plantation in Xinavane, Mozambique. On top of year-round irrigation application, the plantation endures a high inter-annual variability in water availability with a short and intense rainfall season and a long dry season. The plantation covers nearly 18000 hectares of sugarcane, which is produced all year round. These characteristics make it a suitable playground to investigate the influence of waterlogging in agricultural monitoring from space.

1.4. RESEARCH OUTLINE

This thesis consists of several chapters, which have been published as a series of peer-reviewed articles. Chapter 2 provides a description of the study site and data collected. The data and some of the code generated within this chapter have been made publicly available and references to these datasets are provided. In Chapter 3, an overview is provided on how waterlogging is overlooked in satellite based evaporation algorithms to assist irrigation, what its impact is on agriculture, and potential pathways to observe waterlogging from space. Hereafter, in Chapter 4, we demonstrate how radar observations respond to sucrose accumulation in the sugarcane crop benchmarked to optical observation. Chapter 5 dives deeper in the response of radar to sucrose accumulation and shows how waterlogging influences sugarcane monitoring from space. Finally, in the Conclusion the main findings and their implications will be summarized.

2

CASE STUDY AND GROUND DATA

Ahi tengissene timbilo ta hina ku fana ni mati

Let us purify our hearts and be like water (Changan saying)

The research conducted in this dissertation evolves around a case study in Xinavane, Mozambique. Multiple fieldwork campaigns were conducted to gather the ground database that enabled the research. The following chapter gives a description of the case study and the ground data collected. In addition, information is provided on where to access the data and parts of the code.

Parts of this chapter have been published in Elsevier Physics and Chemistry of the Earth (den Besten et al., 2020)

2.1. CASE STUDY

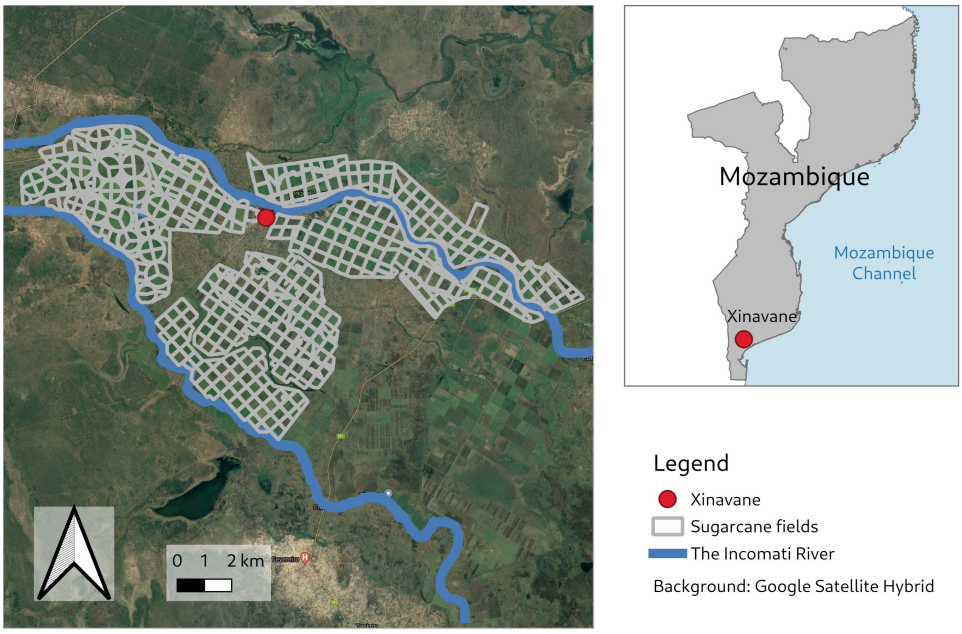

Figure 2.1: The location of the case study: a sugarcane plantation in Xinvane, Mozambique

The location of the research conducted in this dissertation is in Xinavane, Mozambique. In Xinavane, a large (±18000 ha) plantation is located, as illustrated in Figure 2.1. The plantation is established within the lower reaches of the Incomati river basin. As a result of the location, the plantation in Xinavane is in competition over water with an increasing population in the catchment and water users in upstream South Africa and Swaziland, where numerous other sugarcane plantations are located (Santillán-Fernández et al., 2016; Zaag van der & Carmo Vaz, 2003).

To grow sugarcane in Xinavane, irrigation is required all year round. The long-term average annual precipitation in the area is 721 mm/year, measured from 1967 to 2017 by a local weather station. However, to grow sugarcane in Xinavane a lot more water is needed. The maximum crop evaporation in Xinavane is around 1800 mm/season (den Besten et al., 2020). Chukalla et al., 2022 found the potential evaporation ranging between 1800 and 2200 mm/season. In addition, den Besten et al., 2020 documented mean actual evaporation per field ranged between 1390 and 1483 mm/season for different fields. Similarly, Chukalla et al., 2022 reported actual evaporation rates of 1350 mm/season assessing four seasons. These numbers imply a significant amount of irrigation water is required to sustain sugarcane production in Xinavane. In addition, the big difference between actual and potential evaporation rates indicate room for improvement to optimize crop water use (Chukalla et al., 2022; den Besten et al., 2020).

Figure 2.2 illustrates Xinavane's struggle with water. The gray line represents the av-

erage soil water content of the catchment of the Corumana dam. The dam, located further upstream of the Incomati river, is the most important reservoir for irrigation at the plantation. The blue line in Figure 2.2 represents the water level measured in the dam. From 2012 until 2014, the plantation experienced three successive years of heavy rainfall and high river levels which adversely affected the operations within the plantation. These events were followed by two consecutive drought years in 2015 and 2016, associated with El Nino (Gelcer et al., 2018). In the years 2017 and 2018 the annual rainfall was also below average. Clearly, this was not enough to replenish the reservoir to pre-El Niño conditions.

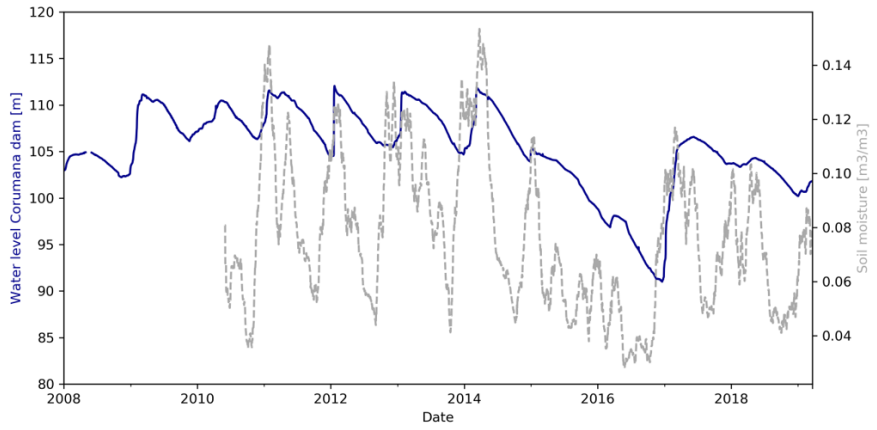

Figure 2.2: A representation of the average soil water content measured with SMOS of the catchment of the Corumana dam and respective dam levels.

In this dissertation, the area of interest covers ± 7510 hectares (see figure 2.1). In this area, irrigation is centrally organized by the agricultural department of Xinavane. Different irrigation techniques (e.g. furrow, sprinkler, drip) are used in the plantation, of which sprinkler is the most common practice. In practice, irrigation is applied every 10-12 days approximately. Irrigation water is provided by different pumping stations, which pump water from the Incomati river into irrigation channels. Drains and drainage channels are supposed to divert excess water into basins before the drainage water is pumped out of the plantation.

Most of the ground data were collected during a project named IWACA-Tech, which aimed to improve water use efficiency at irrigation systems using advanced remote sensing technology[1]. During the project, several fieldwork campaigns were conducted to understand the irrigation and production issues in the plantation and to test and implement solutions proposed by partners in the project. One of the outcomes of the project was a peer-reviewed article presenting a high resolution evaporation algorithm

[1] www.iwacatech.com

(See appendix A). The spatial evaporation estimates provide the irrigation and agricultural managers with information on actual crop water use and biomass development, which is relevant to both crop monitoring and irrigation water management (den Besten et al., 2020). In addition, during the fieldwork a large spatio-temporal variability of yield within the plantation was observed. Several student research projects showed production issues related to waterlogging and salinization.
[2] [3]

2.2. AVAILABLE GROUND DATA

Data and knowledge were shared by the agricultural department of Xinavane's estate for this research. This included production data at field level, but also meteorological data, and elevation spatial maps to understand the geomorphology. The dataset contains the following spatial and temporal variables:

Agronomic info of 387 fields (20ha) from 2002-2021 12 years:

- Sugarcane and sucrose yield (Tons/ha)
- Quality yield metrics: percentage of sucrose, water, brix and fibre (percentage of fresh weight)
- Ratoon years (year)
- Length growing season (days) [datapoints: 3463]
- Harvest date (Day Of Year)
- Irrigation type (categorical)
- Soil type/ clay percentage (percentage) [shapefile/ points]
- Location with areas that face permanent waterlogging (binary) [shapefile] (Vilanculos & Mafalacusser, 2012)

Meteorological data (1 weather stations):

- Temperature (daily, mean Celsius)
- Precipitation (mm/day)
- Wind speed
- Radiation
- Relative Humidity

LIDAR observations: LIDAR from which the following spatial layers are calculated on a pixel level (13x13m) or field level:

[2] Multi-Disciplinary Student Project
[3] Master Thesis

- Digital Elevation Model
- Slope
- Topographic Wetness Index
- Convex-Concave features in a field
- Height Above Nearest Drainage - HAND (considering man-made pumping stations/ drainage)

The ground data are bundled in a package called Sugarmomma and can be used by citing this dissertation.

3

WATERLOGGING IN IRRIGATED AGRICULTURE

Too much of anything is never good.

Mom

This chapter provides a scientific perspective on the topic of waterlogging by consulting literature in the disciplines of agronomy, hydrology, and remote sensing. As waterlogging is an increasingly important issue in irrigated agriculture with detrimental impact on crop productivity, the current impact of waterlogging on irrigated agriculture and the presence of waterlogging in different remote sensing techniques and evaporation algorithms is assessed.

This chapter is published in the special issue of MDPI *Remote Sensing for Agricultural Water Management (RSAWM)* (den Besten, Steele-Dunne, de Jeu, et al., 2021)

3.1. INTRODUCTION

In irrigated agriculture, waterlogging is a common problem with a detrimental impact on crop productivity (Houk et al., 2006). Waterlogging prevents aeration of the root-zone and induces secondary soil salinization, as salts are unable to leave the soil profile (Wallender, Tanji, et al., 2011). Waterlogged soil conditions affect plant physiology by causing low oxygen availability in the roots, a reduction of the availability of nutrients, and a change in microbial activity. These effects of waterlogging hamper crop growth and yield significantly (Shaw et al., 2013). For example, (Dennis et al., 2000) estimated a EUR 180 million annual loss in wheat production due to waterlogging in Australia.

Worldwide, roughly twenty percent of irrigated land is burdened by waterlogging and secondary soil salinization resulting from over-irrigation or poor sub-surface drainage (FAO, 2016c). This is especially the case for (semi-)arid areas with high evaporation rates (Steduto et al., 2017). Researchers have reported issues related to waterlogging around the world, such as in Australia (Christen et al., 2001; Shaw et al., 2013; Ward et al., 2002), Pakistan (A. Singh, 2016), India, amongst other countries (Poddar et al., 2011; Valipour, 2014).

For example, waterlogging and secondary soil salinity in the Lower Arkansas River of Colorado causes significant damage to agriculture (Houk et al., 2006). The agricultural land in this basin has been irrigated since the 1870s, and reported issues with waterlogging date back to the beginning of the 20th century. Waterlogging increased over the decades as a consequence of continuous irrigation and inadequate drainage, causing the water table to rise within the rootzone. Moreover, 25 percent of the agricultural area in the Lower Arkansas River basin has a water table at less than 1.5 meter. (Houk et al., 2006) calculated agricultural profits are approximately 40 percent less as a consequence of waterlogging and associated soil salinity.

In the last 50 years, the global area equipped with irrigation has almost doubled (Neumann et al., 2011). The global coverage of irrigated areas is expected to increase alongside the projected rise in global population (You et al., 2011). Moreover, the future increase in population calls for sustainable agricultural intensification, as the majority of the world's arable land is already cultivated (Cassidy et al., 2013; Mueller et al., 2012; Pfister et al., 2011). Irrigated crop production globally is 2.5 times more productive than rain-fed crop production (Mashnik et al., 2017). Therefore, irrigation is internationally promoted as a technique to help sustain future food demand (Mueller et al., 2012).

The increase in irrigated areas is expected to increase fresh water abstraction rates. Nowadays, agriculture already accounts for approximately seventy percent of the total freshwater withdrawals (FAO, 2016a). Studies show that the socio-economic impact, due to an increased demand on our freshwater resources may be just as large as the pressure resulting from climate change (Ferguson & Maxwell, 2012; Fischer et al., 2007).

Therefore, to manage freshwater in a sustainable manner and optimize productivity, it is necessary to focus on enhancing water use efficiency and water productivity in irrigated agriculture (Bhaduri et al., 2016). Here, monitoring plays a crucial role: to track (crop) water use and assess opportunities for improvement. Satellite remote sensing can be a powerful tool in monitoring and evaluating crop water use (Atzberger, 2013; Bastiaanssen et al., 2000). Optimizing irrigation water use, in an irrigation scheme for example, can benefit from frequent spatial evaporation updates on the actual develop-

ment of the crop and its water requirement (Calera et al., 2017; Vanino et al., 2018; Vuolo et al., 2015), as farmers tend to over-irrigate in the absence of objective information on crop status and water requirement (Vanino et al., 2018).

Satellite based evaporation algorithms are increasingly common in irrigation scheduling, to irrigate the right quantity at the right time (Calera et al., 2017; Vanino et al., 2018). In these evaporation algorithms crop stress is directly or indirectly inferred through satellite data by spectral indices, thermal bands, or passive microwave observations, where the term crop stress is inferred to include all kinds of crop stresses, such as water stress (Glaz et al., 2004), nutrient stress (N. Inman-Bamber & Smith, 2005), or stress resulting from disease or pest (Franke & Menz, 2007). Therefore, if these algorithms are used for irrigation purposes, stress resulting from other stresses than water deficit may cause overirrigation. For example, stress resulting from waterlogging can be wrongly interpreted as a need for irrigation, while adding more irrigation water might in fact worsen waterlogging problems (Jones, 2018).

Considering the above, monitoring waterlogging could therefore contribute to the prevention of waterlogging in irrigated agriculture. By identifying which areas are prone to waterlogging, irrigation could be reduced or drainage improved. This would improve both irrigation water use as well as crop productivity. Also, an operational monitoring system can provide agriculturalists information on land trafficability, drainage, or crop selection (Shaw et al., 2013).

Satellite remote sensing has the potential to monitor and identify waterlogging in agricultural fields. However, there is limited research available on waterlogging within the remote sensing community (Choubey, 1997; Mondal & Pal, 2018; S. K. Singh & Pandey, 2014). Literature focussed on waterlogging in irrigated agriculture is even more limited (Chowdary et al., 2008; El Bastawesy & Ali, 2013). Therefore, the aim of this chapter is to provide a perspective on how waterlogging could be monitored in irrigated agriculture. This chapter starts by reviewing literature on the topic of waterlogging within the disciplines of agronomy and hydrology. Then, literature in the in satellite remote sensing community is assesed to understand what has been done so far with waterlogging. Here, different remote sensing based evaporation algorithms are assessed to discuss the presence of waterlogging in the algorithms. Next, several approaches are reviewed that have proved successful in the field of inundation detection and discuss how they might be adapted to address the challenges associated with monitoring waterlogging in irrigated agriculture. Finally, these aspects will be synthesized to present a roadmap towards the development of a methodology to monitor waterlogging with remote sensing for sustainable irrigated agriculture.

3.2. WATERLOGGING AND ITS IMPACT

Waterlogging is the accumulation of excess water in the rootzone (Ritzema, 2016). Agronomists also define soil submergence, where even the aerial (above-ground) plant tissue is partly or completely flooded (Fukao et al., 2019). When a soil is waterlogged or submerged, pores are predominantly filled with water. However, to sustain proper crop growth a good soil needs to consist of a combination of soil, air, and water. Both waterlogging and soil submergence can create a situation where there is less than 21 percent oxygen in the soil, this is called hypoxia (Fukao et al., 2019; Sasidharan & Voesenek, 2015). Anoxia

occurs when there is a complete absence of oxygen (Sairam et al., 2008).

The response of crops to (partial) submergence or waterlogging differs (Parent et al., 2008). In general, when plants are partially submerged, shoot elongation may be suppressed to keep carbohydrates for when flooding disappears. On the other hand, when a plant is fully submerged, rapid elongation can occur to reach the surface of the water. The influence of waterlogging, partial submergence, and full submergence all negatively affect the yield. In this thesis, waterlogging is defined as the situation where the rootzone is deprived of oxygen, irrespective of partial or full submergence.

The absence or scarcity of oxygen under waterlogged soil conditions hampers the gas exchange in and around the plant, as water slows down the gas diffusion necessary for major physiological processes in the plant (Sasidharan & Voesenek, 2015). Vital processes such as photosynthesis and transpiration are heavily affected by waterlogging as these require exchange with atmospheric gases (Sairam et al., 2008; Sasidharan & Voesenek, 2015). The absence of oxygen inhibits or prevents the roots from taking up ions. This disturbs the water potential in the cells of the plant and leads to a decrease in stomatal conductance (the degree of stomatal opening) (Irfan et al., 2010).

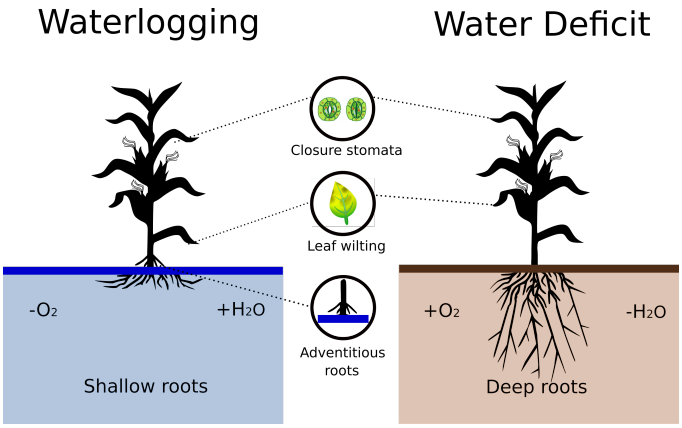

Figure 3.1: The similarities in response to the crop on above-ground features in times of waterlogging (left) and water deficit (right). The situation and response of the crop beneath the surface is different.

There are many effects of physiologic and morphological responses to oxygen deficit to aerial plant tissue, and they are crop and variety dependent. Generally, above-ground symptoms of waterlogging include wilting of the plant, leaf yellowing, reduction of plant growth and grain yield (Kaur et al., 2020; Shaw et al., 2013). Importantly, leaf wilting of the plant is often interpreted as water deficit stress (Shaw et al., 2013). Morphological adaptations or symptoms as stomatal closure or leaf wilting can occur both under crop stress due to water deficit as well as due to waterlogging, see Figure 3.1.

Waterlogging inhibits root development, leading to a decrease of root length and weight (Zhou et al., 2020). Ultimately, the damage to the root system negatively impacts the nutrient and water uptake of the crop, and may result in a physiological water deficit above ground (Gomathi et al., 2015). To survive waterlogged soil conditions crops can

develop adventitious roots (Bellini et al., 2014). The adventitious roots grow from the stem and closer to the surface in order to access oxygen (Kaur et al., 2020).

The impact of waterlogging on crop yields can vary in different regions due to the variation in climatic conditions, soil types, crop type, crop variety, crop age, and management differences (Kaur et al., 2020). Each crop and variety responds differently to waterlogging, and the duration of waterlogging is key to the impact on crop yield (Irfan et al., 2010). Figure 3.2 provides an overview of the effect of waterlogging duration on the yield for different major crops based on data collated from the literature. Raw data can be found in appendix A.

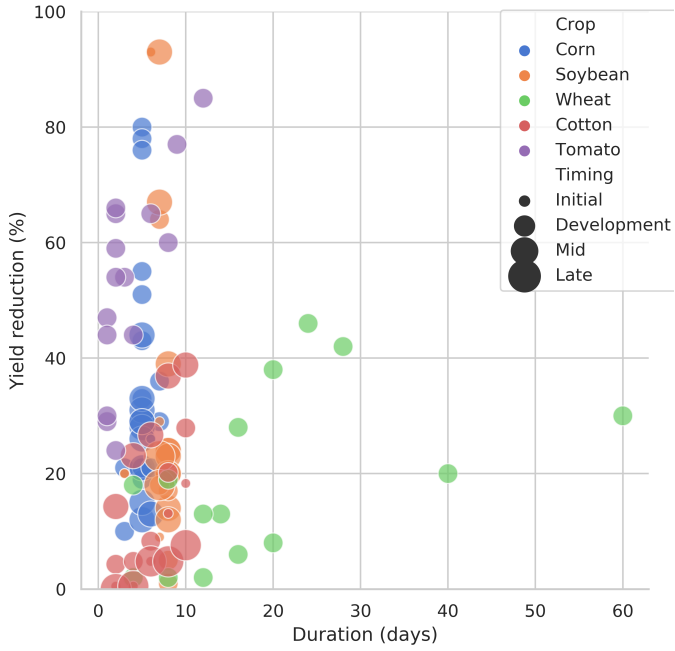

Figure 3.2: The relation between duration of waterlogging (in days) and yield reduction (in percentages). Each dot represents a study result from the literature. The size of the dots illustrate the onset of waterlogging within the growing season.

From Figure 3.2 it can be observed that the selected crops experience a reduction in yield when waterlogging occurs. Most terrestrial crops are sensitive to water excess in the rootzone (Sasidharan & Voesenek, 2015). However, some crop types are more resistant to waterlogging than others. For example, a few study results on wheat show a yield reduction of 30 percent where waterlogging prevailed for 60 days (Arguello et al., 2016; Marti et al., 2015; Pampana et al., 2016). On the other hand, most tomato varieties already experience severe yield reduction after a few days of waterlogging (Ezin et al., 2010; Mohanty et al., 2020; Tareq et al., 2020).

Note that the effect of duration can differ for the same crop type in Figure 3.2 as

some experiments use different varieties or a different onset of waterlogging within the growing season. In all development stages waterlogging is an issue. However, the impact differs because of different coping mechanisms in the crop stages (Kaur et al., 2020; Zhou et al., 2020). For example the impact of waterlogging on corn and soybean growth is largest in the initial or development stage (Kaur et al., 2017; Linkemer et al., 1998; Ren et al., 2016; Rhine et al., 2010; Shah et al., 2012; Sullivan et al., 2001). Germination and seedling establishment are frequently mostly impacted by waterlogging (Kaur et al., 2020).

There are also crops more resistant to waterlogging. For example, paddy rice is cultivated on flooded soils. However, when completely submerged, paddy rice yield may be negatively affected (Irfan et al., 2010). Another example of a waterlogging-resistant crop is sugarcane, which can withstand weeks of waterlogging or inundation (Avivi et al., 2020; Glaz et al., 2004). Nonetheless, long-term or permanent waterlogging is detrimental to sugarcane productivity and can result in secondary soil salinization (Rietz & Haynes, 2002; Warrence et al., 2002).

An example of the effects of waterlogging to crop productivity can be observed in an irrigated sugarcane plantation in Xinavane, Mozambique, see figure 3.3. In this plantation, there are a lot of productivity issues associated with waterlogging (den Besten et al., 2020; Vilanculos & Mafalacusser, 2012). During a large soil survey waterlogged areas were documented (Vilanculos & Mafalacusser, 2012). From figure 3.3 it is visible that the majority of the waterlogged areas coincide with low crop productivity. Waterlogging is also noted as a driver behind yield instability in other areas (Martinez-Feria & Basso, 2020). By assessing temporal variability in maize, soybean, wheat and cotton yield in the US Midwest (Martinez-Feria & Basso, 2020) prove largest in-field variability can be found in depressional areas, where waterlogging occurs in wet years.

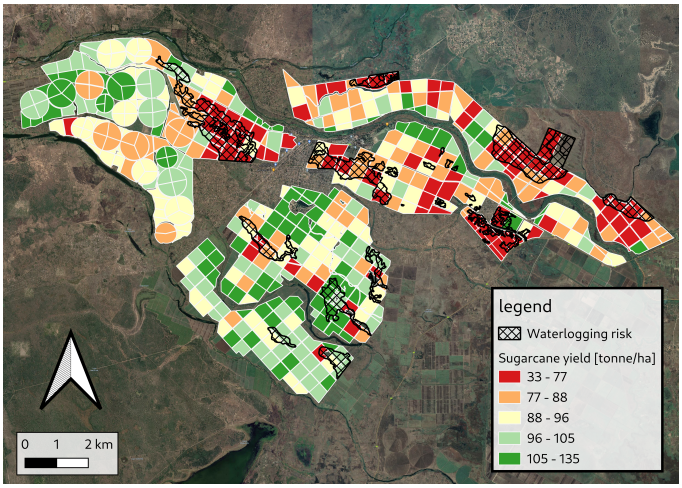

Figure 3.3: An overview of the average yield per field in Xinavane between 2008-2019 in Tonne Cane per Hectare (TCH). The black striped shapefile displays the areas with waterlogging issues (Vilanculos & Mafalacusser, 2012).

For the majority of the experimental results in Figure 3.2, the focus lies on the effect of waterlogging with a duration of <10 days to assess the impact on yield. The effect on crop yield can already be significant in a few days. Therefore, both transient or permanent waterlogging needs to be monitored and prevented for optimal crop productivity. Monitoring waterlogging is especially useful in areas where it can be controlled, such as in irrigated or drainage agriculture.

The spatial extent of waterlogging varies from small-scale depressions to large-scale shallow groundwater tables. Waterlogging is related to absence of or limited drainage, and occurs in local depressions, poorly constructed irrigation schemes, (irrigated) wetlands, or areas with impermeable soils, for example (Ritzema et al., 2008). Small-scale depressions in a field may induce waterlogging, but a shallow groundwater table may also enhance the development of waterlogged soils. To prevent or mitigate waterlogging adequate drainage is required (Ritzema et al., 2008; Valipour, 2014).

Geographically, waterlogging occurs in both natural and human induced circumstances. In natural circumstances, waterlogging may occur when there is a high water table and water is continuously or at once added to the surface by rain or a flood event (Shaw et al., 2013). These naturally waterlogged areas can be found globally in wetlands, river basins, or lakesides, for example (Z. Wang et al., 2019). Waterlogging may also be caused by human interventions such as irrigation, wrongly designed drainage methods, and other surface alterations (e.g. ridges) (H. Chen et al., 2020; Z. Wang et al., 2019). Due to continuous irrigation, waterlogging is prevalent in agricultural areas in mostly arid and semi-arid areas where irrigation is needed to sustain agricultural production.

Previous research within hydrology and agronomy focused on modeling and monitoring waterlogging in irrigated agriculture to optimize crop productivity. For example, the crop models SWAGMAN, DRAINMOD, and APSIM take the effect of water excess stress on crop yield into consideration in agricultural management (Shaw et al., 2013). Recently, efforts were made to model waterlogging in irrigated paddy rice to understand human interventions in the irrigation schemes and the resulting yield reduction of waterlogged area (H. Chen et al., 2020). To simulate waterlogging in irrigated agriculture, natural processes need to be considered, but also the hydraulic structures created by humans and the interventions taken place within the system are of importance (e.g. irrigation, gates) (H. Chen et al., 2020). The model developed by (H. Chen et al., 2020) is able to predict accurate water levels within the irrigated rice system, but it requires a lot of data. Moving towards an operational monitoring system for waterlogging, satellite remote sensing could provide a less data-intensive solution. There is need for an operational monitoring system that identifies waterlogged areas to support decision-making in irrigation scheduling, drainage, or crop selection (H. Chen et al., 2020; Shaw et al., 2013).

3.3. WATERLOGGING AND SATELLITE REMOTE SENSING

There is limited research on waterlogging within the remote sensing community (Choubey, 1997; Mondal & Pal, 2018; S. K. Singh & Pandey, 2014), especially in an irrigation context (Chowdary et al., 2008; El Bastawesy & Ali, 2013). Within the agricultural water management community, (A. Singh, 2016) reviewed literature to analyze the applications and GIS techniques available for the management of water in irrigated agriculture. Most of

the techniques available focus on delineation of waterlogged areas, where the use of optical data in these studies are common. For example, (Choubey, 1997) uses the infra-red band to delineate waterlogged areas. Normalized Difference Vegetation Index (NDVI) and Normalized Difference Water Index (NDWI) are also common indices used to delineate waterlogged areas (Chowdary et al., 2008; Dwivedi et al., 2007; Mandal & Sharma, 2011; S. K. Singh & Pandey, 2014). Ultimately, the results are generally static risk maps delineating perennial and/or permanent waterlogged areas. The analysis of temporal variation in, for example, Enhanced Vegetation Index (EVI) or Land Surface Temperature (LST), are particularly useful for identifying waterlogged croplands (Fei et al., 2014).

The use of Digital Elevation Models (DEM), with or without the combination of optical data, has also played a role in research on delineation of waterlogging within remote sensing (El Bastawesy & Ali, 2013; S. K. Singh & Pandey, 2014). (El Bastawesy & Ali, 2013) mapped waterlogging hazard with the help of hydrological parameters analyzed with GIS. A DEM was used to visually interpret the natural sinks in the area under study. Another example is (S. K. Singh & Pandey, 2014), where the extent of waterlogging is spatially analyzed with Modified Normalized Difference Water Index (MNDWI) and a DEM.

However, as pointed out in section 3.2, waterlogging is a process that changes in space and time in response to physical surface changes, precipitation and/or irrigation application. The aforementioned studies result in delineation of waterlogged areas, but do not monitor the actual areas subject to waterlogging over time. Ideally, an operational system should track the extent of area waterlogged in time. This is essential to provide agriculturalists with timely information on land trafficability and drainage to support decisions related to crop choice and land management practices. Furthermore, information on the waterlogging state is essential to correctly identify the underlying source of crop stress, and to improve irrigation advice based on satellite-based evaporation models (den Besten et al., 2020; Shaw et al., 2013).

Several researchers have demonstrated the potential of satellite remote sensing for irrigation scheduling, but also to assess the water use on global and catchment scale (Bastiaanssen et al., 2000; Weiss et al., 2020). Examples of remote sensing based evaporation algorithms can be found in Table 3.1. Table 3.1 shows that several of these methodologies are now downscaled to fine spatial and temporal resolution with the help of data from new satellites or improved algorithms (He et al., 2019; Martens et al., 2018). This opens up an era of research to integrate valuable remote sensing information for field-scale water management (Weiss et al., 2020).

In all remote sensing based evaporation algorithms in Table 3.1, crop stress is directly or indirectly incorporated through satellite data by spectral indices, thermal bands, or passive microwave observations. The observed crop stress includes all kinds of crop stresses, such as water stress (Govender et al., 2009), nutrient stress (Jackson, 1986), or stress resulting from disease or pest (Franke & Menz, 2007). In current remote sensing based evaporation calculations any kind of crop stress will translate into a need for irrigation.

However, waterlogging will also result in the closure of stomata or leaf wilting (see figure 3.1), which in turn affects the surface temperature or eventually NDVI observed by the satellite (Jones, 2018). In current evaporation algorithms, there is a dominant

focus on water deficit, and stress resulting from water-logging may be overlooked or misinterpreted as water deficit stress. Scientific reviews on remotely sensed evaporation algorithms for irrigation focus mainly on water deficit stress (Barbagallo et al., 2009; Bastiaanssen et al., 2000; Calera et al., 2017; P. H. Gowda et al., 2008; Khanal et al., 2017; Maes & Steppe, 2012), and do not consider stress resulting from waterlogging. If such algorithms would be used for irrigation scheduling, this might in fact worsen waterlogging problems (Jones, 2018).

To illustrate this, the irrigated sugarcane plantation in Xinavane, southern Mozambique, is considered. Many fields in the plantation are burdened by permanent waterlogging, see figure 3.4. Figure 3.4 B, C, and D give a snapshot of a visual (RGB, Sentinel-2B), NDVI (Sentinel-2B), and Thermal image (B10, Landsat-8) in a field where waterlogging is occurring on the particular dates displayed (den Besten et al., 2019). From groundwater and field observations the centred field in figure 3.4 B, C, and D is waterlogged: groundwater levels are within the rootzone and the centre of the field is fully submerged (den Besten et al., 2019). From figure 3.4 B you can see the effects of permanent waterlogging (and soil salinization): in some parts the sugarcane is barely growing. The latter is also visible in figure 3.4 C and D. The parts where sugarcane is barely growing results in a lower NDVI and higher surface radiometric temperature due to the exposure of bare soil.

Thermal Infrared bands and NDVI are common and important building blocks for ET algorithms, see Table 3.1. Often the surface radiometric temperature is partitioned by using NDVI/LAI to retrieve soil and canopy temperature which are crucial to calculate latent heat. However, in the case of waterlogging underneath a canopy the algorithm will be able to visualize the effects of waterlogging only once the adverse effects of waterlogging already occurred. Namely when the NDVI/LAI is low due to hampered crop growth (see bare soil spots figure 3.4 C).

The latter example is illustrative of how waterlogging can be overlooked or misinterpreted as water deficit stress when these algorithms are used for irrigation. Nevertheless, it is important to include waterlogging stress to inform sustainable irrigation water use and productivity. In this context, (Jones, 2018) also pointed out that it is critical to distinguish water deficit-related stomatal closure from the responses to other stress, which can also lead to stomatal closure. Therefore, monitoring waterlogging can be of help to interpret evaporation algorithms in irrigated agriculture.

Table 3.1: An overview of different remote sensing based evaporation algorithms and their characteristics. The spatial and temporal resolutions are the highest resolutions found in literature. LST: Land Surface Temperature, NIR: Near infra-red, FPAR: fraction of photosynthetically active radiation

Name	Spatial res	Temporal resolution	Crop stress product	Crop stress bands	Source
MODIS ET	30m	Daily	EVI, NDVI, LST	TIR, Red, NIR	(Mu et al., 2007), (He et al., 2019)
SEBAL	30m	Daily	EVI, NDVI, LST	TIR, Red, NIR	(Bastiaanssen et al., 1998; Hong et al., 2009)
GLEAM	100m	Daily	VOD, Microwave SM	X, C, L-band	(Miralles et al., 2011), (Martens et al., 2018)
Alexi	5-10km	Daily	LST, fPAR	TIR, Red, NIR	(M. C. Anderson et al., 2007; M. Anderson et al., 2010)
DisAlexi	30m	Every 5-16 days	LST, fPAR	TIR, Red, NIR	(M. Anderson et al., 2010; Kustas et al., 2003)
SSEB	120m	Daily	LST, NDVI	TIR, Red, NIR	(P. Gowda et al., 2009; Senay et al., 2007)
TSEB	30m	Every 8 days	LST, NDVI	TIR, Red, NIR	(French et al., 2015; Norman et al., 1995)
METRIC	30m	Every 8 days	EVI, NDVI, LST	TIR, Red, NIR	(Allen et al., 2007; French et al., 2015)
WaPOR	30-100m	Every 10 days	LST, NDVI	TIR, Red, NIR	(FAO, 2018)
PT-JPL	70m	Daily	NDVI	Red, NIR	(J. B. Fisher et al., 2008)

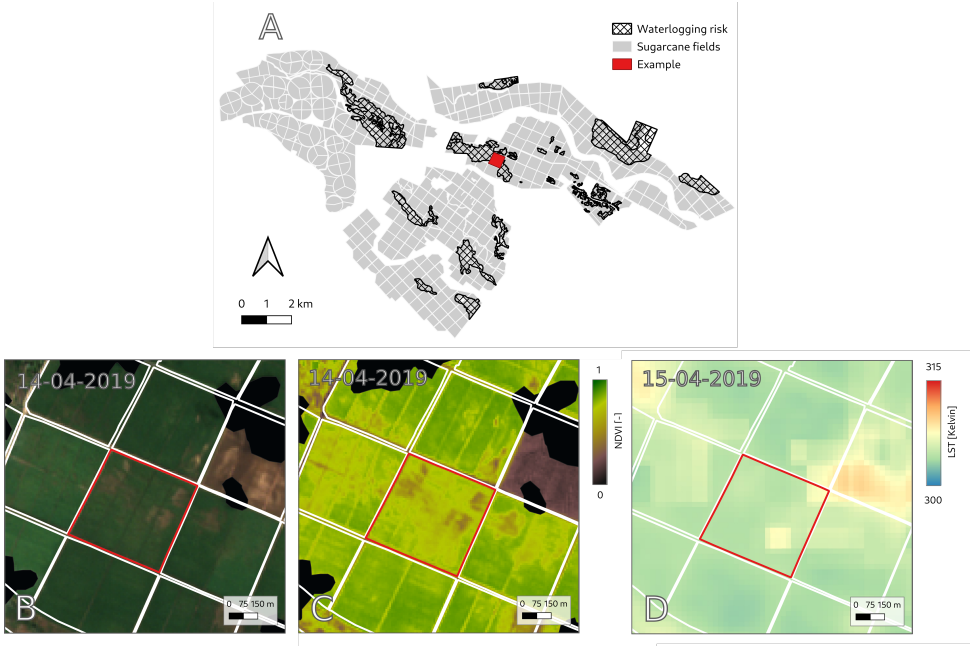

Figure 3.4: A) the extent of permanent waterlogging documented by a sugarcane plantation in Xinavane, Mozambique (Vilanculos & Mafalacusser, 2012). B) a snapshot of a true-color composite by Sentinel-2B on the 14th of April 2019. C) a snapshot of NDVI observed by Sentinel-2B on the 14th of April 2019. D) a snapshot of surface radiometric temperature (B10) observed by Landsat-8 on the 15th of April 2019.

3.4. DETECTION OF WATERLOGGING WITH DIFFERENT REMOTE SENSING TECHNIQUES

Detection of surface water with satellite remote sensing is based on the difference between radiometric properties and temperature of water and other surfaces (Prigent et al., 2016). There are several theoretical possibilities to detect surface water or waterlogging with satellite data: by using passive microwave sensors, optical (VIS) or Near-infrared sensors (NIR), Synthetic Aperture Radar (SAR), or scatterometry. The advantages and disadvantages of each of the first three techniques to detect waterlogging with satellite imagery will be assessed. A summary can be found in Table 3.2.

First, waterlogging can be detected by passive microwave frequencies (Basist et al., 2001; Giddings & Choudhury, 1989; Sippel et al., 1994). By combining data from different wavelengths, polarizations, and/or viewing angles, it is possible to retrieve information of the soil surface. Due to the high contrast in dielectric properties between water and dry soil, microwave observations are particularly suitable for sensing water in the topsoil or on the surface (Ulaby et al., 1981).

Passive microwave observations show sensitivity to the underlying surface wetness that enables detection of surface water even in densely vegetated areas (Choudhury,

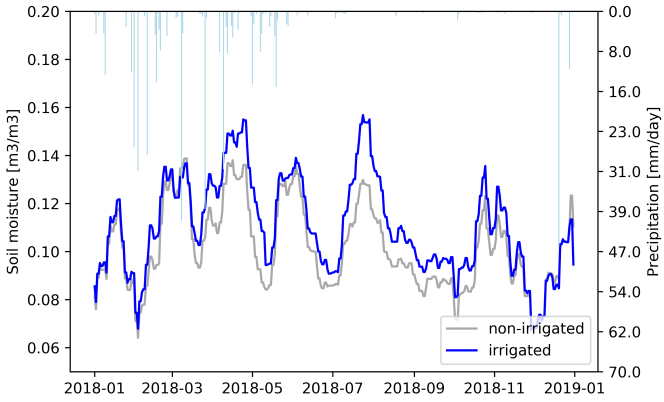

Figure 3.5: Timeseries of satellite soil moisture for an irrigated (blue) and non-irrigated reference area (gray) as derived from enhanced L-band microwave observations of NASA SMAP (Richard de et al., 2016). The lightblue bars on top indicate precipitation events measured by a meteorological tower within the irrigated area.

1989; Hamilton et al., 1996; Prigent et al., 2001; Sippe et al., 1998; Sippel et al., 1994). The polarization difference increases with increasing soil wetness (Choudhury, 1989). For example, soil moisture to a depth of 0.8mm can be sensed with the Ka-band (37 Ghz) frequency (Shang, 2017). A combination of different frequencies has also been used to detect surface wetness (Achutuni, 1996; Scofield & Achutuni, 1996).

Higher frequency passive microwave channels, such as Ka-band, are partly influenced by atmospheric circumstances and vegetation and ideally should be corrected for those (Prigent et al., 2007). Low frequency passive microwave channels, such as the L-band radiometer on SMOS and SMAP, are less affected by canopy and atmospheric conditions (Parrens et al., 2017) and are well suited to soil moisture monitoring.

The difficulty in using passive microwave observations to detect waterlogging is that their resolution is coarse. Observations at lower frequencies have a lower spatial resolution than observations at higher frequencies (e.g. L-band's spatial resolution is in the order of 36 km). There are operational products that downscale brightness temperature observations. For example, NASA provides a downscaled 9 km resolution brightness temperature and soil moisture product (Chaubell et al., 2016). This enhanced L-band product has, to our knowledge, not yet been used in research to detect surface water.

To illustrate the potential value of passive microwave remote sensing here, Figure 3.5 shows a comparison of satellite derived soil moisture from L-band observations over the sugarcane plantation in Xinavane and from a reference area with no irrigation. Here a downscaled version of SMAP L-band observations based on a new deconvolution method (Richard de et al., 2016) and converted to soil moisture with the Land Parameter Retrieval Model gridded at 100 m is used (van der Schalie et al., 2017). Outside of the rainy season the average soil moisture is higher than the reference area without irrigation. Despite the coarse spatial resolution, L-band passive microwave observations are capable of detecting differences in surface soil moisture even under the dense sugarcane canopy.

Secondly, it is possible to detect surface water with VIS and NIR sensors. The physical radiation over different wavelengths in the VIS and NIR domain are distinctly different for water, compared to other surfaces. Longer wavelengths in the VIS and NIR bands are absorbed more by water than shorter VIS. Due to these spectral response patterns, water bodies can be delineated per pixel (Lillesand et al., 2015). In addition, VIS and NIR sensors observe at a high spatial resolution, e.g. Sentinel-2 at a 10 meter spatial resolution (Pekel et al., 2016).

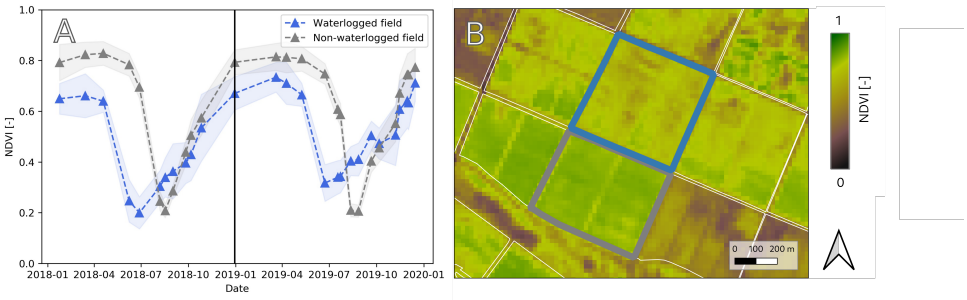

Figure 3.6: A) NDVI timeseries observed by Sentinel 2B of a waterlogged (blue) and non-waterlogged field (gray). The black vertical line denotes the observation date of the snapshot in B. B) NDVI snapshot on 30-12-2018 of the waterlogged (blue border) and non-waterlogged field (gray border).

Nevertheless, figure 3.6 A shows a NDVI time-series (Sentinel-2) of a water logged and non-waterlogged field in the sugarcane plantation Xinavane, Mozambique (See Figure 3.3). The NDVI values in the timeseries of the waterlogged field are lower compared to the non-waterlogged field, as a result of hampered crop growth due to waterlogging. This confirms there is information within the visual spectrum on waterlogging. In addition, the standard deviation in the field dealing with waterlogging is larger. The latter is visible in figure 3.6 B, where a snapshot of the two fields show the waterlogged field (blue) shows less uniformity than the non-waterlogged field (gray).

A limitation of this technique is the inability to acquire observations under cloudy conditions (Prigent et al., 2020). Since waterlogging may also result from intensive rainfall events, the inability to have observations under cloudy conditions hampers the ability to continuously monitor waterlogging. In addition, VIS and NIR data are sensitive to the reflectance at the top of the canopy and cannot penetrate a dense canopy to provide information from the underlying surface (Lillesand et al., 2015).

Third, active microwave observations may also provide information on waterlogging. SAR transmits a microwave pulse and measures the backscattered power of each returning signal (Lillesand et al., 2015). These observations can be obtained in different wavelengths and polarizations. Generally, open water surfaces are distinguished by low backscattering coefficients (Prigent et al., 2016). Data from SAR are able to detect surface water bodies underneath vegetation (Martinez & Le Toan, 2007; Pierdicca et al., 2017). For example, SAR can detect water beneath a slender leaf crop such as rice (Pierdicca et al., 2017). However, the signal is influenced by vegetation and the signal saturates under a thick canopy (Tsyganskaya et al., 2018b).

Table 3.2: Disadvantages and advantages of different remote sensing techniques to detect waterlogging.

	Disadvantages	Advantages
Passive microwaves	coarse spatial resolution, downscaling needed, saturation (crop specific)	almost daily observations, detects beneath canopy (frequency dependent)
VIS and NIR	cloud interference, saturation	inundation easily detected, high spatial resolution,
SAR	saturation (crop specific)	high spatial resolution, no cloud interference detects beneath canopy (frequency dependent)

Unlike VIS and NIR data, SAR data are less influenced by atmospheric effects and observations can be made on cloudy days (Prigent et al., 2020). In addition, SAR provides data at high spatial resolution. Sentinel-1, for instance, provides SAR backscatter at a 5 x 20 meter resolution (Torres et al., 2012). Sentinel-1 data has a revisit time of six days with platform A and B, but coverage varies around the globe. For example, for the sugarcane plantation in Xinavane there is an observation every 12 days. To observe waterlogging, however, high temporal resolution is required, since most terrestrial crops are negatively effected by waterlogging in a matter of days (see section 3.2).

The spatial and temporal resolutions of current available satellite products will limit the operationability of monitoring waterlogging in irrigated agriculture. Future missions, with higher spatial and temporal resolutions can become game-changers in the future. For example, ESA's ROSE-L mission will provide high spatial and temporal resolution L-band data that is especially of interest to flood mapping, in particular below vegetation (Davidson et al., 2019). Also, Global Navigation Satellite Systems - Reflectometry (GNSS-R) signals can be an interesting data source to monitor waterlogging (Jensen et al., 2018).

Several sources of remote sensing data contain useful information on waterlogging. Combining them provides complementary information on waterlogging at a range of spatial and temporal scales, and provides a way to circumvent the limitations of the individual data streams.

3.5. DOWNSCALING USING ANCILLARY DATA

In addition to combining observations from different parts of the electromagnetic spectrum, the use of ancillary data can provide a means to downscale to the higher spatial resolutions needed to monitor within-field waterlogging. In this regard, future research on monitoring waterlogging can benefit from the work done so far within monitoring inundation. Recently (global) inundation products were introduced that combine different satellite products with passive microwave remote sensing, also referred to as hybrid approaches (Parrens et al., 2019; Prigent et al., 2016; Schroeder et al., 2015). By combining different satellite products, different sensitivities to surface properties are differentiated, but also higher spatial resolutions are obtained (Prigent et al., 2020). Two examples are Global Inundation Extent from Different Satellites (GIEMS) and Surface Water Microwave Product Series (SWAMP) (Papa et al., 2010; Schroeder et al., 2015).

Table 3.3 gives an overview of the characteristics of these inundation products. In re-

cent years several researchers have attempted to downscale global and regional surface water products to higher spatial resolutions (Aires et al., 2013; Galantowicz et al., 2017; Parrens et al., 2019; Prigent et al., 2016). These methodologies all require high resolution ancillary data to improve the resolution of the passive microwave observations. (Prigent et al., 2016) distinguishes two strategies to improve the resolution of coarse scale surface water products: (1) downscaling by using high spatial resolution satellite observations; (2) downscaling by using topography information. Although waterlogging requires even higher spatial and temporal resolutions, these existing methodologies set a basis for an approach to monitor waterlogging.

In these inundation products the underlying assumption is the passive microwaves signal used is linked to the fraction of land inundated (Galantowicz, 2002; Parrens et al., 2019; Prigent et al., 2016). However, in irrigated agriculture there is a very important additional driver besides topography and precipitation, namely irrigation and man-made drainage. The underlying assumption used in current inundation models need to add derivatives of irrigation effects or detection of irrigation in order to monitor waterlogging.

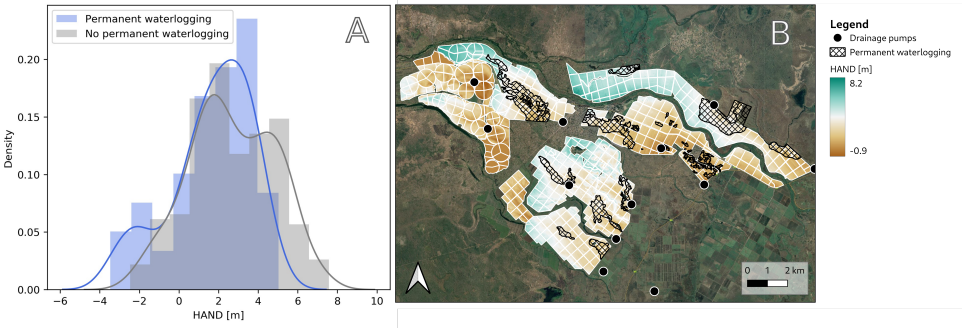

Figure 3.7: A) A kernel density estimation and histogram of the distribution of the average HAND per field with waterlogging issues (blue) and without waterlogging issues (gray) as reported by (Vilanculos & Mafalacusser, 2012). B) A spatial overview of the HAND throughout the plantation considering drainage pumps.

Table 3.3: Two examples of high resolution inundation products using topography for downscaling.

Product	Spatial resolution	Temporal resolution	Remote sensing products used
GIEMS-D3 (Aires et al., 2017)	90 m	Monthly (1993-2007)	19 and 37 GHz [cloud filtering: 85 GHz] Radar 5 GHz NDVI DEM (HydroSHED) Global Lands and Wetlands database
SWAF-HR (Parrens et al., 2019)	1 km	3 days	1.4 GHz DEM (MERIT) Global surface water occurrence dataset

To monitor waterlogging future studies should focus on how to include human-made drivers inducing waterlogging. Future scientific studies need to focus on: (1) monitoring waterlogging with ancillary data by looking at the temporal variation, and (2) waterlogging occurrence from drainage parameters deducted from high spatial resolution

DEMs. These DEMs can be developed with data from LIDAR or Unmanned Aereal Vehicles (UAVs). A determining factor in suitability for DEM to monitor waterlogging is the vertical accuracy, which is still too large in available global satellite products, e.g. TanDEM-X with a vertical accuracy of two meters (G. J. Schumann & Bates, 2018).

For example, in the sugarcane plantation in Mozambique permanently waterlogged areas occur in poorly drained areas, see figure 3.7. The Height Above Nearest Drainage (HAND) was computed with LIDAR observations, considering drainage points and pumps of the irrigation system. Figure 3.7 shows the distribution of HAND is different in waterlogged fields compared to non-waterlogged fields. This illustrates topographical information withholds information on waterlogging or the potential to be waterlogged (Galantowicz, 2002).

3.6. CONCLUSION

Waterlogging is a localized phenomenon (e.g. ponds within a field) and can induce crop stress within a few days. Within agronomy, studies on crop stress focus more on water deficit stress, as compared to stress resulting from waterlogging. However, waterlogging is a common and adverse problem in (irrigated) agriculture. Most terrestrial crops are susceptible to waterlogging, but the intensity of the negative effects depend on crop type and variety, duration, timing, amongst other factors. Within (irrigated) agriculture, waterlogging needs to be prevented to optimize yield, water productivity, and soil quality. Furthermore, failure to tackle persistent waterlogging can induce secondary soil salinization, a process that is hard to reverse.

The above-ground effect of waterlogging on crops is hard to distinguish from water deficit stress, as responses like stomatal closure and leaf wilting occur in both situations. Currently the origin of crop stress is not distinguished by remote sensing based evaporation algorithms and these may therefore be erroneously interpreted as a need for irrigation. In sum, before evaporation estimates from satellite data can play a role in optimizing the field-scale water use in irrigated areas, evaporation algorithms must be able to identify water stress only in case of water deficit in the root-zone. Here, monitoring waterlogging can play a role.

Efforts in modelling waterlogging are data-intensive and it is worthwhile to explore whether satellite remote sensing provides opportunities for an operational system to monitor waterlogging. In recent years studies within remote sensing on irrigated agriculture have focussed on static delineation of waterlogging. However, waterlogging is a dynamic process that requires frequent monitoring. Future research to create a remote sensing based monitoring system to prevent waterlogging can learn from research on the remote sensing of inundation.

To demonstrate the information on waterlogging present in different remote sensing data products, an irrigated sugarcane plantation in Xinavane, Mozambique, is used as a case study. The plantation faces issues with waterlogging and, therefore, use the information to illustrate how different sensing techniques may contain information on waterlogging. However, each sensing technique has its own limitations. Consequently, there is not just one sensing technique suitable to monitor waterlogging. Opportunities to monitor waterlogging lie in hybrid approaches combining different satellite products to optimize temporal and spatial resolution.

Future scientific routes should focus on complementing remote sensing data with ancillary data by looking at the temporal variation, and waterlogging occurrence from drainage parameters deduced from high spatial resolution DEMs (with LIDAR or UAVs).

Remote sensing can be used to identify areas that are frequently subject to waterlogging, information that can be used to make smarter crop choices and to improve drainage. Remote sensing data from multiple sources can be combined with ancillary data to monitor transient waterlogging at high temporal and spatial resolution. This can provide real-time information on trafficability, and potential crop damage. Most importantly, this provides an essential input to evaporation estimation algorithms used for irrigation support. In addition to conserving water resources, the correct attribution of crop stress to waterlogging rather than water deficit stress would ensure that waterlogging is not further exacerbated by the application of additional irrigation.

4

MONITORING SUGARCANE CANOPIES

You, Venerable One, may indeed be a seeker, for, striving toward your goal, there is much you do not see which is right before your eyes.

Herman Hesse

The previous chapter gave a perspective on how waterlogging is present in satellite remote sensing observations in irrigated agriculture. The original aim of this chapter was to study field time series of different vegetation indices. Surprisingly, time series analysis revealed the sensitivity of Sentinel-1 backscatter to sucrose accumulation. This is an important finding to be considered when observing agricultural canopies and waterlogging from space.

This chapter is published in *Frontiers in Remote Sensing* (den Besten, Steele-Dunne, Aouizerats, et al., 2021).

4.1. INTRODUCTION

Sugarcane is an important source for both sugar and ethanol production, where the quantity and quality of soluble sugar in the plant, named sucrose, determines the final sugar yield. Sucrose production develops over the season in the stem of the sugarcane plant (J. Wang et al., 2013). Sucrose accumulates in high concentrations in the stem. Different sucrose concentrations have been reported by cultivars around the world, ranging between 10 and 15 percent of fresh weight (G. Inman-Bamber, 2013).

Monitoring sugarcane and its sucrose content during the growing season can provide essential information to several users, such as individual producers, sugarcane mills, or commodity traders (Abdel-Rahman & Ahmed, 2008). This is because monitoring and yield forecasting helps to evaluate production processes, adjust on-site management, and estimates the potential industrial production (Bocca et al., 2015). Currently, the most common method for yield estimation in the field is still based on historical records and expert knowledge (Shendryk et al., 2021). Specialists estimate yield based on visual assessment, basing their estimation on knowledge, historical yield data, land characteristics, weather, and the manifestation of pests and diseases (Bocca et al., 2015).

Previous studies have researched the relation between sugarcane yield and vegetation indices computed from satellite data (Bégué et al., 2010; Lofton et al., 2012; Molijn et al., 2019; Morel et al., 2014). Common techniques are based on optical indices (e.g. NDVI). For instance, Morel et al. (2014) found integrated NDVI values over the growing season best related to yield on a field scale. Fernandes et al. (2017) investigated how NDVI timeseries and neural networks can be combined to predict regional sugarcane yield in Brazil. Unfortunately, the integration of new yield estimation techniques into the decision making process of sugarcane production remains slow (Bocca et al., 2015).

Few studies have focused on Synthetic Aperture Radar (SAR) data and its relation to sugarcane or sucrose yield. Limited studies have assessed the capability of SAR data to monitor sugarcane biomass or estimate sugarcane yield. Shendryk et al. (2021) focused on predicting yield with machine learning, where Sentinel-1 data was used as a predictor variable. Molijn et al. (2019) explored the suitability of Sentinel-1 data to monitor biomass throughout the growing season. However, in none of these studies was SAR data directly compared to a large yield database.

This chapter will show how sucrose accumulation affects Sentinel-1 backscatter. Sentinel-1 backscatter and Planet optical data are used and compared. The analysis starts by assessing the variation of different vegetation indices over the growing season. Hereafter, the relationship of different vegetation indices to sugarcane yield over the season is compared. Finally, a modeling study was set up to mimic the impact of sucrose accumulation on the dielectric constant. The modeling study will provide explanation on the behavior of Sentinel-1 backscatter and supports the potential to monitor potential sucrose yield with satellite data.

4.2. SUGARCANE GROWTH

Around the world sugarcane is grown in subtropical and tropical conditions. While Brazil and India are the largest sugarcane producers worldwide, accounting for 21 percent and percent respectively (FAO, 2021a), the continent of Africa accounts for five percent of

the total sugarcane production (FAO, 2021b). Where Brazil produces sugarcane mostly under dryland conditions, the majority of the sugarcane grown on the African continent is sustained with irrigation (Dubb et al., 2017).

Sugarcane can be grown as a plant cane or ratoon crop (G. Inman-Bamber, 2013). When sugarcane is grown as a ratoon crop, it is not replanted annually but grown from the preceding plant. As it is cost-effective, ratooning is the most common practice within the sugarcane growing countries (Surendran et al., 2016). Sugarcane is planted and harvested all year round. Harvest dates depend on the sugar mill and ideally, cane growth is planned to sustain maximum capacity (Bocca et al., 2015).

Compared to other perennial crops, sugarcane has a relatively long growing season and is harvested after a period of between 12 and 18 months. Physiological changes controlled by different mechanisms define different growth stages. In general, sugarcane growth is divided by the following four periods: an initial stage (30 days), tillering stage (90 days), development stage (150 days), and the final stage (90 days) (Doorenbos & Kassam, 1979; Silva et al., 2015). Throughout the analysis the growth stages will be referred to.

The initial stage is characterised by the germination of the original stool. The onset of biomass growth and sucrose accumulation coincides with the development of the leaf canopy, during the tillering stage (G. Inman-Bamber, 2013). During the development stage the sugarcane plant focuses more on elongation of the stem, which is an important sink for sucrose development (Cock, 2001; G. Inman-Bamber, 2013). In the final stage, senescence is the dominant process (Martins et al., 2016). During this process the leaves turn yellow as chlorophyll content decreases. This process is combined with water loss in the plant and therewith increases the sucrose concentration in the plant (Bégué et al., 2010). In irrigated sugarcane, irrigation is often stopped at the end of the season to maximize the accumulation of sucrose (G. Inman-Bamber, 2013).

4.3. DATA AND METHODS

4.3.1. FIELD DATA ACQUISITION

This chapter uses crop yield data from a sugarcane plantation located on the banks of the lower Incomati river in Xinavane, Mozambique. The plantation grows ratoon sugarcane under irrigated conditions in a subtropical climate. From April to December, the local sugar mill opens and the sugarcane fields are harvested (den Besten et al., 2020; den Besten, Steele-Dunne, de Jeu, et al., 2021). The focus of this research lies on 387 fields that make up the majority of the area owned and grown by the Tongaat Hulett group, where agricultural management is centrally organized. The average field-size is approximately 20 hectares (den Besten et al., 2020). The sugarcane in the plantation is planted in rows 1-1.5 meter apart. The dominant sugarcane varieties in the plantation are N25 and N23.

In the analysis, a sugarcane yield data of season 2018-2019 and 2019-2020 was used. After harvest, trucks containing harvested sugarcane are weighed and documented per field. After weighing, several samples are tested for their sucrose content. This process results in data per field on sugarcane yield (tons/hectare, TCH) and sucrose yield (tons/hectare, TSH). The relation between sugarcane and sucrose yield is linear for this

plantation with a correlation coefficient of 0.95 for 688 samples (see Figure 4.1B). Because of this very high correlation and the fact that the sucrose database is not complete, the analysis focuses on the yield data available for sugarcane as a proxy for its sucrose content to maximize the number of available data points.

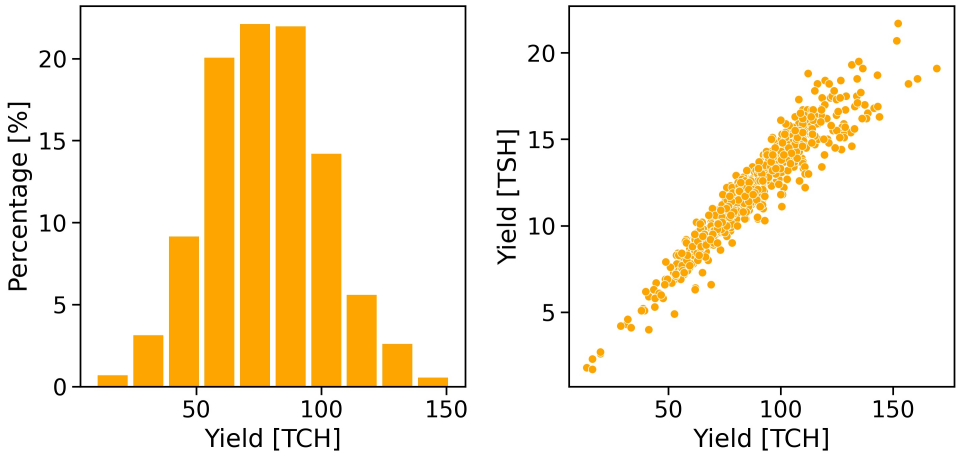

Figure 4.1: A) Distribution of sugarcane yield for season 2018-2019 and 2019-2020 B) Comparison sucrose yield and sugarcane yield (r=0.95).

4.3.2. SATELLITE DATA ACQUISITION AND PROCESSING

For this analysis, time series per season were extracted for different remote sensing products per field based on harvesting dates. Time series dates were expressed in terms of "days after ratooning" to allow for comparison between fields. Time series of the field-averaged Sentinel-1 backscatters at VV and VH polarizations were used, as well as Planet's NDVI product.

SENTINEL-1 BACKSCATTER

Sentinel-1 data was processed by using the Sentinel Application Platform (SNAP) toolbox (ESA, 2021b). During this process a radiometric calibration and terrain correction are applied to convert the data into normalized backscatter and correct for elevation differences respectively. The Sentinel-1 satellites observed with Synthetic Aperture Radar (SAR), captures backscatter at 5.405GHz (C-band) at 5x20m spatial resolution. In southern Mozambique, Sentinel-1 has a revisit frequency of approximately 12 days (ESA, 2021a). Only descending data from both Sentinel-1 platforms were used of orbit number 6 and 79 to minimize observation geometry effects (Vreugdenhil et al., 2018). Finally, the observations were sampled at a 10 by 10 meter resolution.

Backscatter timeseries were extracted from Sentinel-1 observations for each field for VV and VH polarizations. In addition, the cross ratio (CR) was calculated for each field. The CR can be calculated by subtracting VH-VV on a logarithmic scale. In previous researches CR was used to study vegetation dynamics as it reduces the backscatter effect of

soil moisture and soil-vegetation interactions (Khabbazan et al., 2019; Vreugdenhil et al., 2018). CR has been shown to increase with vegetation growth and is, therefore, more representative of the scattering associated with volume scattering from vegetation (Veloso et al., 2017), while the individual VV and VH backscatters include a stronger contribution of soil moisture from rain events as well as irrigation.

PLANET FUSION NDVI

The Normalized Difference Vegetation Index (NDVI) is a widely used vegetation index. NDVI requires red and near-infra red bands and is indicative of the chlorophyll content of a vegetated surface (Rouse et al., 1974). Planet realizes daily global imaging in optical spectrum, observing in RGB and near infra red at approximately 3 meter spatial resolution with commercial satellites. For this chapter Planet's NDVI fusion products was used and up-scaled to Sentinel-1's 10 meter spatial resolution. The Planet fusion product merges PlanetScope observations with Sentinel-2, Landsat-8 and MODIS data (Houborg & McCabe, 2018a). The end result is a daily cloud free NDVI timeseries. The new Planet data improves cross-sensor inconsistencies due to variations in orbital configurations, spectral responses, and radiometric quality. The CubeSat ENabled Spatio-Temporal Enhancement Method (CESTEM) creates a robust NDVI signal that can be used to observe high-frequency vegetation dynamics (Aragon et al., 2021; Houborg & McCabe, 2018a; Planet, 2021).

4.3.3. SUGARCANE DATA ANALYSIS

The sugarcane yield and satellite data were used to understand the effect of sucrose accumulation on different vegetation indices retrieved with satellite data. In addition, a modeling study was done to explain the effect of changes in the vegetation water content as a result of sucrose accumulation on the dielectric constant of vegetation.

YIELD ANALYSIS

First, the variation of NDVI and CR per field was assessed over the growing season. To understand the behaviour of the two vegetation indices in poor and good performing fields, the 10^{th} and 90^{th} percentile of the sugarcane yield dataset for the season 2018-2019 and 2019-2020 was calculated. The 10^{th} percentile was found to be 50.0 TCH and the 90^{th} percentile 108.7 TCH. The average NDVI and CR over time was computed for the selected fields below and above the chosen percentiles.

Second, the VV backscatter, VH backscatter, CR, and NDVI were compared with yield over the growing season. The Pearson correlation coefficient was computed for each day after ratooning for average field values of the satellite derived products and the final sugarcane yield. For each satellite product the five-day moving average of the correlation coefficient was plotted to understand the changes over the growing season.

MODELING STUDY

To understand the effect of sucrose accumulation on radar backscatter a modeling study was performed. Radar backscatter of a canopy is determined by its dielectric properties, size, shape, orientation, and roughness, and the distribution of the canopy (Karam &

Fung, 1989; Steele-Dunne et al., 2017). The dielectric properties of vegetation are described by the dual-dispersion model of Ulaby and El-Rayes (1987). This is a model converting the gravimetric water content into the complex dielectric constant of vegetation (ϵ_v) (Meyer et al., 2019). Ulaby and El-Rayes (1987) assumes ϵ_v is a mixture of three components: a non-dispersive residual component (ϵ_r) [-], a free water component (ϵ_{fw}) [-], and a bound water component (ϵ_b) [-]. Where bound water refers to the water molecules that are in a solution, and free water means refers to water molecules not in compound (Ulaby & El-Rayes, 1987). Ulaby and El-Rayes (1987) define the dielectric constant of vegetation (ϵ_v) as follows:

$$\epsilon_v = \epsilon_r + v_{fw}\epsilon_{fw} + v_b\epsilon_b \tag{4.1}$$

Where v_{fw}: volume fraction of free water [-] v_b: volume fraction of the bulk vegetation-bound water mixture [-]. All the components depend on the gravimetric water content (M_g). Where M_g is the gravimetric moisture content defined as the amount of water [g] per wet biomass [g] (Meyer et al., 2019). The non-dispersive residual component (ϵ_r) is estimated as:

$$\epsilon_r = 1.7 - 0.74M_g + 6.16M_g^2 \tag{4.2}$$

The free water and bound water component of the complex dielectric constant of vegetation in equation 4.1 are defined as follows:

$$\epsilon_{fw} = 4.9 + \frac{75}{1 + \frac{jf}{18}} - j\frac{18\sigma}{f} \tag{4.3}$$

$$\epsilon_b = 2.9 + \frac{55}{1 + (\frac{jf}{0.18})^{0.5}} \tag{4.4}$$

where f is the frequency [GHz], σ the ionic conductivity of free-water solution [Sm^{-1}], and j denotes the imaginary number. The parameter σ was found to be constant (1.27 Sm^{-1}) by Ulaby and El-Rayes (1987). The difficulty of the model is to estimate the distribution of free and bound water. With the help of lab experiments Ulaby and El-Rayes (1987) found a relation between the gravimetric moisture content and the v_{fw} and v_b:

$$v_{fw} = M_g(0.55M_g - 0.076) \tag{4.5}$$

$$v_b = 4.64M_g^2/(1 + 7.36M_g^2) \tag{4.6}$$

Literature on water content and sucrose development in sugarcane over time is not abundant (G. Inman-Bamber, 2013). However, a study by Muchow et al. (1996) reported on a field experiment that documented the development of sucrose, vegetation water, and dry vegetation over the growing season. The location of the experiment was Australia and sugarcane was grown as a ratoon crop under irrigated conditions (Muchow et al., 1996). The experiment entailed sampling of sugarcane on eight moments in the growing season. From these results the gravimetric moisture content was estimated by:

$$M_g = 1 - M_{sucrose} - M_{dry} \tag{4.7}$$

where $M_{sucrose}$ is the fraction of sucrose of the total fresh biomass and M_{dry} the fraction of dry weight of the fresh biomass. Data from (Muchow et al., 1996) were used to model the effect of temporal changes in M_g on the dielectric constant in vegetation. This allows us to explain the observed changes in backscatter and CR. In Table 4.1 the resulting v_{fw} and v_b can be found.

Table 4.1: Free and bound water fractions after several moments in the growing season. v_b and v_{fw} computed with field experiment results Muchow et al. (1996).

Sampling day	**150**	**190**	**220**	**250**	**290**	**350**	**380**	**420**
v_{fw}	0.29	0.23	0.20	0.18	0.15	0.14	0.14	0.13
v_b	0.52	0.50	0.49	0.48	0.45	0.45	0.45	0.44

4.4. RESULTS

Figure 4.2 A and B show the NDVI and CR per field during the growing season, where panel A shows the NDVI and panel B the CR. The red and green lines in Figure 4.2 A and dots in Figure 4.2 B display the NDVI and CR observation values in 10^{th} and 90^{th} percentile fields considering crop yield. The NDVI and CR of the fields with a yield below the 10^{th} percentile and above the 90^{th} percentile are averaged to compute the red and green lines, respectively. From Figure 4.2 A the 90^{th} percentile NDVI development show an increase over the growing season. The 90^{th} percentile reaches a much higher NDVI value. The 10^{th} percentile NDVI development show lower values. The difference between the 10^{th} and 90^{th} percentile line becomes evident during the Development and Final stage, when the biomass is fully developing. The results suggest good performing fields develop high NDVI values over the growing season and poor performing fields develop low NDVI values. Which is in line with previous research on NDVI and sugarcane yield (Bégué et al., 2010; Pinheiro Lisboa et al., 2018).

Figure 4.2 B shows an opposite signal compared to NDVI. The CR development of 90^{th} percentile line shows a decrease over the growing season, starting in the Development stage. The average CR values of the 10^{th} percentile fields are more constant from the end of the Tillering stage onward. Interestingly, the CR values of the 10^{th} percentile fields are higher than the 90^{th} percentile fields in the Development and Final stage. Combining with Figure 2A, this suggests that good-performing fields are characterized by high NDVI and low CR. Conversely, poor-performing fields are characterized by low NDVI and higher CR values. To our knowledge, this is the first such analysis of CR in sugarcane. However, in other crops (e.g. corn) the CR increases over time as a result of increase in vegetation water content (Vreugdenhil et al., 2018).

Figure 4.3 visualizes the relation between different satellite products and sugarcane yield over the growing season. The satellite derived products assessed in Figure 4.3 are: VV, VH, CR and NDVI. In Figure 4.3 the Pearson correlation over each day in the growing season is calculated for the final yield and average field value of the satellite derived product for all fields under study. Figure 4.3 shows the correlation between sugarcane

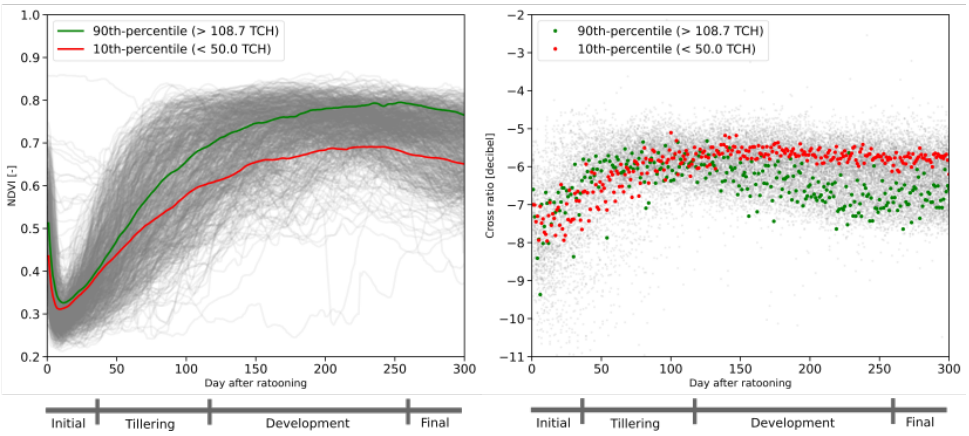

Figure 4.2: (A) NDVI timeseries of the fields under study over the growing season. Each gray line corresponds to a single field. (B) Cross ratio timeseries of the fields under study. The green and red lines display the average values of fields with a yield above the 90^{th} percentile (> 108.7 TCH) and below the 10^{th} percentile (< 50.0 TCH). The bar below the figure indicates the length of the different crop stages.

yield and NDVI is increasing alongside the sugarcane development. The highest correlation is 0.56 on 254 days after ratooning, at the end of the Development stage. In the Final stage, the correlation with yield declines. This is expected since, at this stage, dry-off causes wilting of the sugarcane plant (see section 4.2).

VV and VH show a similar variation in their correlation to yield throughout the growing season. The highest correlation for VV is 0.50 on day 272 and 0.42 for VH on day 116. The correlation to yield for VV and VH start to deviate from each other during the Development stage. VV shows higher correlations to yield compared to the VH, suggesting that VV provides a better indicator of sugarcane growth than VH. This is in contrast to other studies on broadleaf crops and tall leaf stems (e.g. corn) which showed an increasing backscatter signal over the growing season (Macelloni et al., 2001). Macelloni et al. (2001) and Vreugdenhil et al. (2018) showed VH to be more sensitive to crop growth indicators (i.e. Leaf Area Index, Vegetation Water Content). However, the crops considered in those studies do not accumulate sucrose over the growing season.

The CR shows a negative relationship with yield over time. This is an opposite relationship NDVI shows with yield over time. Over the growing season the relation between CR and yield shows an increasing negative correlation with a maximum correlation of -0.47 on day 233. In particular, halfway through the Tillering stage and towards the start of the Development stage, the CR correlation shows a steep decline. Towards the end of the Development stage, the correlation stablizes and remains stable throughout the Final stage. The steep increase in negative correlation between the yield and CR half way the Tillering stage suggests a change in the sugarcane plant growth. Interestingly, this coincides with the period in which the sugarcane plant starts to accumulate sucrose (see section 4.2).

A modeling study was performed to investigate how sucrose accumulation affects

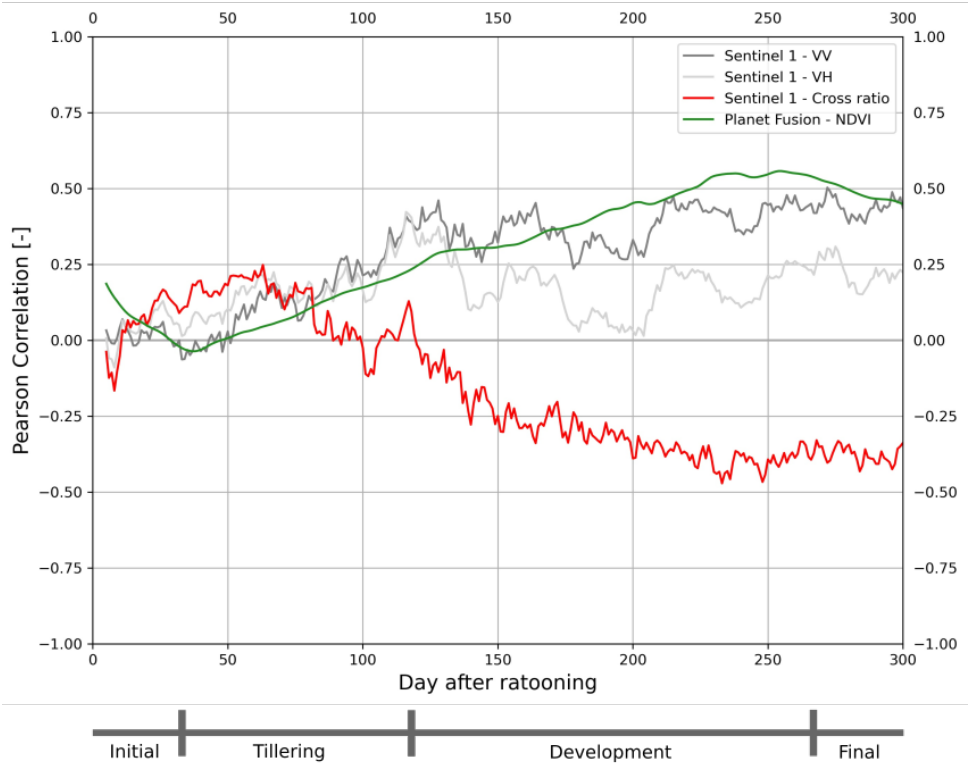

Figure 4.3: Pearson correlation with sugarcane yield for season 2019-2020 for VV and VH polarization, Cross ratio, and NDVI. The bar below the figure indicates the length of the different crop stages

.

the dielectric constant, a key driver of the radar backscatter. Data were used from a field campaign conducted by Muchow et al. (1996), in which they documented the development of sucrose, vegetation water, and dry vegetation over the growing season. The data are visualized in Figure 4.4, where the accumulation of sucrose is evident, particularly during the Development stage.

The accumulation of sucrose within the plant lowers the total gravimetric water content in the plant (section 4.3.3 and equation 4.1). Based on the Dual Dispersion model of Ulaby and El-Rayes (1987), this lowers the dielectric constant of vegetation significantly, see Figure 4.4. Figure 4.4 shows how the dielectric constant of vegetation, particularly the real part, decreases. This decrease explains the decrease in backscatter, which in turn explains the negative correlation between CR and yield.

It is worth noting that a change in the chemical composition of stem water as a result of sucrose accumulation would also affect the dielectric constant, a factor not explicitly considered in Equation 4.6 (McDonald et al., 2002; Ulaby & El-Rayes, 1987). As sucrose is bound to water, an increase in sucrose should increase the amount of bound water

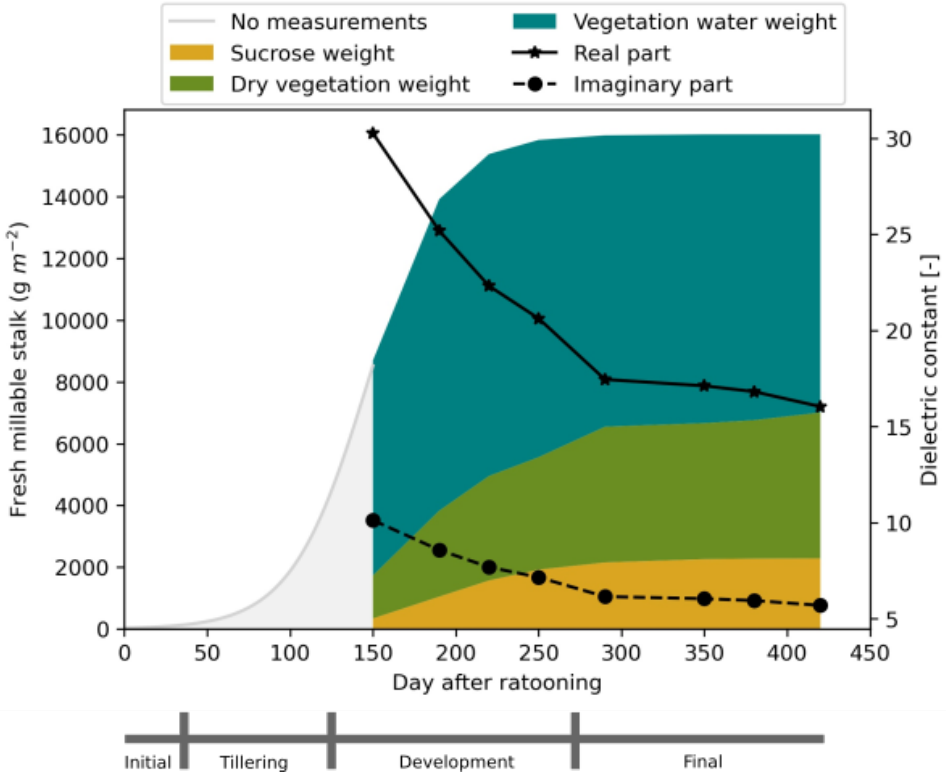

Figure 4.4: Results of a field campaign by Muchow et al. (1996) and the influence of the change in distribution between bound and free particles on the dielectric properties of vegetation. The bar below the figure indicates the length of the different crop stages.

(Moore & Botha, 2013). Bound water has a lower dielectric constant than free water, as the molecules are not free to rotate. Hence, accounting for the impact of sucrose on the bound water fraction is likely to lead to a further decrease in dielectric constant.

As a result of sucrose production within the sugarcane stem, the combined effect of a changing water content and chemical composition affects the backscatter signal through a decrease in dielectric constant directly. This is different from NDVI, which indicates the chlorophyll content of the vegetated surfaces (Rouse et al., 1974). The link between chlorophyll content and sucrose accumulation is indirect. The CR in particular has a distinctive response to the sucrose development and, therefore, proves to contain information on sucrose accumulation in the sugarcane plant. In addition, the results support the CR to be more representative of the scattering associated with the canopy, as was found in other studies (Khabbazan et al., 2019; Veloso et al., 2017; Vreugdenhil et al., 2018).

4.5. DISCUSSION

This chapter shows the relationship between sugarcane yield and vegetation indices from Sentinel-1 backscatter and Planet NDVI. The results show a negative correlation between the CR and sugarcane yield over the growing season. Previous studies on the CR reported the ability to observe changes in vegetation structure and accumulation of fresh biomass (Veloso et al., 2017; Vreugdenhil et al., 2018). However, no comparable studies exist where the CR is compared to yield in sucrose accumulating crops.

Contrary to the results using CR, NDVI develops a positive correlation to yield over the growing season. In other words, where good performing fields are characterized by low CR values and high NDVI, poor performing fields are characterized by high CR values and low NDVI. Other researchers have found positive correlations with NDVI and sugarcane crop yield (Bégué et al., 2010; Morel et al., 2014). In these studies the integral of NDVI over the growing season was compared to final sugarcane yield or the maximum value within a growing season. In addition, Bégué et al. (2010) found lower NDVI values in the final stage for fields with a higher sucrose content. This can be explained by the leaf senescence, which causes the chlorophyll content to drop. And could explain why the results show a decrease in correlation with NDVI towards the end of the growing season.

A modeling study was used to show how the dielectric constant of sugarcane is affected by the change in the sugarcane's internal composition (El-Rayes & Ulaby, 1987; Ulaby & El-Rayes, 1987). Contrary to other crops, the chemical composition of plant water in sucrose-producing crops, like sugarcane, changes over the growing season. Sucrose is produced from the Tillering stage through to the Development stage. This decreases the amount of free water and increases the bound water in the sugarcane stem over the growing season (J. Wang et al., 2013; R. Wang et al., 2011). The combined effect of a decrease in vegetation water content and change in chemical composition of the vegetation water due to sucrose accumulation in the sugarcane stem alters the backscatter signal (McDonald et al., 2002).

The alteration of the backscatter signal is visible in the CR over the growing season which shows a negative correlation to sucrose yield. This shows the CR is able to observe sucrose accumulation during the growing season. Hence, the CR is indicative of the sucrose content in the sugarcane plant. To improve understanding of the effect of sucrose accumulation on the backscatter signal, more research should focus on the effect of sucrose accumulation on the partitioning between free and bound water in vegetation. Within the current estimation of gravimetric moisture content in Ulaby and El-Rayes (1987) the development of bound water in sucrose accumulating crops are underestimated. The estimation of apportioning free and bound water is currently based on, predominantly, corn leaf experiments by Ulaby and El-Rayes (1987). More studies should focus on experiments with sucrose accumulating vegetation (e.g. agave).

In this chapter, it has been proven that CR computed with Sentinel-1 backscatter can be used to observe sucrose accumulation in sugarcane. Although this thesis focuses on sugarcane, Sentinel-1 backscatter could also be of use to monitor quality and/or sucrose accumulation in other crops (e.g. agave). In addition, combining optical and backscatter observations is expected to be of value for crop monitoring and yield prediction. Future studies along the same line, therefore, should focus on combining these different data

products.

5

THE INFLUENCE OF WATERLOGGING ON SUGARCANE MONITORING

I told you. Too much of anything is really never good.

Mom

The previous chapter showed the impact of sucrose accumulation in Sentinel-1 backscatter. In this chapter the aim was to analyze if, and how, waterlogging is present in Sentinel-1 backscatter. This was done by comparing several seasons and by benchmarking against different remote sensing observations. The analysis elaborated on how to observe sucrose development in Sentinel-1 backscatter and the results showed the influence of waterlogging on Sentinel-1 backscatter observations.

This chapter is published in *Remote Sensing of Environment* (den Besten et al., 2023).

5.1. INTRODUCTION

The global production of sugarcane is driven by the demand for raw sugar and (bio-) ethanol (Shabbir et al., 2021). Over the last few decades researchers have managed to breed the perennial grass to produce high contents of sucrose. Furthermore, sucrose is the soluble sugar present in the stem of the sugarcane crop and, as a result of breeding, sugarcane species accumulate high concentrations of sucrose. Additionally, the concentration of sucrose in the sugarcane stem can be as high as 18 percent of fresh weight (Mustafa et al., 2018).

Improving operational and management practices in the sugarcane production chain are key to sustainable intensification, in order to ultimately close the current yield gaps with less pressure on the environment (Bordonal et al., 2018). An example is to improve current manual sugarcane monitoring to adjust on-site management (Bocca et al., 2015). Here, information on the presence of waterlogging plays a role due to waterlogged soil conditions affecting plant physiology and hampering crop growth and yield significantly (den Besten, Steele-Dunne, de Jeu, et al., 2021; Shaw et al., 2013). Academic literature reports the cause of waterlogging in irrigated agriculture to be a result of over-irrigation or poor sub-surface drainage (FAO, 2016c). In rain-fed agriculture, Martinez-Feria and Basso (2020) found waterlogging to be an important driver behind yield instability in the US Midwest.

Satellite remote sensing can play a role in improving current sugarcane production practices through monitoring (Bégué et al., 2018; Cancela et al., 2019; Mancini et al., 2019; McCabe et al., 2016). Unfortunately, the integration of new remote sensing techniques into the decision making process of sugarcane production remains slow (Bocca et al., 2015). Previous studies have researched the relationship between sugarcane yield and vegetation indices computed from satellite data (Bégué et al., 2010; Lofton et al., 2012; Molijn et al., 2019; Morel et al., 2014). Common techniques are based on optical indices (e.g. NDVI) (Morel et al., 2014) and focus on machine learning (Fernandes et al., 2017; Shendryk et al., 2021).

Vegetation indices retrieved from backscatter are also starting to proliferate (Steele-Dunne et al., 2017). Researchers have shown the capabilities of cross- and co-polarization backscatter channels to monitor sugarcane (Baghdadi et al., 2009; Molijn et al., 2019; Som-ard et al., 2021). For example, Baghdadi et al., 2009 concluded cross-polarizations are slightly better for monitoring sugarcane and, therefore, Molijn et al., 2019 did not consider co-polarization.

Vegetation indices retrieved from radar are sensitive to different characteristics than indices derived from optical sensors. Microwave energy responds to the dielectric properties of the crop canopy, but also to the structure of the crops, such as the size, and orientation of leaves, stalk, and fruit (McNairn & Brisco, 2004). The dielectric properties are strongly influenced by the water content in the plant (Ulaby & Jedlicka, 1984). In addition, for sugarcane, den Besten, Steele-Dunne, Aouizerats, et al., 2021 showed how a change in the internal characteristics of sugarcane during the growing season influences the radar backscatter. As a result of sucrose accumulation, the dielectric constant of the canopy decreases and the strength of the observed backscatter signal also decreases.

Unfortunately, studies relating large sugarcane yield datasets to backscatter are scarce (den Besten, Steele-Dunne, Aouizerats, et al., 2021; Shendryk et al., 2021). In addition,

it is not known how or the extent to which waterlogging beneath a thick canopy, such as sugarcane, affects different radar polarizations and polarization ratios. Expanding knowledge on how Sentinel-1 backscatter responds to sugarcane yield variability and waterlogging is crucial to help the interpretation of the radar vegetation signals. In addition, information on the presence of waterlogging itself is valuable to several agricultural practices (e.g. drainage issues, trafficability, irrigation).

Therefore, the aim of this chapter was to understand how Sentinel-1 backscatter responds to sugarcane yield variability and waterlogging. Here we present how backscatter observations can be used to monitor sugarcane yield and how the observations are influenced by waterlogging. The ultimate goal was to increase understanding on how to simultaneously monitor sugarcane and waterlogging using Sentinel-1 SAR data. To research the issue we focused on an irrigated sugarcane plantation in Xinavane, southern Mozambique, a site with numerous reported issues related to waterlogging (den Besten, Steele-Dunne, de Jeu, et al., 2021).

5.2. SUGARCANE GROWTH

Sugarcane is grown in subtropical and tropical regions. Harvest dates are ideally determined to match optimum supply to the nearest sugar mill (Bocca et al., 2015). The majority of sugarcane plantations or farms grow sugarcane as a ratoon crop (G. Inman-Bamber, 2013). This is a common and cost-effective practice around the world, where sugarcane is not replanted after harvest, but grown from the preceding plant (Surendran et al., 2016).

Sugarcane is ideally harvested at maximum sugar accumulation in the stem. The average length of the growing season in Xinavane is twelve months (den Besten et al., 2020). The growing season can be divided into different growth stages. In the analysis presented in this chapter, the following four growth stages were defined: the initial stage (30 days), the tillering stage (90 days), the development stage (150 days), and the final stage (90 days) (Doorenbos & Kassam, 1979; Silva et al., 2015).

Sugarcane is a peculiar crop as it accumulates sucrose both inside and outside the cells (both symplast and apoplast) (J. Wang et al., 2013). The sugarcane plant deposits the sucrose in the stem vacuoles and cells around it. During the tillering stage, the sugarcane plant starts accumulating biomass. The biomass growth takes place particularly in the leaf canopy (G. Inman-Bamber, 2013). Hereafter, in the development stage, the growth emphasis is on the stem, which is an important sink for sucrose development (Cock, 2001; G. Inman-Bamber, 2013). In this stage, the sucrose accumulation starts to play a significant role. See figure 5.1 (A) and (D). Sucrose forms as a hydrogen bond, and the development of stalk moisture and sucrose are therefore closely linked to each other (N. Inman-Bamber et al., 2009). Over time, the sucrose accumulation ensures that a fraction of the water in the fresh stalk is substituted with sucrose, see figure 5.1 (A) (Muchow et al., 1996).

Throughout the growing season, the vertical distribution of sucrose and Vegetation Water Content (VWC) inside the sugarcane plant changes as well. From our experience in Xinavane, we know that the vertical distribution inside the sugarcane plant changes during the growing season. However, to our knowledge, quantitative data on this have not been published to date. A few researchers have attempted to capture the changes

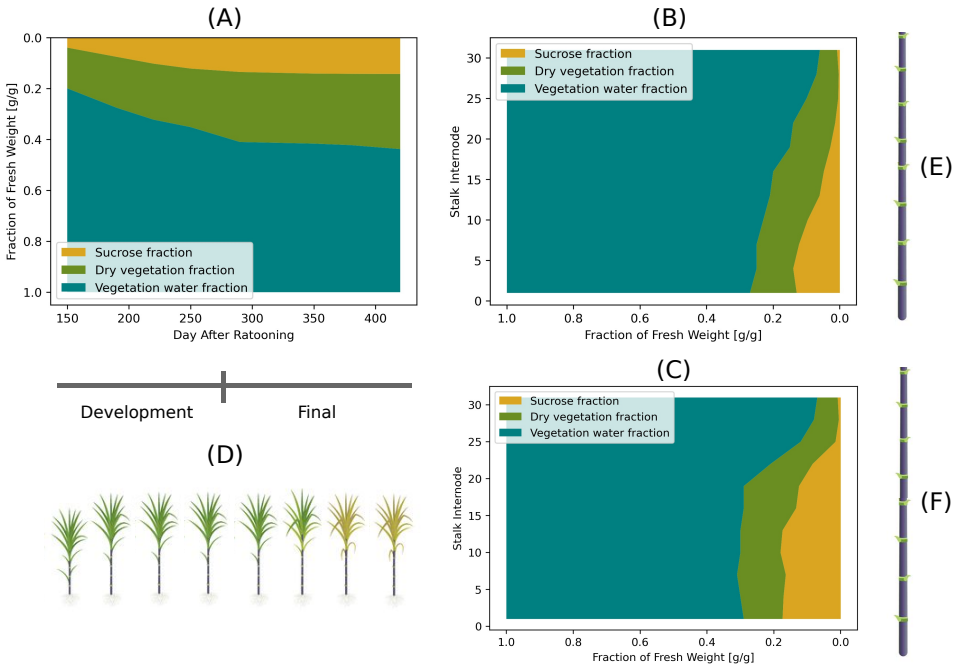

Figure 5.1: A schematic diagram of the vertical and temporal distribution of sucrose in the sugarcane stalk. (A) shows the temporal change of sucrose, vegetation, and water distribution over the development and final phase (Muchow et al., 1996); (B) and (C) the vertical distribution for a low and high yielding variety respectively. (N. Inman-Bamber et al., 2009) For reference purposes (D), (E), and (F) illustrate the physical development of the canopy and vertical structure of the sugarcane stalks.

of the vertical distribution over time by sampling different varieties in the development stage. These results showed the sucrose distribution in lower yielding varieties was stored mostly in the lower inter-nodes, whereas in the higher yielding varieties the sucrose is distributed more homogeneous in the stalk, see figure 5.1 (C) and (D) (N. Inman-Bamber et al., 2009). Nodes are referred to as the place where leafs develop on the stalk, see figure 5.1 (E) and (F).

5.3. DATA AND METHODS

The research presented in this chapter focused on different satellite remote sensing observations for an irrigated sugarcane plantation. Optical and passive microwave observations were used to benchmark Sentinel-1 observations, in order to understand the seasonal characteristics and expose differences. Ground data were used to understand how radar observations in different polarizations and their ratio relate to sucrose yield. Section 5.3.1 will explain the origin and characteristics of the data and Section 5.3.2 will provide a description of the data analysis.

5.3.1. DATA

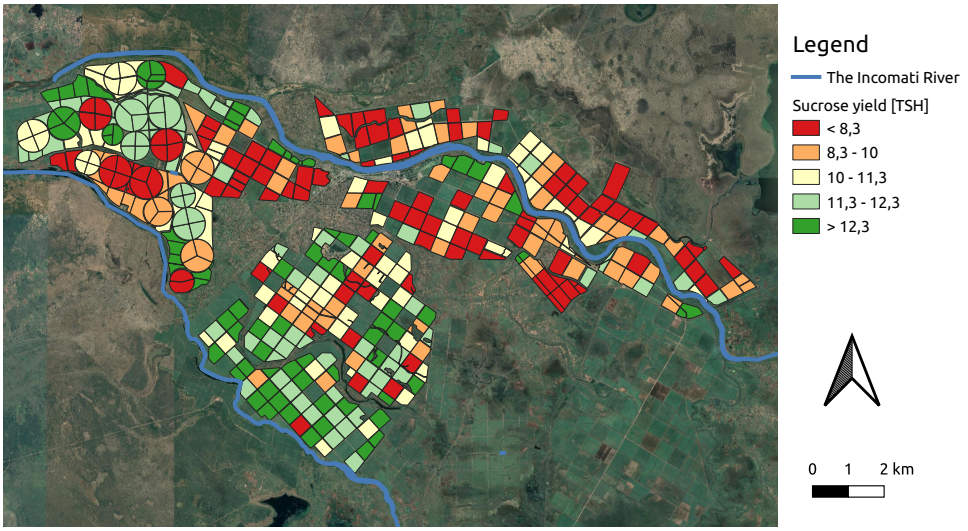

Figure 5.2: Location of fields under study in Xinavane, Mozambique. The colors indicate average yield for the seasons 2019-2021 for 299 fields.

YIELD DATA

Crop yield data were obtained from a sugarcane plantation located on the banks of the lower Incomati river in Xinavane, Mozambique (see Figure 5.2). The local sugar mill runs from April to December and during these months sugarcane is harvested and milled. The sugarcane produced in the plantation is converted to raw sugar at the sugar mill. In the plantation, ratoon sugarcane is grown under irrigated conditions (den Besten et al., 2020). The average field-size is approximately 20 hectares (den Besten et al., 2020). The sugarcane in the plantation is planted in rows 1-1.5 meter apart. The dominant sugarcane varieties in the plantation are N25 and N23, accounting for 86 percent (Butler, 2001). The research presented focused on 299 fields that are owned and managed by the Tongaat Hulett group.

To harvest the sugarcane, fields are burnt to ease the manual harvest process and remove leaves. After the fire ceases, the harvest labourers cut the stalk from the roots at ground level. The harvested sugarcane is then collected by trucks allocated to specific fields. The trucks containing harvested sugarcane are weighed and documented per field. After weighing, several samples are tested for their sucrose content. This process results in data per field on sugarcane yield (tonnes of cane per hectare, TCH) and sucrose yield (tonnes of sucrose per hectare, TSH).

For this research the sucrose yield (TSH) obtained by the sugar mill was considered for the seasons 2018-2019, 2019-2020, and 2020-2021. The preceding seasons correspond to 2019, 2020, and 2021 in Figure 5.3 (A). These years were taken because of robust availability of satellite data during these seasons and contrasting years in terms of soil water content. Seasons 2015-2019 experienced a rainy season below average, in contrast to seasons 2020 and 2021 in Figure 5.3 (den Besten et al., 2020). Interestingly, Figure 5.3 (A) shows the mean sucrose yield was lower in seasons 2020 and 2021.

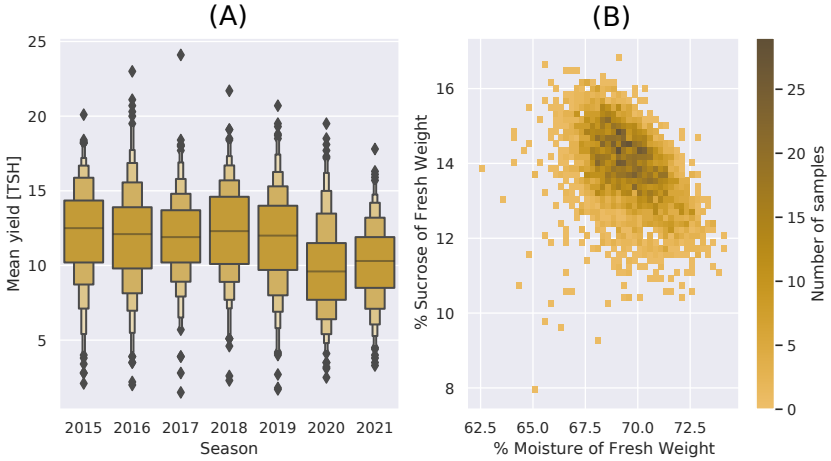

Figure 5.3: (A) shows a boxplot of mean sucrose yield for seasons 2015 until 2021 (B) shows the relation between measured sucrose and moisture percentage of fresh weight of seasons 2018-2021 for the 299 fields

In addition, Figure 5.3 (B) shows the percentage of sucrose and moisture of fresh weight measured at harvest. This is to illustrate the high percentage of sucrose concentration in the stalk (up to 16 percent). There is a negative correlation between sucrose and moisture content at harvest, further illustrating the relation between sucrose and moisture content in the sugarcane stalk (see section 5.2).

SOIL WATER CONTENT AND LAND SURFACE TEMPERATURE

During the analysis, Soil Water Content and Land Surface Temperature as derived from the Land Parameter Retrieval Model using passive microwave observations were used (Owe et al., 2008; van der Schalie et al., 2017). A downscaling method was applied to the passive microwave brightness temperatures to get to a spatial resolution of 100m (Richard de et al., 2016). The basis for Soil Water Content was SMAP's L-band (1.41GHz) passive microwave observations at 06:00AM at equatorial passing (descending) and the a effective field of view footprint is a 39 km by 47 km ellipse. The observations represent the Soil Water Content in the first 0-5 cm of the soil. To compute Land Surface Temperature AMSR-2's Ka-band (36.5GHz) data were used, which observes at 01:30AM (descending) with a spatial resolution of 7km x 12km (Holmes et al., 2009; Owe et al., 2008).

For the analysis, the Soil Water Content was used to understand the temporal variation in soil moisture over the three seasons. The data products are too coarse to identify individual irrigation events (den Besten, Steele-Dunne, de Jeu, et al., 2021). Nevertheless, it is very valuable for identifying wet or dry periods. Certainly, in combination with observations from the field, a period with prolonged waterlogging could be identified in season 2020-2021, see figure 5.4 and section 5.3.2. In Figure 5.4 (C) we zoom in on the soil water content during the identified waterlogging peak where (II) indicates a week during the waterlogging peak and (I) a week before of the waterlogging event.

Figure 5.4 (A) also shows the average daily Land Surface Temperature for all the fields under study. The LST reflects the seasonality in the plantation, with higher temperatures before and during the rainy season and lower temperatures during winter. LST was used in the analysis to understand seasonal dynamics and to understand the role of temperature on sucrose development.

SENTINEL-1 RADAR BACKSCATTER

Sentinel-1 GRD data were processed using Google Earth Engine and the Sentinel-1 Toolbox. During this process, a radiometric calibration and terrain correction were applied to convert the data into normalized backscatter and correct for elevation differences. The Sentinel-1 satellites observed with Synthetic Aperture Radar (SAR), captures backscatter at 5.405GHz (C-band) at 5x20m spatial resolution. Descending data from Sentinel-1 A and B were used. Figure 5.5 (A) shows the available observations that were used throughout the season. In southern Mozambique the majority of the revisit frequency between 4 to 6 days, with a few exceptions in 2018 as a result of maintenance (ESA, 2021a). Figure 5.5 (B) provides a snapshot of Sentinel-1 VH polarization. Finally, the observations were sampled at a 10 by 10 meter resolution.

Backscatter time series were extracted for each field with daily average values of VV and VH polarizations, see Figure 5.2 (B) for the respective field boundaries. The cross ratio (CR) was also calculated for each field. The Cross Ratio can be calculated by subtracting VH-VV on a logarithmic scale. Previous work showed CR reduces the backscatter effect of soil moisture and soil-vegetation interactions (Khabbazan et al., 2019; Vreugdenhil et al., 2018). The individual VV and VH backscatters contain artefacts of soil moisture, rain events, and irrigation for example (Molijn et al., 2019). The CR relates more to the volume scattering from vegetation and increases with vegetation growth (Veloso et al., 2017).

PLANET FUSION NDVI

The Normalized Difference Vegetation Index (NDVI) requires red and near-infrared bands and is widely used as an indicator of the chlorophyll content and density of a vegetated surface (Rouse et al., 1974). In this study PlanetScope satellite data were used. PlanetScope provides near-daily global imaging at optical wavelengths, observing in RGB and near-infrared at 3-5 meter spatial resolution. This study used the Planet Fusion surface reflectance product, which represents a comprehensive harmonization and fusion methodology based on the CubeSat Enabled Spatio-Temporal Enhancement Method (CESTEM) (Houborg & McCabe, 2018a, 2018b; Planet, 2021). Planet Fusion leverages rigorously calibrated publicly accessible datasets from Sentinel-2, Landsat 8/9, Moderate Resolution Imaging Spectroradiometer (MODIS), and Visible Infrared Imaging Radiometer Suite (VIIRS) in concert with the higher spatial and temporal resolution data provided by Planet's medium resolution constellation of 200+ CubeSats for full fleet interoperability. Planet Fusion includes rigorous, temporally driven, cloud and cloud shadow detection and advanced harmonization to reduce cross-sensor inconsistencies resulting from variations in orbital configurations, spectral responses, and geometric and radiometric quality. The end result is a next generation analysis ready surface reflectance product that can be used to derive daily, cloud-free, and gap-free NDVI time series data characterized by enhanced radiometric stability and consistency across space and time to

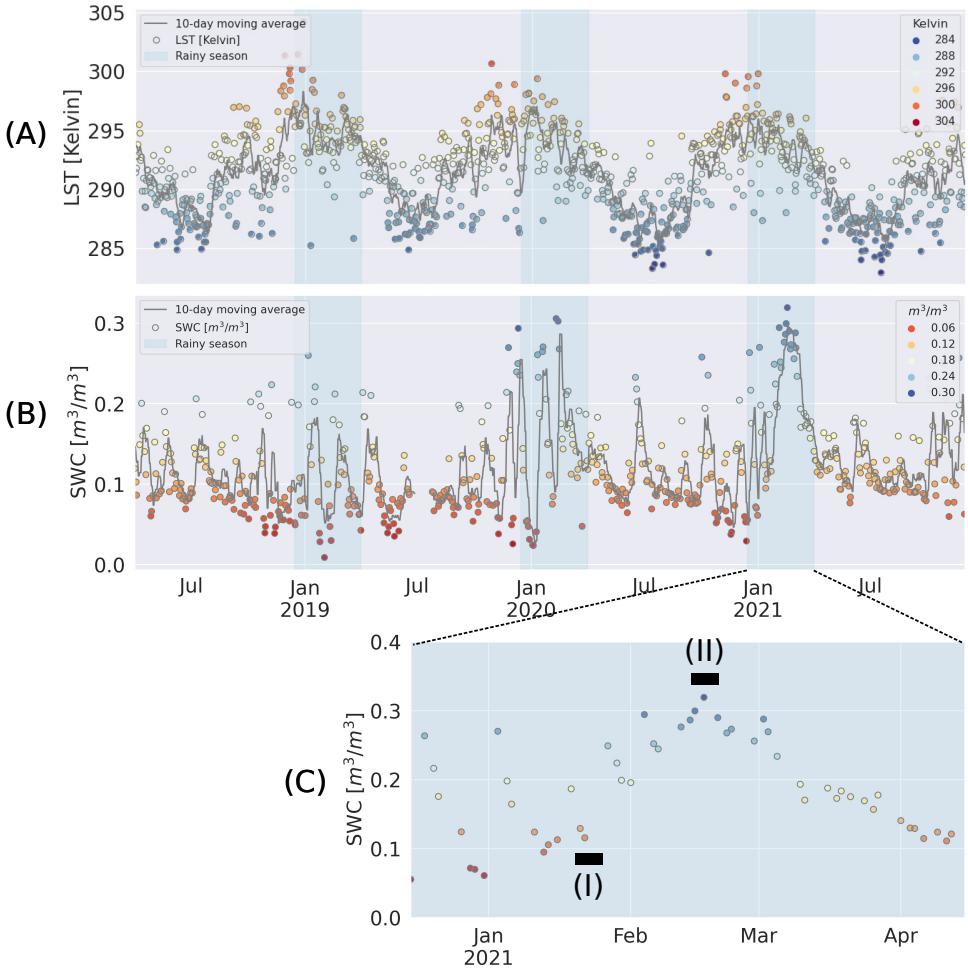

Figure 5.4: (A) Land Surface Temperature and (B) soil water content averaged for all the fields under study from April 2018 until December 2021. The individual observations are indicated with colored dots. The gray line shows a moving average with a 10 day timeframe. The blue shading indicates the rainy season. (C) detailed view of the rainy season of 2021. (I) and (II) indicate before and during the waterlogging peak, respectively.

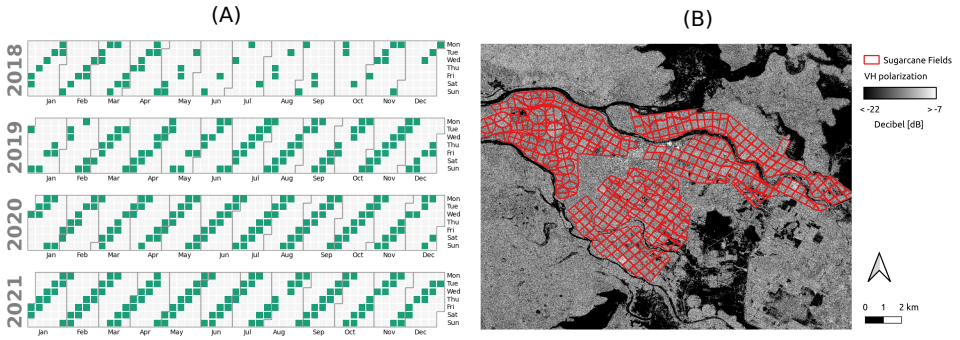

Figure 5.5: (A) Green squares are days of Sentinel-1 observations used in the analysis (Tomkwok, 2022). (B) Snapshot of Sentinel-1 observation (2021-02-17) with fields under study in Xinavane, Mozambique.

support studies on high-frequency vegetation dynamics (Aragon et al., 2021; Houborg & McCabe, 2018a; Planet, 2021). Finally, the observations were resampled at a 10 by 10 meter resolution to meet the spatial resolution of Sentinel-1 for a more accurate comparison.

5

5.3.2. DATA ANALYSIS

CLASSIFYING FIELDS BY SUCROSE YIELD

First, the variation of vegetation indices per field were assessed over the growing season. To understand the response of the vegetation indices to sugarcane yield variability, the 25^{th}, 50^{th}, and 75^{th} percentiles of the sucrose yield (TSH) dataset were calculated. From these percentiles four groups were created, respectively $< 25^{th}$, 25^{th}-50^{th}, 50^{th}-75^{th}, $> 75^{th}$. These yield constraints were used to mask the field time series and generate averages for different performance groups and different indices. A rolling mean of fifteen days was used to visualize time series.

SEASONALITY IN SUCROSE DEVELOPMENT

Previous studies have found a connection between ratooning month, sugarcane biomass accumulation and sucrose yield (van Heerden et al., 2010). Due to seasonal variations in radiation, the relationship between biomass and intercepted radiation is affected by ratooning month. This means that radiation use efficiency for sugarcane varies depending on the ratooning month (Donaldson et al., 2008). Figure 5.4 A shows how Land Surface Temperature (LST) varies during the year and figure 5.6 shows that yield is indeed affected by choice of ratooning month. Figure 5.6 shows the difference in yield in the plantation can potentially be as much as 3 TSH [=20 percent] comparing the average yield in August and November.

Figure 5.6 illustrates how the LST in the period of Day After Ratooning (DAR) 150-200 relates to the seasonality in yield. This implies, in order to compare other influential factor besides temperature, ratooning dates or month need to be considered. Therefore, the data were further sorted by ratooning month which ranges from May to November. April and December were excluded from the analysis due to insignificant number of fields

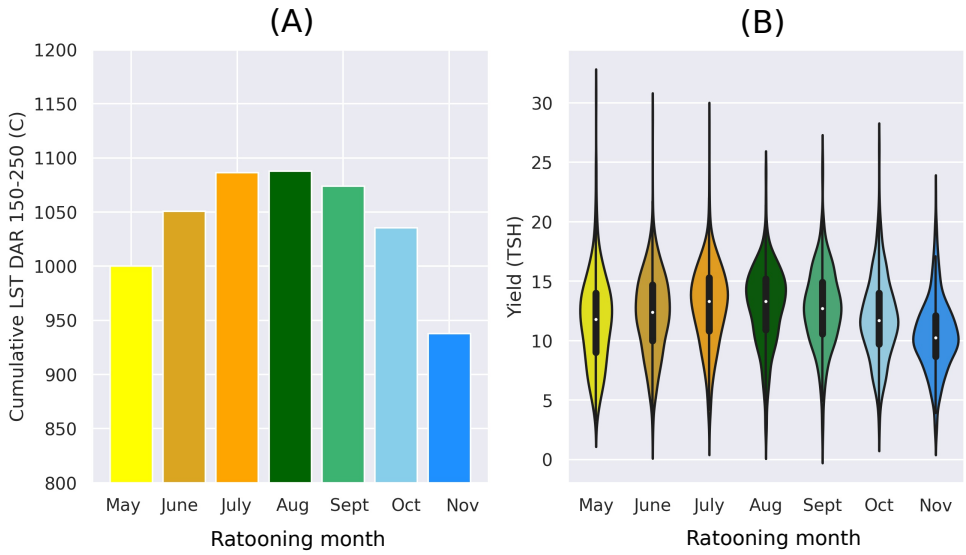

Figure 5.6: (A) cumulative Land Surface Temperature between DAR 150-200 for fields with similar ratooning months (B) violin plot for average sucrose yield per ratooning month for season 2019, 2020, and 2021

harvested during these months. The categorization aimed to understand the effect of ratooning month on crop growth and how the vegetation indices are affected by other factors (e.g. large rainfall events).

INTER-ANNUAL VARIABILITY

To demonstrate the difference between seasons, the average of the different observations for a specific Day of Ratooning was created for different growing seasons. Three seasons were used to compute these averages, season 2018-19, season 2019-2020, and season 2020-2021. In addition to time series, Pearson correlations between sucrose yield and polarizations, CR, and NDVI were also provided. The average value of these polarizations and indices in the last 150 days before the ratooning date were related to sucrose yield to understand the relationship to yield in different seasons.

THE INFLUENCE OF WATERLOGGING ON SUCROSE MONITORING

In this section the mean backscatter over the time series of the VV, VH, and CR is visualized for fields ratooned in a given month. To illustrate the effect of waterlogging on backscatter we focused on the wet period in season 2020-2021 (see Figure 5.4 (C)). The agricultural department in Xinavane confirmed that intense rainfall events combined with high groundwater levels due to the rise of water levels in the Incomati river, resulted in prolonged waterlogging during this period. To start with, the SWC and backscatter were compared in a season with a relatively dry rainy season (2018-19) and a relatively wet rainy season (2020-21) for similar ratooning months. Second, we compared data from at the waterlogging peak [2021-02-11:2021-02-18], to data from the local minimum before the waterlogging peak [2021-01-12:2021-01-19]. Each period contained

three radar observations, which were averaged before visualizing the difference as a function of growth stage.

5.4. RESULTS AND DISCUSSION

5.4.1. OBSERVING DIFFERENT SUCROSE LEVELS

Figures 5.7 shows the behaviour of VH and VV backscatter and the CR during three different growing seasons. Figures 5.7 (A), (D), and (G) show that the increase in biomass leads to an increase of around 5dB in VH backscatter. Similar to the results of Molijn et al., 2019, there is a rapid increase at the start of the season and a slower decrease after the maximum is reached. However, the results are similar among the yield performance categories, particularly early in the season.

In contrast, results from the VV polarization in Figure 5.7, (B), (E), and (H), are markedly different for the four yield performance classes. By the end of the season, the difference between the lowest and highest performing categories is 1.5dB in VV compared to 0.5dB in VH. The maxima are more distinct in VV compared to VH, and the rate of decrease after the maximum is also different. One reason for the clear distinction among yield categories in VV may be the predominantly vertical structure due to the sugarcane stalks. In addition, the stalk is the main reservoir of sucrose in the sugarcane crop (J. Wang et al., 2013) and sucrose yield data is directly linked and measured from the fresh stalk biomass, section 5.2. Stalk biomass is lower in lower performing fields and higher in higher performing fields (N. Inman-Bamber et al., 2009).

The combined influence of the differences between VH and VV is encapsulated in the CR. Figure 5.7 (C), (F), (I), shows a clear distinction among the yield categories in the CR. The CR of lower yield categories increases more slowly, and reaches a maximum 50 to 75 days later than the higher yield categories. The maximum values themselves are higher for the lower yield categories. The most notable feature, though, is the divergence after the maximum has been reached. The CR from the lowest yield category stays close to its maximum until harvest, while the CR of the highest yield category has the sharpest decline. By the end of the season, the difference in CR between the highest and lowest yield categories can be as high as 1dB (Figure 5.7 (F)). Furthermore, den Besten, Steele-Dunne, Aouizerats, et al. (2021) used published data and modeling to argue that sucrose accumulation decreases the dielectric constant of sugarcane, thereby lowering the Sentinel-1 backscatter. A decrease of the dielectric constant due to an increase in sucrose concentration was also observed by Sumranbumrung et al., 2021. This explains why higher performance categories show lower CR values over the growing season, and vice versa. Figure 5.7 (C), (F), (I) confirms the CR is indicative of the measured VWC, as pointed out by other studies (Veloso et al., 2017; Vreugdenhil et al., 2018).

Recall that the vertical distribution of moisture and sucrose is not uniform, and is different for higher and lower yielding sugarcane (Figure 5.1) (N. Inman-Bamber et al., 2009). In higher yielding sugarcane, the ratio of moisture to sucrose is more vertically homogeneous, while there is a gradient in lower yielding stalks. However, even in higher yielding sugarcane, there is little to no sucrose at the top of the plant. Note though, that the dynamics of total backscatter are not necessarily dominated by the top of the canopy, or some sensing depth from the top of the canopy. Recent modeling at L-band

has also shown that contributions to total backscatter depend on the vertical distribution of moisture, or more generally on the vertical variations in dielectric constant (Vermunt et al., 2022). InSAR studies have also shown that the phase center can be close to the surface even for relatively high frequencies (Joerg et al., 2018; Steele-Dunne et al., 2017). This explains why, even at C-band, Sentinel-1 backscatter is sensitive to dynamics in sucrose accumulation within the stalk and allows for a distinction between sugarcane with high and low sucrose yield.

In Figure 5.8 the development of VH, VV, CR, and NDVI over all three growing seasons are visualized. Figure 5.8 (D) and (E) shows CR and NDVI are able to distinguish different performance groups over the growing season. In particular, the lowest performance category deviates early in the season from the other categories. This may suggest poor performing fields are more easily detectable early in the season. The maximum of the VH, VV and CR radar data is observed earlier than the maximum in the optical indices. This was also observed by Molijn et al., 2019. More importantly, while the lowest category deviates from the others in the optical indices early in the season, the distinction between all four classes is clearer in the radar data. In particular there is a delay between the classes during the development stage. In addition, Table 5.1 shows the correlation between backscatter and sucrose yield in the different seasons. The VV polarization and sucrose yield show moderate positive correlations in Season 2018-19 and Season 2019-20.

5.4.2. SEASONALITY IN SUCROSE DEVELOPMENT

Figure 5.9 (A), (B), and (C) shows the influence of ratooning month on the evolution of backscatter. The influence of the choice of ratooning month on crop yield is visible in VV, VH, and CR. In VV, VH and CR the fields ratooned in October and November rise to their maximum faster than other months. However, in the VV and VH data these fields end up distinctly lower at the end of the growing season. This is very consistent with Figure 5.6 (B), which shows that fields ratooned in the months October and November have a lower yield compared to other ratooning months.

Compared to NDVI in Figure 5.9 (D), the development is similar to the individual polarizations. Fields ratooned in October or November, for instance, rise faster, but finish with the lowest average values. This illustrates the importance of temperature on sucrose development. Fields ratooned in October or November experience high temperatures at the start of the growing season.

In addition, Figure 5.9 illustrates the difference in temporal behavior between optical and radar timeseries. Where NDVI shows a clear distinction between ratooning months, it is evident backscatter records more than vegetation. For example, in Figure 5.9 (C) the CR for ratooning month November shows a steep rise due to high initial temperatures and reaching a maximum at DAR 75. After reaching this maximum a second high is reached at DAR 100, coinciding with the onset of the rainy season, which commences at the end of December or January (see section 5.3.2). This is also visible in the ratooning month of August in the CR, a second peak is reached around DAR 200 in Figure 5.9 (C), which coincides with the onset of the rainy season. These additional peaks are not visible in NDVI in Figure 5.9 (D). It is known that backscatter is sensitive to soil moisture and the soil surface in early growth stages (De Roo et al., 2001; Pierdicca et al., 2017). However,

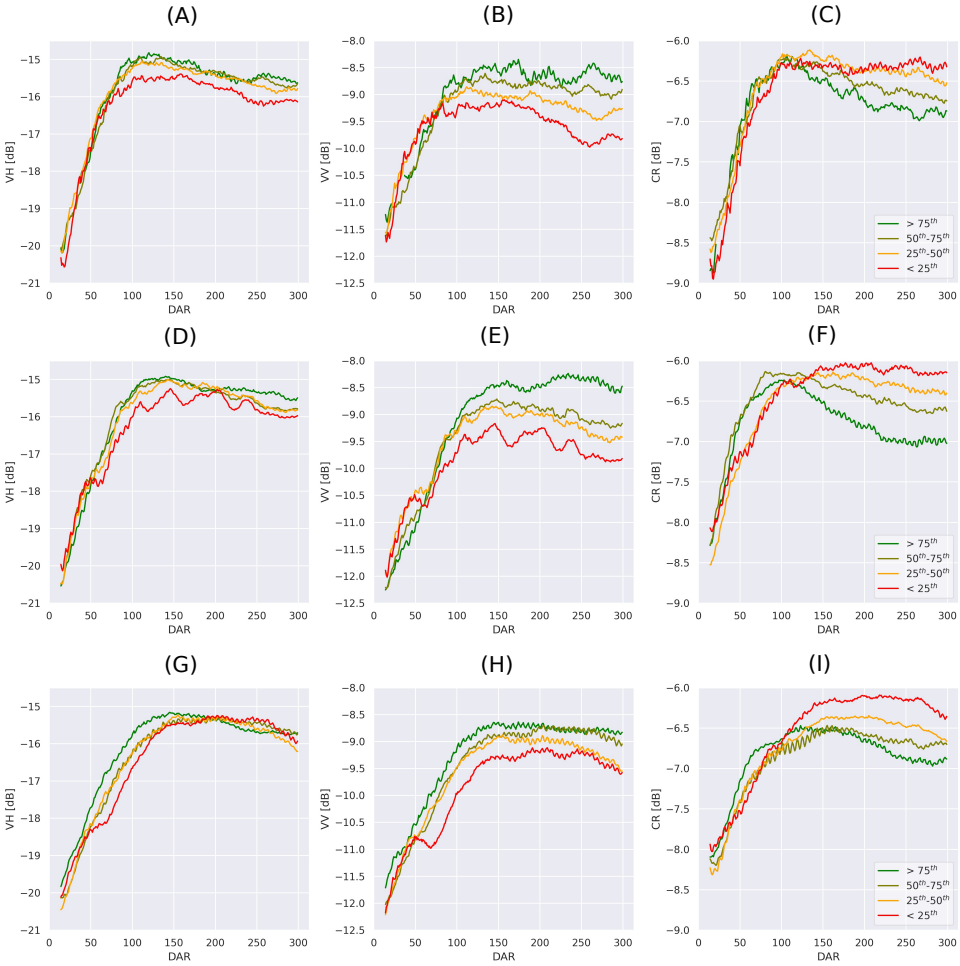

Figure 5.7: The figures in the first columns (A), (D), and (G) show the development of VH over the growing season. Subsequently, the figures in the second column (B, E, and H) represent the VV and third column (C, F, and I) represent the CR. Each row represents a different season: 2018-2019, 2019-2020, and 2020-2021 (Day after Ratooning) respectively. The different colors represent the different sucrose yield percentiles over the growing season.

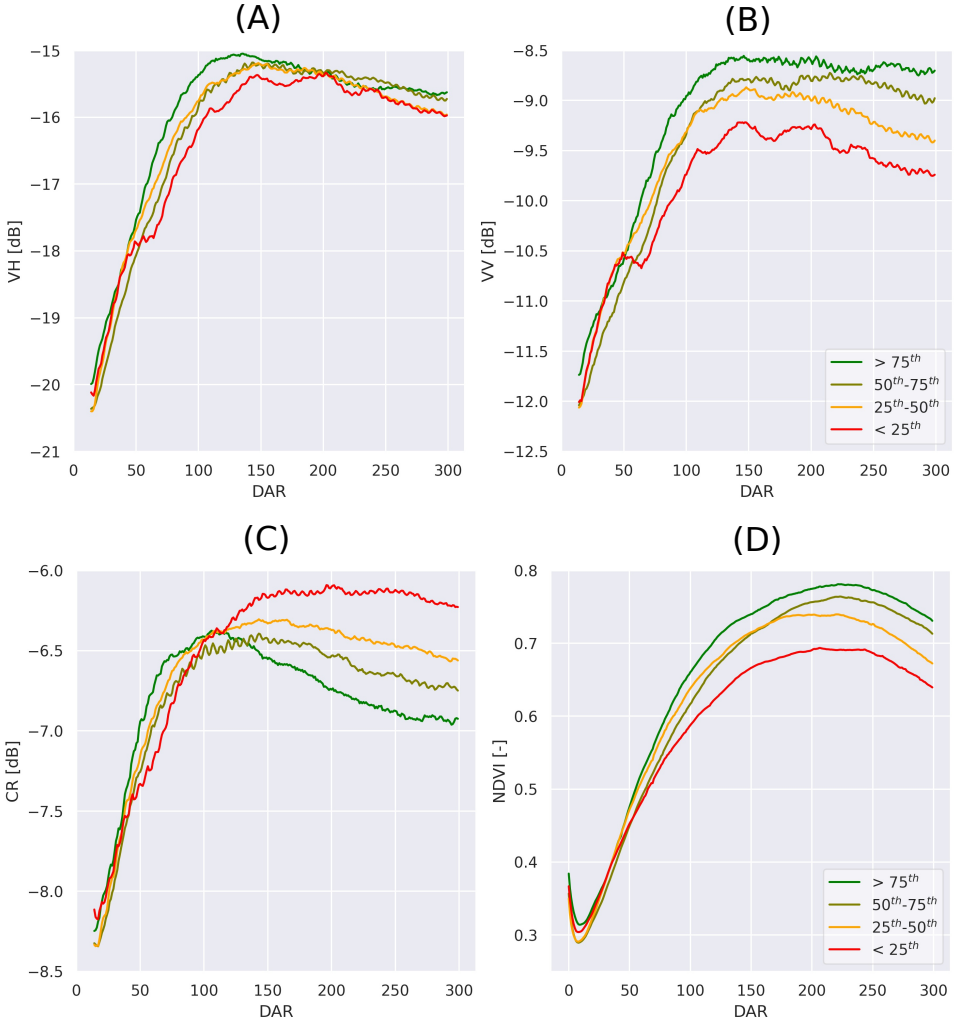

Figure 5.8: The development of (A) VH, (B) VV, (C) CR, and (D) NDVI over the growing season combining all seasons (Day after Ratooning). The different colors represent the different sucrose yield percentiles over the growing season.

it may be worthwhile to also consider the effect of extreme wet periods throughout the growing season.

5.4.3. INTER-YEAR VARIABILITY

Table 5.1: This table shows the Pearson correlation between mean backscatter in the last 150 days of the growing season observed in different polarizations, the CR, NDVI, and sucrose yield (TSH) for seasons 2018-19, 2019-20, 2020-21 and all three seasons together.

	Season 2018-19	**Season 2019-20**	**Season 2020-21**	**All seasons**
VV	0.55	0.52	0.22	0.53
VH	0.22	0.21	-0.11	0.19
CR	-0.48	-0.54	-0.49	-0.56
NDVI	0.58	0.6	0.34	0.6

Table 5.1 shows generally higher correlations between NDVI and sucrose yield than backscatter observations and sucrose yield in different seasons. For backscatter, the CR and VV give highest correlations to the yield. The correlation with CR is variable ranging from -0.48 - -0.56, whereas the correlation between VV and sucrose yield lay between 0.22 and 0.55. Interestingly, all correlations except CR are affected in season 2020-21. The VH backscatter and sucrose yield in season 2020-21 is even negative opposing the correlation in other seasons.

Figure 5.10 shows the mean over the growing season for VV, VH, CR, and NDVI as a function of day after ratooning. In Figure 5.10 (C) and (D) it is clearly visible season 2020-21 is behaving differently than other seasons. The graphs show a delay in the sugarcane development. Figure 5.11 (A), (C), and (D) show the standard deviation is also different in season 2020-21. In this season a long wet period was documented, resulting into prolonged waterlogging, see section 5.3.2.

5.4.4. THE INFLUENCE OF WATERLOGGING ON SUGARCANE MONITORING

Figure 5.12 shows (A) the average Soil Water Content and (B) average VH polarization for fields with a ratooning month in June in two different seasons, season 2018-2019 (red) and season 2020-2021 (blue). Figure 5.12 illustrates the response of VH backscatter due to the rainy season. In both seasons an increased Soil Water Content in Figure 5.12 (A) in mid-February and a drydown towards April is visible in VH backscatter in Figure 5.12 (B). The rainy season was less intense in season 2018-2019 than in 2020-2021, which resulted in a long waterlogging event in 2021. Considering the waterlogging event, as identified in section 5.3.2, the blue shaded area (II) identifies the peak of the waterlogging event in 2021 and (I) before the waterlogging event. The difference between VH backscatter at the height of the peak (II) and before the rise of the peak (I) is also visible in Figure 5.12 (B) in season 2020-2021. Similar figures for different ratooning months can be found in the appendix B.

To further quantify the effect of the waterlogging event on backscatter, Figure 5.13 shows the difference in the period before the large soil water content peak in season

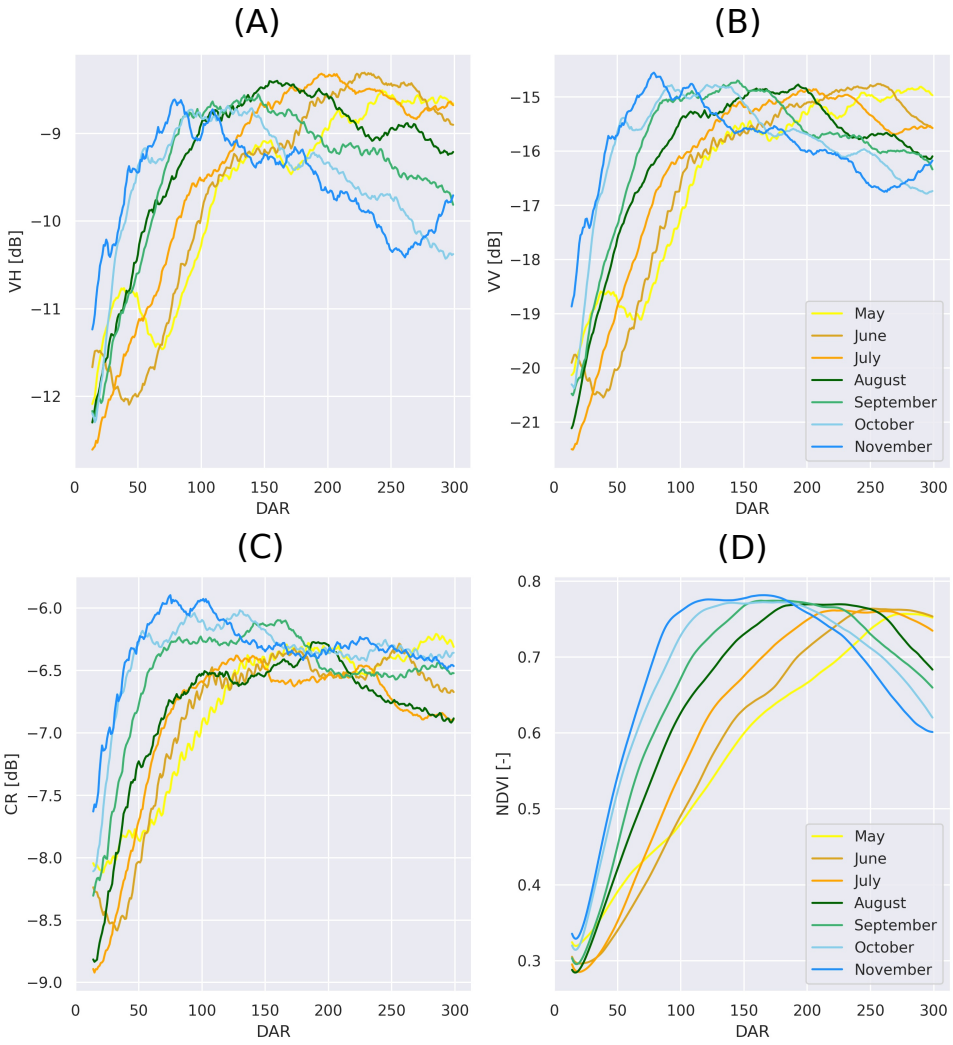

Figure 5.9: The average (A) VH, (B) VV, (C) CR, and (D) NDVI over the growing season (Day After Ratooning) for different ratooning months. The colors indicate the different ratooning months

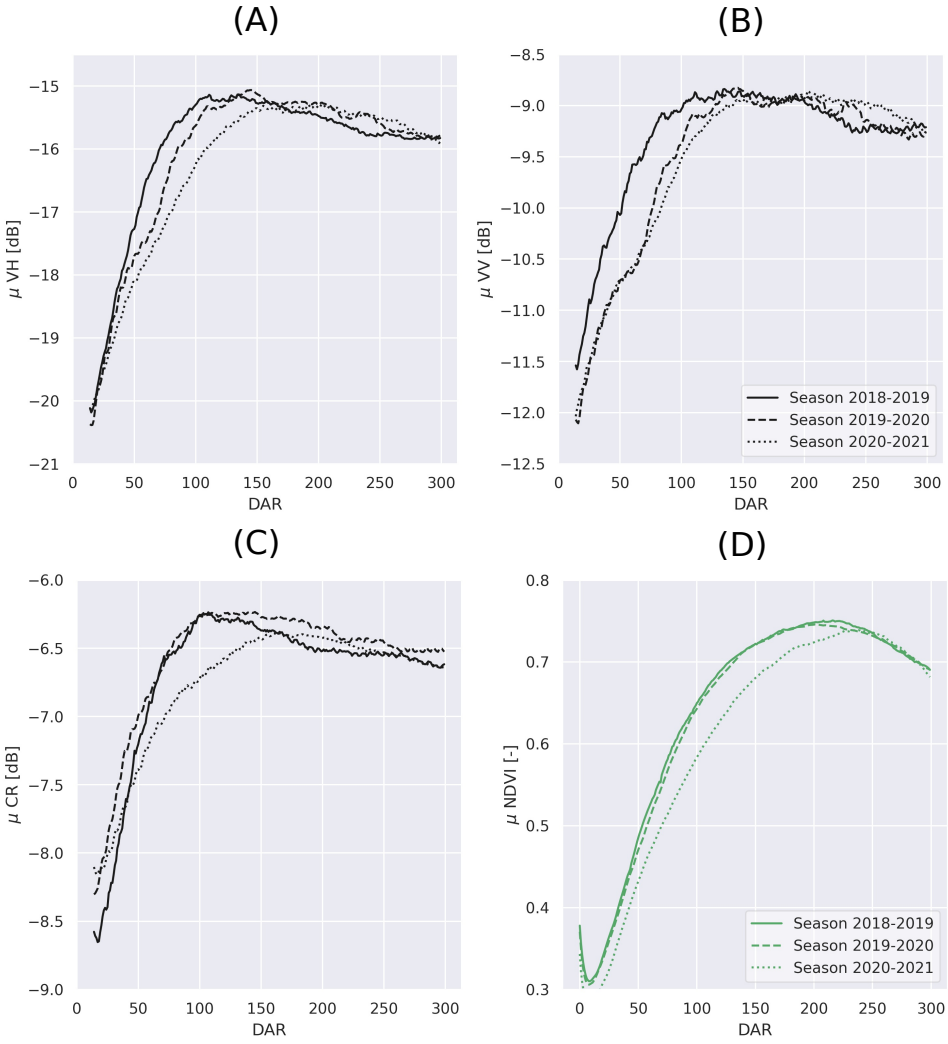

Figure 5.10: The average (A) VH, (B) VV, (C) CR, and (D) NDVI over the growing season for seasons 2018-2019, 2019-2020, and 2020-2021 (Day after Ratooning).

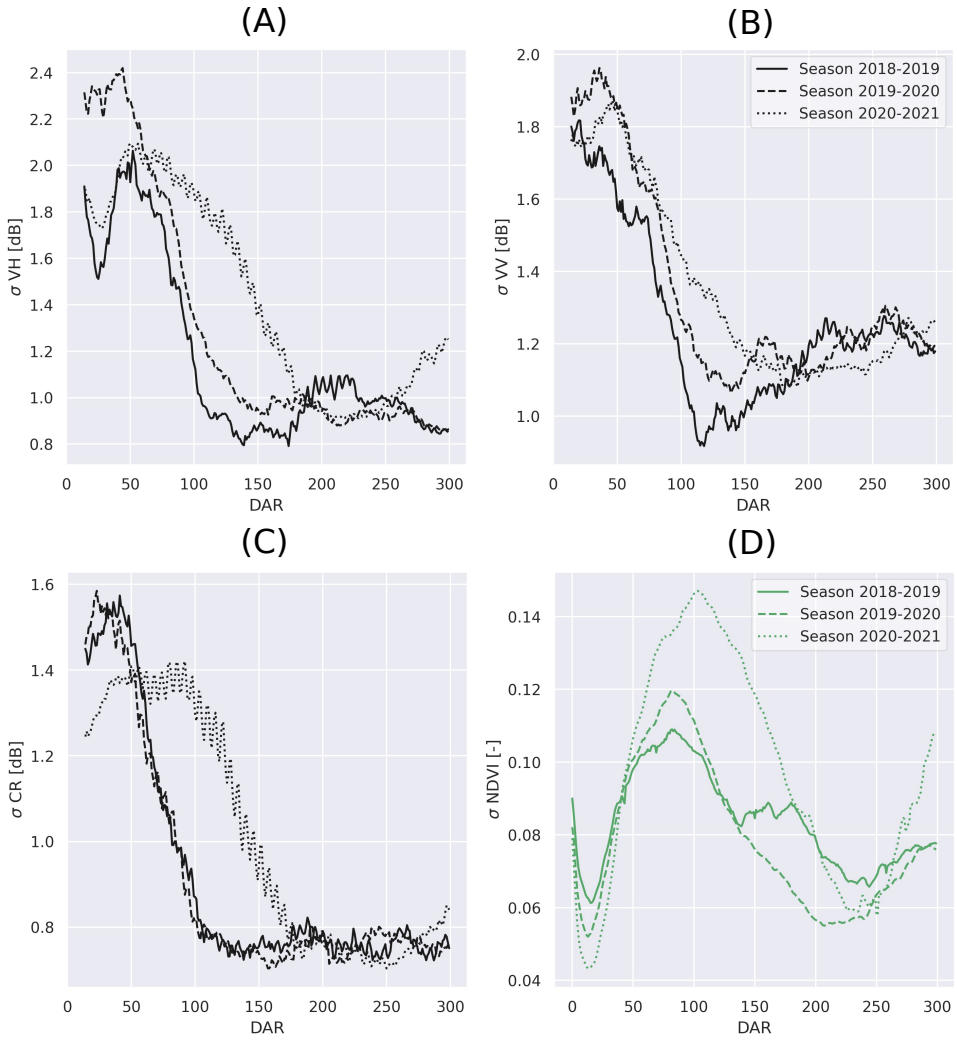

Figure 5.11: The standard deviation VH, VV, CR, and NDVI over the growing season for seasons 2018-2019, 2019-2020, and 2020-2021 (Day after Ratooning).

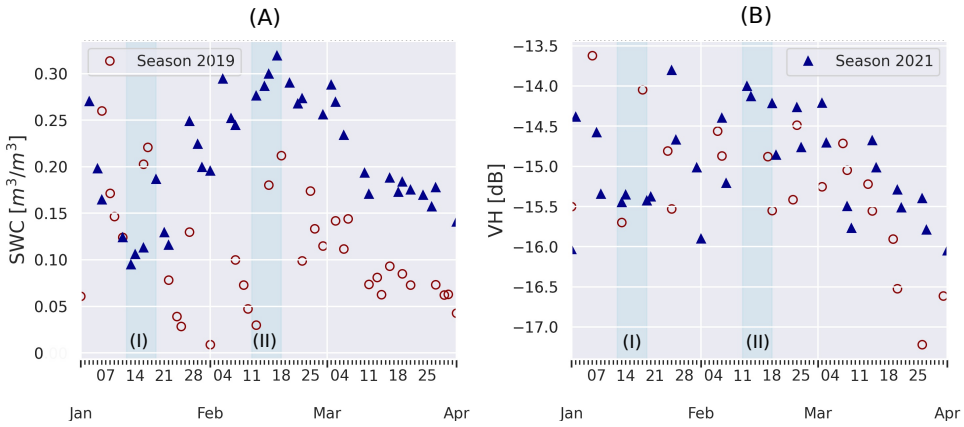

Figure 5.12: The average Soil Water Content (A) and average VH backscatter (B) for fields ratooned in August for Season 2018-2019 and 2019-2020. The graphs zoom in on the period of the 1st of January until the 1st of April. (I) and (II) indicate the period before and during the waterlogging event in Season 2020-2021.

2020-21 and during the peak for different ratooning months. The difference shows backscatter increases as a result of the event and is visible in VH, VV and CR. The waterlogging event causes differences between 0.45 dB and 1 dB for VV, and between 1.12 to 1.47 dB for VH. The higher values in November in the individual polarizations indicate that the effect of waterlogging is more visible at earlier stages of the crop growth, i.e. when the canopy is not fully developed yet. The results of CR in Figure 5.13 also indicate that the effect of waterlogging may be translated through to the cross ratio. Therefore, the CR contains information on waterlogging.

Though few studies have explicitly considered waterlogging, these differences can be considered in the context of what is known about flooding under vegetation more generally. Lang et al., 2008 researched the difference of flooded and non-flooded forest in HH polarization (C-band) and recorded an average difference of 2.45 db depending on the incidence angle. Sentinel-1 data was also used to detect temporary flooded vegetation (TFV) to improve flood algorithms (Tsyganskaya et al., 2018a). Tsyganskaya et al. (2018a) found, in different parts of the world, that VH and VV increased during flooding events and the increase was due to the interaction between standing water and the vertically oriented vegetation which increases the double- or multi-bounce interactions (Tsyganskaya et al., 2018a).

Despite sugarcane's thick canopy, Figure 5.13 shows that waterlogging is visible in all crop stages. It seems that the effect of waterlogging is more evident at earlier stages of the growing season (ratooning month November) in the individual polarizations. The results imply Sentinel-1 backscatter contains both information on waterlogging under the canopy as well as sucrose development in the stalk. Therefore, CR could potentially play a role in the discrimination of waterlogging.

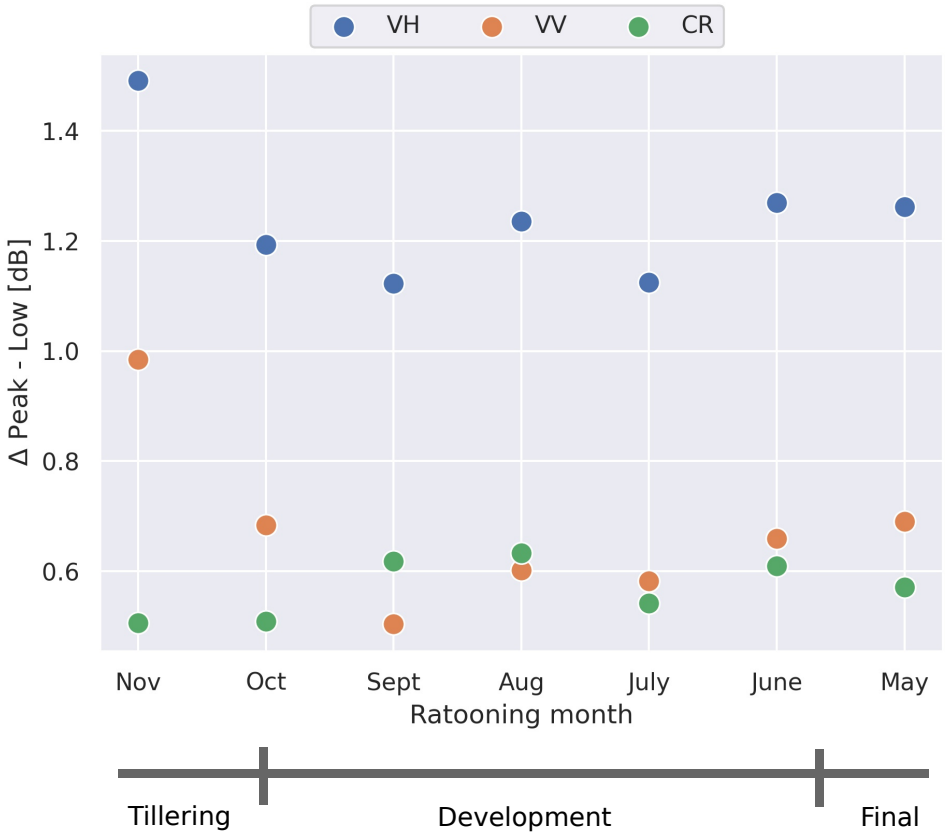

Figure 5.13: The difference between backscatter during and before the waterlogging peak averaged for fields with similar ratooning months

5.5. CONCLUSION

The aim of this research was to understand how Sentinel-1 backscatter responds to sugarcane yield variability and waterlogging. We demonstrated the possibility to monitor sugarcane yield throughout the season, the effect of ratooning month on sugarcane development, and how waterlogging under the canopy is observed within different stages during the sugarcane development. All this valuable information is evidently present in Sentinel-1 backscatter.

The results showed VV backscatter contains information on sucrose development. The VV backscatter responds to the stalk characteristics which is also the reservoir of sucrose in the sugarcane crop. The CR represents the VWC in the stalk and the results demonstrated the influence of the distribution in availability of moisture and sucrose in the stalk on total observed backscatter. The fraction of sucrose and VWC changes over the growing season and the vertical distribution of sucrose and VWC varies as well. The results showed both influence the observed backscatter.

In addition, the results demonstrated the influence of choice in ratooning month on the sucrose yield and consequently backscatter. By considering ratooning month and comparing sucrose yield with different backscatter observations, we discovered the influence of waterlogging beneath the sugarcane canopy. Especially the VH backscatter was found to be sensitive to waterlogging beneath a canopy. However, waterlogging was also visible in the CR, which demonstrates the CR can be used to discriminate waterlogging from regular crop growth conditions. Moreover, the analysis implies the influence of waterlogging is present in all stages of the sugarcane growth, despite a thick sugarcane canopy.

The results of this research indicate that Sentinel-1 backscatter contains both information on waterlogging under the canopy as well as sucrose development in the plant. As the influence of waterlogging is detectable on a field-scale, it gives confidence that Sentinel-1 backscatter can be used to monitor waterlogging. Also, the influence of waterlogging can be flagged to help interpret vegetation signals retrieved with Sentinel-1 backscatter.

We recommend future studies and applications on crop monitoring with backscatter to consider waterlogging or inundation within the growing season. In addition, more experimental research is needed to understand the vertical and temporal distribution of sucrose and moisture and its effect on backscatter for different crops. This is necessary to improve understanding of the actual sensing depth of backscatter and to understand the contributions of different surface and crop characteristics on backscatter retrievals. Here, modelling studies could contribute to increased understanding of the backscatter signal.

Sentinel-1 backscatter contains a lot of information relevant to monitor sugarcane development. Nevertheless, more collaboration is needed between radar remote sensing experts and application users to extract relevant and actionable information about the surface and canopy. In addition, such collaboration would allow remote sensing scientists to benefit from the great wealth of data collected on the ground by agriculturalists every season.

6

CONCLUSION

The research presented in this dissertation aimed *to extend knowledge on what the influence of waterlogging is on agricultural monitoring with satellite remote sensing.* This is an essential step towards monitoring waterlogging from space. To do so, agronomic ground data were collected from an irrigated sugarcane plantation. Different satellite remote sensing technologies were assessed, modeled, and compared to the gathered field data. In particular, we demonstrated with this thesis the detrimental impact of waterlogging on agriculture and the potential to use C-band radar for sucrose monitoring and waterlogging on a field-level, benchmarked with optical and passive microwave data. The results have implications for evaporation estimates for irrigation calculations, remote sensing of sucrose accumulating crops, and remote sensing of waterlogging in agriculture.

6.1. NEW FINDINGS AND IMPLICATIONS

6.1.1. ON THE INFLUENCE OF WATERLOGGING ON IRRIGATION ESTIMATES WITH SATELLITE REMOTE SENSING

The case study presented in Chapter 3 showed that, even in Xinavane's semi-arid environment, waterlogging is a major issue burdening crop productivity. The results demonstrated currently available evaporation estimates from satellite data interpret waterlogging stress as a need to irrigate. This implies that before evaporation estimates from satellite data can play a role in optimizing field-scale water use in irrigated areas, evaporation algorithms must be able to unambiguously identify water stress due to water deficit in the root-zone. In addition, by assessing different remote sensing techniques in the context of waterlogging, the analysis showed the signature of waterlogging or crop response to waterlogging varies among different satellite remote sensing observations. Consequently, integrating observations of multiple sensors and potentially ancillary data (e.g. DEMs) will help to unravel how to monitor waterlogging with satellite remote sensing.

6.1.2. ON MONITORING SUCROSE ACCUMULATING CROPS

The comparison of optical vegetation indices, radar vegetation indices, and sugarcane yield (Chapter 4) in the plantation gave an interesting and unexpected result. Contrary to expectations, the results showed a negative correlation between the CR and sugarcane yield over the growing season. A modeling study proved that the negative correlation is a result of a change in the sugarcane's internal composition which effects the dielectric constant of sugarcane canopies. The chemical composition of plant water in sugarcane changes over the growing season. Sucrose is produced from the Tillering stage through to the Development stage. This decreases the fraction of free water and increases the fraction of bound water in the sugarcane stem over the growing season. Results from the modelin study showed that this change in composition due to an increase in sucrose accumulation lowers the backscattered signal. It was found that the distribution of sucrose and moisture changes in time, but also that the vertical profile of the sucrose-moisture distribution changes over the growing season. As a result, the vertical profile of the fraction of sucrose to plant water influences the dielectric constant and, hence, the backscattered signal.

The results confirmed that the CR is especially sensitive to the VWC in the plant. In addition, the results contributed to fundamental knowledge that a change in chemical composition of the crop influences the dielectric properties of the crop canopy. Hence, canopies containing a lot of fruit (e.g. pineapple) or change in chemical composition over time in the crop (e.g. agave) may exhibit variations in their dielectric properties due to their chemical composition. Therefore, applications or studies of radar observations including such agricultural canopies should be considered with care.

Previous research highlighted VH as the polarization containing the most relevant information to sugarcane monitoring. The results in this dissertation showed VV backscatter contains valuable information on stalk development. The VV backscatter responds to the stalk biomass, which is also the reservoir of sucrose in the sugarcane crop. Therefore, we should not underestimate the potential value of VV polarization data for monitoring crops with a structure similar to sugarcane should not be underestimated (e.g. narrow-leaf crop, dominant vertical stalk).

6.1.3. ON MONITORING WATERLOGGING

The influence of waterlogging on Sentinel-1 backscatter was detected through benchmarking with passive microwave observations, optical vegetation indices, and production data. Despite a thick sugarcane canopy, an increase in VH and VV polarizations was observed as a result of waterlogging. The increase was present at all stages during the growing season. The difference in backscatter as a result of waterlogging was highest in the VH backscatter. Also, the effect of waterlogging is translated through to the CR. As the influence of waterlogging is detectable on a field-scale and throughout the growing season, it gives confidence that Sentinel-1 backscatter can be used to monitor waterlogging. In addition, the influence of waterlogging can be flagged to help interpret vegetation signals retrieved with Sentinel-1 backscatter.

6.2. DIRECTIONS FOR FURTHER RESEARCH

6.2.1. RADAR REMOTE SENSING OF SUCROSE ACCUMULATING CROPS

A majority of the fundamental research on (active) microwave remote sensing was conducted in the eighties and beginning of nineties (Ulaby et al., 2014). However, as the results in this dissertation show, there is still a lot to discover to fully understand radar backscatter observations over agricultural canopies. For example, Ulaby and El-Rayes, 1987 developed the Dual Dispersion dielectric model to understand the nature of variation in dielectric constant as a result of different vegetation components and their respective contribution to the measured dielectric constant of vegetation. These components relate to the volume fraction of free water, bound water, and vegetation. The model was, however, fitted to experiments on corn leaves. Therefore, it would be beneficial to expand experimental research with different crops. Especially crops and/or crop components that accumulate sucrose over the growing season would be of interest here, to improve our understanding of the effect this has on the dielectric constant of vegetation.

Recently, Sumranbumrung et al. (2021) presented a model to characterize the dielectric properties of a sugarcane solution to be used in lab analyses in cane milling. This model adds a term to include the effect of ionic activity and is fitted to in-situ measurements. Sumranbumrung et al. (2021) also found the dielectric constant was inversely proportional to sugar concentrations at all investigated frequencies and temperatures. The dielectric constant decreases markedly with increasing sugar content, which is explained by a decrease of free water molecules in samples with higher sugar concentrations. This in turn affects mostly the real part of the dielectric constant. In addition, an increase in bound water in higher sugarcane concentration decreases the relaxation frequency. The relationship between dielectric loss factor (imaginary part) and sugar concentration was directly proportional at a lower frequency band before reaching the relaxation region (< 9-10GHz). For C-band, the results showed no significant differences between different concentration samples and loss factor. This illustrates that the effect of an increase in bound water due to higher sugar concentration may influence the dielectric loss factor more in other frequencies (observation bands). Moreover, Ulaby and Jedlicka, 1984 showed bound water especially influences the imaginary part of the dielectric constant below frequencies of 5GHz. This is an important consideration for future studies with lower frequency observations, such as L-band (e.g. ROSE-L).

With the research presented in this dissertation, a start is made to understand the sensitivity of radar backscatter and the dielectric constant to different levels of sucrose during crop development. Future studies on sucrose sensitivity can use the data presented in this thesis as there is still a lot more to explore. For instance, a thorough sensitivity analysis of the sucrose-water distribution can be done with the quality yield metrics provided in Chapter 2. Concentrations of sucrose could be further understood and estimated through comparison of backscatter and other variables (e.g temperature) observed around the harvest date. When consistent relationships are found, the information can be used to provide input to forecast sucrose levels.

In addition, the results of Chapter 4 on vegetation monitoring of sucrose accumulating crops, point out similar studies in other geographies and larger scale studies are needed. Consequently, to understand how what we found in Mozambique also occurs in other regions of the world. Continued improvement of our understanding of backscat-

ter timeseries is important, as a radar time series on a sucrose accumulating crop may be falsely interpreted as being affected by e.g. drought, while the opposite might be the case. In that regard, revisiting fundamental research is necessary and the need for field-work to support it.

6.2.2. COMBINING SENSORS TO DETECT WATERLOGGING

The results presented in the different chapters pointed out the relevance of combining different sensors. Chapter 4 and 5 showed how benchmarking with different sensors helps to enhance understanding of backscatter's capability to monitor sugarcane and detect waterlogging. For instance, by benchmarking the CR with NDVI, unexpected behavior in the radar vegetation signal was identified in Chapter 4. Likewise, in Chapter 5, the influence of waterlogging on radar vegetation indices was understood by benchmarking against soil water content retrievals from passive microwave observations.

In Chapter 3 it was hypothesized that opportunities to monitor waterlogging lie in hybrid approaches combining different satellite retrievals. The results in Chapter 4 and 5 reveal that this is indeed the way forward to monitor waterlogging. For the further development of monitoring waterlogging from space, it is crucial to enhance knowledge on the larger scale biophysical dynamics on field-scale or intra-field variation. For instance, in further research on waterlogging, the contribution of waterlogging to backscatter observations should be isolated. This can be done by incorporating other sensors determining the likelihood of the occurence of waterlogging in the radar backscatter when a temporal and/or spatial change in the signal is observed.

6.2.3. THE RIGHT RESOLUTION TO MONITOR WATERLOGGING

Throughout this dissertation the main sample size for the analysis was field level. This helped to interpret the different signals with each other and proved to assist the analysis, because of the abundant yield data collected at field-level. However, as mentioned in Chapter 3, waterlogging is a phenomena that also drives intra-field variability (Maestrini & Basso, 2018). Therefore, in order to monitor waterlogging it is essential to explore how intra-field spatial patterns relate to waterlogging in future research. This can be done by, clustering spatial patterns through space and time and linking them to larger processes as precipitation or irrigation.

Furthermore, the work done in inundation and detection of surface water mostly take a pixel-based approach (Pulvirenti et al., 2015; Tsyganskaya et al., 2018a). However, due to the complex nature of observing agricultural crops, which are highly variable in time and space, it is difficult to start at pixel level to understand when and where waterlogging is occurring. Therefore, starting with field-level or intra-field clusters is highly recommended.

6.2.4. IRRIGATION ESTIMATES WITH SATELLITE REMOTE SENSING

As concluded in Chapter 3, evaporation models used to calculate irrigation requirements interpret waterlogging stress as a need to irrigate. To prevent over-irrigation resulting from incorrect interpretation of crop stress, irrigation estimates can benefit from additional spatial and temporal information on the presence of waterlogging. Future research on the topic may want to include information on waterlogging in the crop stress

module in evaporation algorithms to prevent irrigation where it is not necessary. Follow-up research can focus on evaluating the effect on variable rate irrigation when including information on waterlogging Barker et al., 2018. Moreover, limited research within the domain of remote-sensing-based evapotranspiration for irrigation has focused on the actual benefit of using such calculations in the field to meet agricultural reality (Maguire et al., 2022). Therefore, to understand the technical limitations of such algorithms for daily agricultural practices, more adoption-impact studies should be conducted.

6.2.5. VEGETATION MONITORING WITH RADAR OBSERVATIONS

The results presented demonstrate that radar backscatter contains a lot of information relevant to monitor sugarcane development and other agricultural canopies. Nevertheless, more collaboration is needed to distinguish the information from the surface or canopy. Before radar retrieved vegetation indices can play a role in monitoring vegetation consistently, forecasting biomass or yield, waterlogging within the growing season must be considered. We recommend future studies or applications on crop and vegetation monitoring with backscatter to consider waterlogging or inundation within the growing season.

The contribution of different vegetation components to the temporal variation of backscatter observed needs more attention. This thesis and research by Vermunt et al., 2020, Khabbazan et al., 2022, and Molijn et al., 2019, highlight the influence of factors other than total internal vegetation water content and their dynamics on backscatter observations over agricultural canopies. The results show SCW and waterlogging affects the backscatter observations used to monitor agricultural crops. To understand the contribution of the individual components to backscatter variation over time, their contributions need to be recognized, understood, and isolated. The latter can benefit from (1) experimental research combined with modelling studies, but also (2) higher spatial level studies where mono-culture or similar vegetation is present (e.g. US corn, soybean, or wetlands). In both cases, a good ground dataset is required to conduct the research.

In addition, in Water Cloud Models and VOD retrievals from active microwave observations, the effect of multiple scattering from soil vegetation interactions is neglected (Frappart et al., 2020). El Hajj et al., 2019 also notes deviating results with the development of VOD mapping from C-band over rapeseed. The deviating results are attributed to an increase in soil moisture and waterlogging, causing the multiple or double bounce scattering mechanism to rise. This goes to show that the effect of double bounce mechanism in radar VOD retrievals should be considered and not neglected, especially when the objective is to assist agricultural monitoring.

6.2.6. THE INFLUENCE OF VERTICAL PLANT WATER DYNAMICS TO TOTAL BACKSCATTER

This research shortly demonstrates the current unknowns on the contribution of vertical variation in dielectric constant to total backscatter. The results in Chapter 5 point out sucrose accumulation starts in the lower nodes of the sugarcane stalk and gradually moves up the stalk during the growing season. This means that the vertical distribution of moisture (and sucrose) is of importance in understanding backscatter variation over agricultural canopies. The latter resonates with the need for improved understanding on

backscatter and the vertical crop water dynamics as also noted by Vermunt et al., 2022.

The general prevailing view is that backscatter observations of vegetation capture the above ground biomass (Liu et al., 2021). To further improve knowledge on the effect of the vertical distribution of plant water on radar backscatter, collaboration with agronomist could lead to improved understanding of the vertical distribution of biomass and plant water. For several crops the vertical distribution of biomass in the canopy is known (e.g. corn) (Mourtzinis et al., 2015; Vermunt et al., 2022). In order to simplify, vertical dynamics could be understood by solving the vegetation backscatter as a function of the vertical gradient of water in the crop. By collaborating with agronomists such gradients could be understood on a larger scale for different crops.

6.2.7. ON MACHINE LEARNING

Chapter 4 points out the opportunities that backscatter observations provide to observe quality characteristics inside the crop canopy which are complementary to optical vegetation indices. More research is needed to study the synergy between optical and radar backscatter in observing agricultural canopies. In sugarcane research, studies have attempted to immediately use machine learning approaches in their analysis (Shendryk et al., 2021). However, these approaches miss out on the opportunity to first understand which data should go into the machine learning algorithm. There is still a lot that needs to be understood on how radar remote sensing observations connect to what is happening on the ground. Therefore, radar backscatter studies may first need to focus on understanding the signal before it can feed in to machine learning algorithms.

6.2.8. THE EFFECT OF CANOPY DENSITY AND IRRIGATION

A limitation of this study, and an opportunity for future research, is the need for a more careful consideration of canopy density and irrigation on results obtained with Sentinel-1 backscatter. Chapter 5 shows the presence of waterlogging in backscatter. However, to further understand the effect of the attenuation effect the above-ground canopy may have on the results, spatial estimations on canopy cover can help. Here indices as LAI retrieved from NDVI may be relevant to consider as well. Similarly, the presence of row space and direction may be of interest as well. Consequently, the sensitivity of backscatter to changes underneath a canopy can be estimated as a function of canopy cover or crop density. Such a sensitivity study could help in further identification and development of waterlogging from radar observations.

In addition, due to the absence of reliable irrigation data, we assumed the effect of irrigation on the results were uniform. With a large plantation-wide waterlogging peak we were able to identify waterlogging on a field-scale. As we move to finer (temporal) resolutions and longer wavelengths in the future (Torres et al., 2012) artefacts of irrigation may be more present in the observations. This could be advantageous in order to detect waterlogging, but also leads to an additional variable to consider. If, in the future, we are able to isolate irrigation events on a field-level, the information can be used to understand the spatial response of backscatter to additional water applied. The spatial response after irrigation events will further help to understand spatial patterns related to waterlogging, which are dominant in local depressions (Martinez-Feria & Basso, 2020).

6.3. CONCLUDING REMARKS

As demonstrated in this thesis, field data collected from producers proved to be very helpful in the interpretation of vegetation indices retrieved with satellite remote sensing. Despite the fact different characteristics are measured, for instance stalk yield instead of fresh biomass or VWC, a lot can be learned from comparing the two. Therefore, more research should be done with larger producer data sets and, especially, radar-retrieved data.

For instance, within sugarcane the focus so far has been on smaller scale experiments (e.g. Molijn et al. (2019)), which are very relevant to fundamental understanding and reference purposes. The relevance of larger production datasets should not be underestimated, as they may well contribute to fundamental knowledge. Researchers can benefit from the great wealth of data collected on the ground by agriculturalists every season. This will require improved collaboration with researchers and people on the ground.

In addition, since there is so much to study to further understand the dynamics of vegetation, it may also be very helpful for researchers to work more closely together with producers to see what is the main interest of people in the field. This is needed in order to keep the promises made that our Remote Sensing community repeats in this thesis and many other academic literature: e.g. *"RS technologies can be used to support site-specific management decisions at various stages of crop production, helping to optimize crop production while addressing environmental quality, profitability, and sustainability"* (Khanal et al., 2020). We all have to work together more closely to make these promises come true.

ACKNOWLEDGEMENTS

Knowledge is the epitome of human connection. Other than our current citation system encourages, your work is never individual. I was incredibly fortunate to have a very encouraging environment around me from family and friends, to supervision and colleagues. They all helped me to fulfill this PhD quest.

To start with my supervisors: Susan, Richard and Pieter. Susan you are such an inspiration! You taught me so much about radar and research in general. You gave me space to learn, fall and get up again, to be myself. Richard dankjewel voor alle kansen die je me hebt gegeven, je onuitputtelijke bron aan kennis over aardobservaties, en je eindeloze geduld met alle grote veranderingen van de afgelopen jaren. Pieter, eigenlijk ben jij de aanstichter van dit boekje. Door de ontmoetingen bij Hotel Limpopo is er op een gegeven moment een project onstaan, waaruit meer samenwerking voortvloeide. Dankjulliewel.

I would like to thank the staff from the agricultural department at Tongaat Hulett in Xinavane. Everybody at the department was always super cooperative and I learned so much from the fieldworks. In particular Evaristo, Esperanca, and Michael who made Xinavane feel like a second home. And of course my good friend Milton, who set up his own organization after we last met (please checkout: Community Friends Association-COFA, which is supported by Sangha de Bloem).

Of course also a very very big thank you to my colleagues at VanderSat, acquired by Planet. VanderSat was an amazing breeding environment to explore new ideas and conduct interesting research. I feel very blessed to have been part of it. The journey continues with Planet. A special thanks to the Biomass Proxy team, with whom we will bring radar remote sensing to the real world.

And to my friends and family. Thank you for resisting my complains about this, at times, self-imposed suffering. You are amazing, really. Especially, de Besjes (cute little Elin), de Cabo's, Celine (a.k.a. Bob), de Boutalebs, My Waterchicks, Zaz, Sjon, Flubber, Tes, Harry, Alis, and others in my heart. And most importantly, my cariños who have learned me to live and love paso a paso over the last years: Leo and Iñaki.

Estamos Juntos!

A

APPENDIX A

A.1. INTRODUCTION

Globally agriculture accounts for approximately seventy percent of the total fresh water withdrawals (FAO, 2016a). To cope with the increasing competing demands for water in river basins it is necessary to focus on enhancing water use efficiency and water productivity in irrigated agriculture which is the largest water consumer sector. Due to its importance and urgency this goal is referred to in the UN sustainable development goals (SDGs) under the target 6.4 which calls for substantial increase in water-use efficiency to address water scarcity.

The predominant irrigation technique, globally, is surface irrigation which accounts for 86% of the total (Berg & Carter, 1980; FAO, 2016a). Surface irrigation is considered an irrigation method with a low water use efficiency. Poor field water management practices in surface irrigation often result in drainage issues and erosion (Berg & Carter, 1980), salinization (Aroca, 2012), and low field irrigation application uniformity (Raine & Bakker, 1996). These issues all lead to reducing gains, and low land and water productivity (Gunarathna et al., 2018; A. Singh et al., 2018).

Sugarcane, with a global cultivated area of 26 million hectares, is widely used as an industrial crop to produce bioethanol and sugar (Endres et al., 2018). The economic contribution of this commercial crop is of vital importance to some of the African economies such as Mozambique (Jelsma et al., 2010). As a water-intensive crop, sugarcane often requires frequent irrigation (Endres et al., 2018). Its large scale cultivation is known to highly impact freshwater abstraction rates (Olivier & Singels, 2015). The majority of the irrigated sugarcane is irrigated using surface irrigation method (FAO, 2016b) and its productivity is prone to inherent challenges that surface irrigation has.

Proper water management is essential in achieving the target crop yield for sugarcane. The yield is sensitive to both water stress and waterlogging, a situation in which the soil remains saturated with water for prolonged periods. In water stress conditions the plant closes stomata pores to avoid water losses, leading to a decrease in transpiration and subsequently reduced biomass production (Aroca, 2012). Short periods of

water logging mostly do not result in a sugarcane yield decrease, nor decrease in transpiration, but it is observed that if flooding is persistent (>21 days) or if the water tables are very shallow (<15cm) biomass growth can be significantly hampered (Chabot et al., 2002; Glaz et al., 2004). In addition, the salinity of the soil and/or irrigation water decreases the stomatal conductance and photosynthesis and inhibits the growth of sugarcane (Plaut et al., 2000).

Water stress may lead to curling of sugarcane leaves, alteration in chlorophyll content of the plants, reduced leaf area, and stomatal closure (Ferreira et al., 2017; N. Inman-Bamber & Smith, 2005). These symptoms of stress can be observed by the over-passing satellites, which observe vegetation status of the growing crops, and surface temperature, amongst other variables. This data can be used to derive spatial evaporation estimates. These spatial evaporation estimates can be very helpful in efficiently allocating water in especially irrigated agriculture (Bastiaanssen et al., 2000).

Several algorithms have been suggested to retrieve evaporation estimates from data collected by orbiting satellites. For instance, the Two Source Energy Balance (TSEB) (Norman et al., 1995), the Surface Energy Balance Algorithm for Land (SEBAL) (Bastiaanssen et al., 1998), the Atmosphere-Land Exchange Inverse (ALEXI) model (M. C. Anderson et al., 2007), and the Global Land-Surface Evaporation: the Amsterdam Methodology (GLEAM) (Miralles et al., 2011), and the FAO Water Productivity Open-access portal (FAO, 2018). These algorithms apply different methodologies to derive crop water stress and estimate actual evaporation. For example, within GLEAM stress is integrated as a function of the availability of water in the root-zone and canopy size, using microwave soil moisture observations and vegetation optical depth (Miralles et al., 2011). With the Alexi and TSEB models information from the thermal band is used to detect crops stress, based on the principle that canopy temperature increases with increasing crop stress (M. C. Anderson et al., 2007).

To serve the needs of agricultural management at field level and within a field, a high spatial and temporal resolution is required. With the launch of the Copernicus Sentinel-2 satellites, valuable high spatial resolution imagery became available which can assist field-scale and within field agricultural management (Vanino et al., 2018).

Several authors have demonstrated or researched the use of spatial evaporation estimates based on satellite remote sensing to estimate and visualize the crop water requirement to assist irrigation planning (Atzberger, 2013; Bastiaanssen et al., 2000; FAO, 2018; Mulla, 2013; Vanino et al., 2015; Vanino et al., 2018; Vuolo et al., 2015). Detailed evaporation estimates can be used in (irrigation) water management to estimate the crop water requirement or maximum crop evaporation. For instance, this information can be used to irrigate at the proper time and with the proper amount per field. Optimizing irrigation water use, in an irrigation scheme, can benefit from frequent spatial evaporation updates on the actual development of the crop and its water requirement (Calera et al., 2017; Vanino et al., 2018; Vuolo et al., 2015). This is because farmers tend to over irrigate in the absence of objective information on crop status and water requirement (Vanino et al., 2018).

An operational irrigation monitoring system that incorporates near real-time high spatial resolution evaporation information in irrigation decisions and practices will be a significant improvement over the point-based evaporation estimates which are still

common even within relatively hi-tech plantations and irrigation schemes (N. Inman-Bamber & McGlinchey, 2003; Singels et al., 1998). High spatial resolution evaporation estimates enable plantations to monitor water needs at and within the plots, keep track of crop growth, take corrective actions when necessary, and consequently leading to better yields (Calera et al., 2017).

Previous studies demonstrating high spatial resolution evaporation estimates have combined meteorological and satellite data (Vanino et al., 2015; Vanino et al., 2018; Vuolo et al., 2015). Information on Leaf Area Index (LAI) and albedo was retrieved by Sentinel-2 imagery, whereas other data was obtained from a nearby meteorological tower (Vanino et al., 2018). These methodologies use the FAO-56 Penman Monteith method as a basis for their calculations to estimate maximum crop evaporation and irrigation water requirements (Allen et al., 1998).

In this research we focus on a sugarcane plantation in Xinavane in southern Mozambique. The Priestley-Taylor methodology is used to get spatial evaporation estimates (Priestley & Taylor, 1972). Due to the mono-culture in the plantation we are able to develop a sugarcane specific remote sensing evaporation estimate. The application of the Priestley-Taylor (PT) methodology with satellite data has so far shown promising results in several remote sensing based evaporation algorithms and studies (Y. Chen et al., 2014; J. Fisher et al., 2015; Miralles et al., 2011). However, these researches do not apply their research in an irrigated context. Priestley Taylor requires limited data and parameterization and therefore fits the study due to the limited data availability (J. Fisher et al., 2015).

The objective of this study is to present a novel approach for estimating daily actual evaporation at a high resolution of 20 m using a combination of satellite imagery and local weather data. The analysis focuses on a furrow-irrigated area within the plantation, covering 420 hectares. This area was part of a pilot project IWACA-Tech, which aimed at improving water use efficiency at irrigation systems using advanced remote sensing technology[1].

A.2. METHODOLOGY AND DATA

A.2.1. STUDY SITE

The Xinavane plantation is located within the lower reaches of the Incomati river basin, in Mozambique (figure A.1). The irrigated sugarcane plantation in Xinavane is in competition over water with the increasing population and water users in upstream South Africa and Swaziland where numerous sugarcane plantations are located (Santillán-Fernández et al., 2016; Zaag van der & Carmo Vaz, 2003). From 2012 until 2014, the plantation experienced three successive seasons of flooding which adversely affected the operations within the plantation. These events were followed by two consecutive drought years in 2015 and 2016, associated with El Nino (Gelcer et al., 2018). In the years 2017 and 2018 the annual rainfall was also below average.

Twenty-four furrow irrigated fields of the IWACA-Tech project were selected for the analysis, with a total area of approximately 420 ha (figure A.1). The slope runs from Northwest to Southeast in the study area. The irrigation interval is approximately 10-12

[1] www.iwacatech.com

days, and the net irrigation application depth aimed by the agricultural department is 1,350 mm/year. The long-term, 1967 to 2017, average annual precipitation in the area is 721 mm/year.

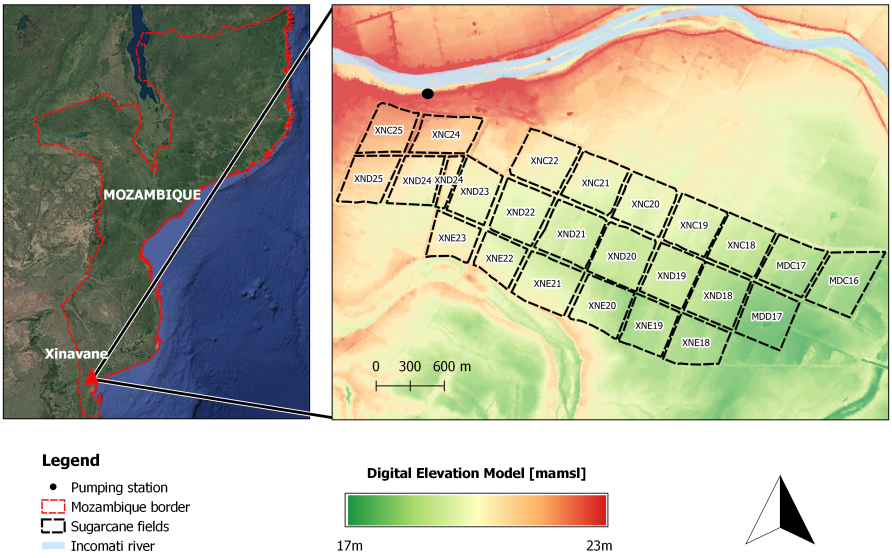

Figure A.1: The left panel shows the location of the sugarcane plantation in Xinavane, Mozambique. The map on the right zooms in to the project site.

A.2.2. SUGARCANE GROWTH CHARACTERISTICS

The furrow irrigated study site plots have a size of approximately 20 ha each. Within the sugarcane plantation, sugarcane is harvested after approximately 12 months when the crop is nearly four meters tall. From April to December fields are harvested based on the production capacity of the factory, meaning the crop stages and length of growing season differ between fields.

Sugarcane is grown as a ratoon crop, so new cane grows from the same root in 8-9 consecutive years. Ratooning naturally leads to a decline in yield over the years, due to several factors, such as soil degradation and fertility (Yadav et al., 2009). Sugarcane growing stage is often divided into four periods: an initial stage (30 days), tillering stage (90 days), development stage (150 days), and the final stage (90 days) (Doorenbos & Pruitt, 1977; Silva et al., 2015). In these different stages the consumptive water use differs and, therefore, it is important to characterize the different stages for agricultural water management. The initial stage commences right after harvest or planting, characteristic for

this stage is the germination of the original stool. After the initial stage, the tillering stage commences, during which the sprouted sugarcane rapidly starts to form shoots and leaves. Next, the smaller shoots die off due to plant competition, and the elongation of the stem starts in the development stage. In this stage, not many new leaves are formed, but energy is used for the growth of existing leaves and the stalk (Cock, 2001). The final stage of the sugarcane crop is characterized by senescence, where the plant cells degrade and the end of the crop cycle approaches (Martins et al., 2016).

A.2.3. FIELD DATA

Data for this research was shared by the agricultural department of Xinavane's estate. This included data on planting dates, harvesting dates, and yields in the period between April 2012 and June 2018. The critical level for yield in the sugarcane plantation is defined at 80 tonnes sugarcane per hectare (tonnes/ha) by the estate management. Fields below the critical level will trigger a diagnostic performance assessment by the plantation management and will be followed up by corrective measures. The set target yield is 105 tonnes cane per hectare.

We also studied the spatial differences in yield during the growing seasons of 2016-2017 and 2017-2018. To compare different fields adequately, fields were selected with the same growing period for an in-depth analysis, since the yield is affected by the harvest date. The selected fields were clustered to good performing (> 90 tonnes/ha), medium performing (80-90 tonnes/ha) and poor performing (< 80 tonnes/ha) fields. Table A.1 presents the selected fields and figure A.1 shows the location of these particular fields. Table A.1 displays the yield of the fields in the year of the analysis, the planting date, and the harvest date with the nearest Sentinel-2 overpass date used as a final date for the analysis.

A.2.4. REFERENCE EVAPORATION

The full workflow proposed in this paper is visualized in figure A.2. In order to take the first step in estimating the actual evaporation spatially with the available data, we first estimated the reference evaporation with Priestley-Taylor (Priestley & Taylor, 1972). The methodology and input used to get the reference evaporation is visualized in the first column of figure A.2. Priestley-Taylor describe the evaporation from saturated surfaces into an unsaturated atmosphere, which is expressed as a function of an equilibrium rate (Viswanadham et al., 1991). According to Priestley-Taylor, the daily evaporation rate can be defined as:

$$E_{PT} = \frac{1}{\gamma} \cdot \frac{s(R_n - G)}{s + \lambda} \cdot \alpha \tag{A.1}$$

where E_{PT} is the daily evaporation flux ($mm\ d^{-1}$), γ the latent heat of vaporization (2.45 $MJ\ kg^{-1}$), s the slope of saturation vapour pressure-temperature relationship ($kPa\ C^{-1}$), α is a dimensionless empirical number and better known as the Priestley-Taylor coefficient [-], R_n the net radiation ($MJ\ m^{-2}\ d^{-1}$), λ the psychrometric constant ($kPa\ C^{-1}$), and G the soil heat flux ($MJ\ m^{-2}\ d^{-1}$), which is assumed negligible when averaged over a day (Price, 1982).

A

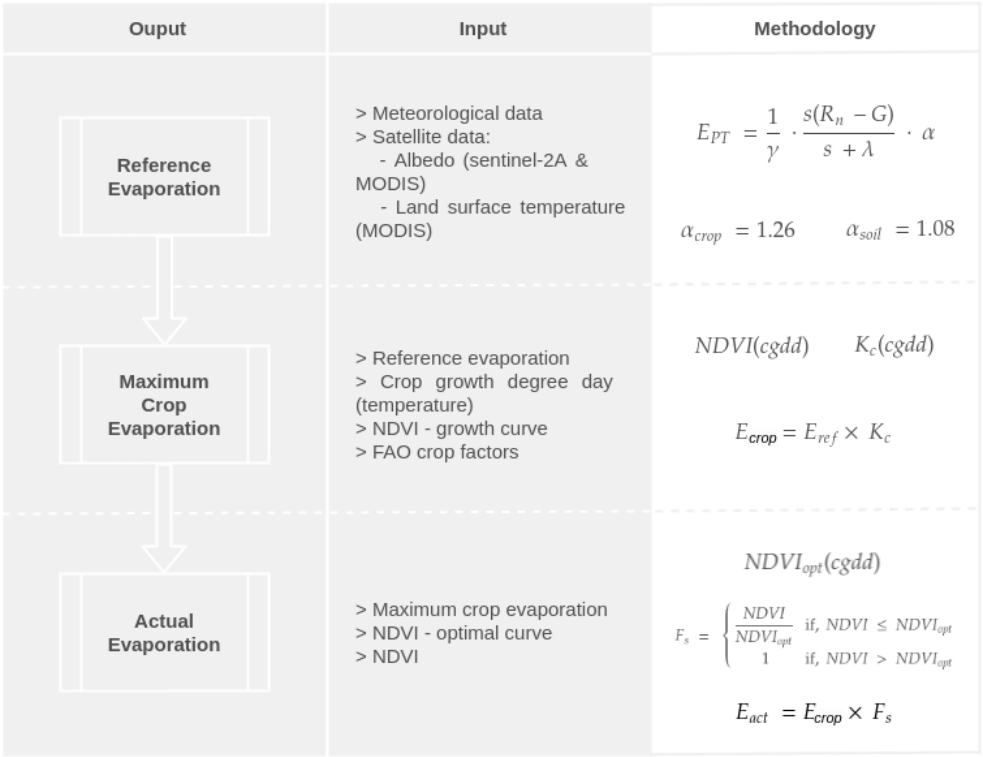

Figure A.2: A visualization of the methodology.

The net radiation is computed by balancing the incoming shortwave radiation and incoming L_{in} and outgoing L_{out} longwave radiation. The latter is calculated through the surface and air temperatures in combination with the Stefan-Boltzman law, to determine the temperature flux for sensible heat. Air temperature data was obtained from the estate's weather station.

Daily Land Surface Temperature and Emissivity (LST and E) at 1 kilometer (km) spatial resolution was derived from the MOD11A1 Version 6 product from the MODIS Terra satellite (Wan et al., 2015). The surface albedo, r_0, controls the partitioning of incoming shortwave radiation R_g. R_g data was also obtained from the local weather station. The net radiation R_n can be calculated as:

$$R_n = (1 - r_0)R_g + L_{in} - L_{out} \tag{A.2}$$

Data on surface temperature from (MODIS), air temperature and incoming shortwave radiation data of the meteorological station were used in combination with spatially distributed albedo maps. Combining spatial satellite data with meteorological data requires combining data layers with different spatial and temporal resolutions. This has been successfully done by other authors, such as Vuolo et al. (2015) and Vanino et al.

(2018). Combining resolutions is possible because not all variables show large variability spatially (e.g. incoming radiation) or temporally (e.g. albedo). To illustrate, incoming shortwave radiation can be covered by daily meteorological point measurement, because there is little spatial variability. In contrast, albedo varies spatially, but shows less variability temporally, and therefore can be estimated with the help of satellite data.

The albedo is calculated using two spectral signature curves: one for sugarcane (Apan et al., 2004) and one for clay soil (Vertisol, obtained from Aster Spectral Library (Meerdink et al., 2018)). The signatures were used to extrapolate the reflection registered within the different bands of Sentinel 2. To continue, the reflection within the same bandwidths as the satellite observations in the spectral signature curves were averaged ($\rho_{b,rc}$) for the respective Sentinel-2 bands. The reflectance observed in the sentinel bands ($\rho_{b,s}$) were divided by $\rho_{b,rc}$, weighted according to the band contribution to the total w_b, and summed to get a correction factor (C_f) to reconstruct the reflection curve for each pixel:

$$C_f = \sum((\rho_{b,s}/\rho_{b,rc}) \times w_b) \tag{A.3}$$

Finally, the albedo was estimated over the extent of spectral reflection curves. Additionally, the computed albedo was scaled with the BRDF/albedo Parameters Daily L3 Global Version 6 of MODIS to correct for overestimation caused by limited observation bands of Sentinel-2 (Schaaf & Wang, 2015). Sentinel-2 data is available at a 5-day interval. For the construction of the albedo daily time series, only Level 2A (Louis et al., 2016) and cloud-free images were used. Missing dates were linearly interpolated. This resulted in daily albedo maps for the study region from April 2016 until July 2018. Given the fact that temporal changes of albedo in a short timeframe are negligible, the linear interpolation method is expected to result in realistic daily values per pixel (Vanino et al., 2018).

The conditions in Xinavane, with relative humidity ranging between 68 and 75 percent and annual mean daily wind speed below 2 m/s, are favourable to obtain optimal reference evaporation estimates with the Priestley-Taylor equation (Cristea et al., 2012). Therefore, the Priestley-Taylor coefficient can remain 1.26 for the vegetated areas (Cristea et al., 2012; Priestley & Taylor, 1972). For soil pixels, the α value is 1.08 as proposed by Miralles et al., 2011.

A.2.5. MAXIMUM CROP EVAPORATION

The reference evaporation obtained using the Priestley-Taylor equation does not account for the growing stage. Generally, to convert reference evaporation to crop evaporation a crop coefficient (K_c) is used that compensates for the crop type and crop growing stage (Allen et al., 1998). Furthermore, the growing cycle of a crop is divided into three or four crop stages and for each of these crop stages, a different crop coefficient is used. The FAO has provided crop coefficients for each crop stage of some common crops (Allen et al., 1998). The methodology and input used to get from reference evaporation to maximum crop evaporation is visualized in the second column of figure A.2.

There is a similarity between the evolution of Kc and the Normalized Difference Vegetation Index (NDVI) (Bausch & Neale, 1987). Vegetation absorbs radiation in the visual spectrum and reflects a large amount of infrared radiation. Therefore, a normalized ratio

A

can be used to identify vegetation activity of which the Normalized Difference Vegetation Index (NDVI) has become the most commonly used index today.

NDVI can be translated into a crop coefficient using a simple linear regression model (Kamble et al., 2013). Kamble et al., 2013 showed a strong linear correlation (r^2=0.91) between the NDVI and the measured crop coefficients. However, for our study, no measured values are available that can be used for regression. Nonetheless, in this study, the crop factors of ratoon sugarcane that are proposed in Allen et al., 1998 will be used to compensate for the growing stage of the sugarcane.

Mean NDVI data per observation along the growing period was obtained for the fields XNC19, XND18,20, and XNE18-21,23. These fields were selected because of their increasing NDVI curve. Next, using the planting and harvest dates of each field, the NDVI data of each crop cycle were obtained. Furthermore, temperature data for each crop cycle was used to convert growing days to Cumulative Growing Degree Days (CGDD), in order to correct for the influence of temperature on the crop development over the growing season (Lofton et al., 2012), see figure A.3. A quadratic regression resulting from the NDVI observations was used to obtain an NDVI curve as a function of CGDD.

According to Allen et al., 1998 and Doorenbos and Kassam, 1979, the initial crop stage has a crop coefficient of 0.4 for ratooned sugarcane and 1.25 when the canopy is at its peak size, and 0.7 at the end of the growing season. These crop factors were used as boundaries to translate the $NDVI_{est}$ to a crop coefficient curve dependent on the CGDD:

$$K_c = -6.24 \times 10^{-7} \times CGDD^2 + 1.51 \times 10^{-3} \times CGDD + 0.4 \tag{A.4}$$

A.2.6. ACTUAL EVAPORATION

In the last part of the analysis, we tested whether crop stress is visible within NDVI and albedo values in different crop stages to test a methodology to correct maximum crop evaporation estimates for crop stress to retrieve actual evaporation. The methodology and input used in this step are visualized in the third column of figure 3. By looking at three performance groups, based on their yield obtained from ground observations (section A.2.3), we assess whether the spectral indices are significantly different from each other in different growth stages. It is assumed that if there is a lot of non-uniformity within a field, then this is related to either mismanagement and/or stress within a field. The non-uniformity should be visible in high spatial resolution spectral indices (Ač et al., 2015).

In order to test if the non-uniformity is present within different crop stages, we first look at the coefficient of variation (CV) of NDVI and albedo within differently performing fields in different crop stages. Then, the statistical significance was tested of the distribution of spectral indices within the different groups. Moreover, the mean value and CV of a field per observation were used as samples for the Mann-Whitney U test. The observations within the groups of fields were at times not normally distributed and the groups showed unequal variances. Therefore the Mann-Whitney U test was found to be most suitable for the analysis (Mann & Whitney, 1947). A significance level of 0.05 was chosen. In each crop stage we tested whether the mean and CV values of NDVI and albedo of the observations within each growth stage were significantly different from each other. In

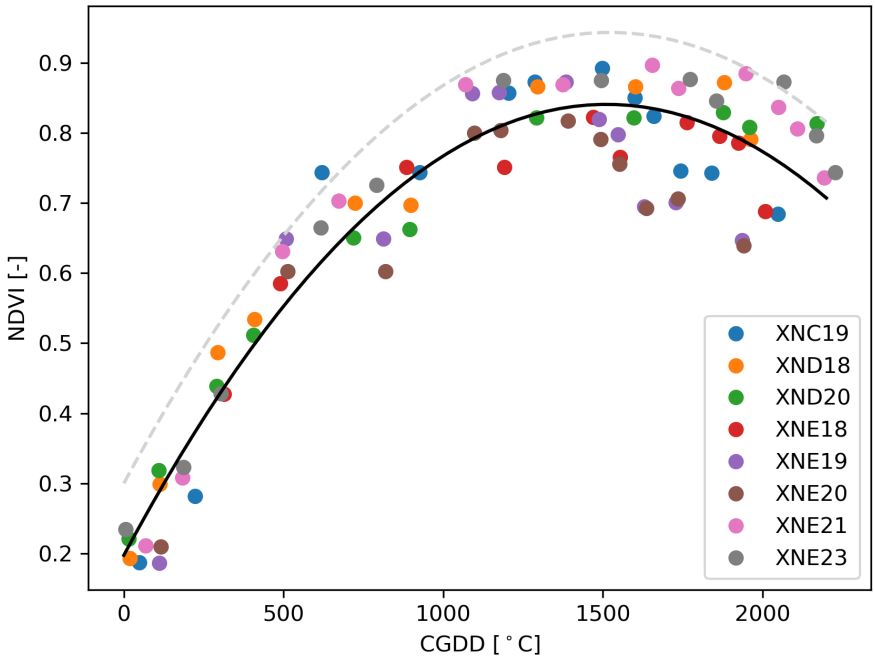

Figure A.3: NDVI observations per field are visualized in relation to CGDD. Fields XNC19, XND18,20, and XNE18-21,23 were used to create a crop growth curve. The black line indicates the quadratic regression curve fitting the NDVI observations $NDVI_{est}$. The dotted grey line indicates the optimal NDVI curve $NDVI_{opt}$.

other words, we tested whether the performance groups could be distinguished based on NDVI or albedo.

Ultimately, the relationship between actual NDVI compared to the optimal NDVI was used to account for stress in the evaporation estimate per time step. The optimal NDVI curve, $NDVI_{opt}$, is assumed to be above the estimated NDVI curve as the boundary between sugarcane and bare soil is set where NDVI is 0.3:

$$NDVI_{opt} = -2.78 \times 10^{-7} \times CGDD^2 + 8.46 \times 10^{-4} \times CGDD + 0.3 \tag{A.5}$$

To compute actual evaporation from maximum crop evaporation, the following stress factor was applied:

$$F_s = \begin{cases} \dfrac{NDVI}{NDVI_{opt}} & \text{for} \quad NDVI \leq NDVI_{opt} \\ 1 & \text{for} \quad NDVI > NDVI_{opt} \end{cases} \tag{A.6}$$

Where a value of 1 indicates no stress and a value of 0 indicates maximum stress.

A

A.3. RESULTS AND DISCUSSION

A.3.1. MAXIMUM CROP EVAPORATION

In figure A.4 the evolution of maximum crop evaporation and albedo over CGDD is presented for five selected fields. A similar analysis was done for other groups within the selected 24 fields, but the results do not differ. Within the two figures we zoom in to the difference in maximum crop evaporation and albedo over the growing season.

In theory, the albedo is affected when crop stress is present (S. Wang & Davidson, 2007). For instance, the albedo of leaves facing water-stress is higher than well-watered leaves (S. Wang et al., 2004). Therefore, working with high spatial resolution albedo estimates may already include crop stress in the maximum crop evaporation calculations. Figure A.4, however, shows that the difference in albedo between fields is marginal.

A difference between the albedo can only be observed in the first 150 CGDD, this can explained by the difference in the start date of the growing season (which is determined by the harvesting date of the previous season). The growing season of fields MDD17, XND24, and XNC18 starts earlier than fields XNE22 and XND19 (see table A.1). In figure A.4b fields MDD17, XND24, and XNC18 therefore show a steeper increase in the first 150 CGDD, which results from a higher albedo in this first part. The albedo increases when sugarcane grows. The sugarcane in fields MDD17, XND24, and XNC18 grow faster at the start. After the difference at the start, the albedo evolution in the different fields have the same shape. Finally, there is barely a difference in cumulative albedo at the end of the season.

The maximum crop evaporation estimates in figure A.4b also confirm insignificant differences between selected fields. The albedo estimates, therefore, do not include crop stress directly. The reason why crop stress is not directly visible in the albedo estimates results from the methodology applied to retrieve albedo estimates, where MODIS is downscaled with Sentinel-2 bands. The evaporation estimates derived in figure A.4a, barely include crop stress and can be used to calculate maximum crop evaporation.

A.3.2. DETECTING CROP STRESS

In figure A.5 we consider the CV of NDVI and albedo within the different performance categories in different growth stages. Similar to the results in figure A.4, the albedo estimates are not able to distinguish between good and poor performing fields, except for the development stage. The CV values in all growth stages are very low (min=0.003, max=0.0325). This indicates a marginal variability in albedo estimates, resulting from the MODIS correction.

However, considering CV values of NDVI are in figure A.5, it is possible to distinguish good, medium, and poor performing fields in the development and final stage. The CV of NDVI shows on average a strong negative correlation between the CV and yield in the last two stages.

NDVI is able to distinguish between good and poor performing fields in the last two stages, see table A.3 in Appendix A. The results of the Mann-Whitney U test to distinguish the different groups within crop growth stages shows the different groups can be distinguished based on the NDVI. However, in earlier growth stages the performance categories are not distinguished by the NDVI.

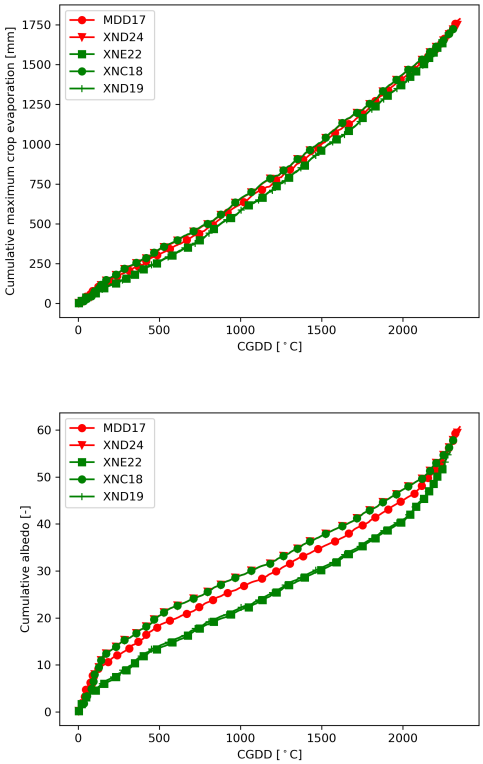

Figure A.4: Figure (a) shows the cumulative maximum crop evaporation in mm for five selected fields (see group 1, table A.1). The red lines indicate the cumulative maximum crop evaporation for fields with a poor yield in seasons 2016/2017. The green lines indicate fields with a medium or good yield. Figure (b) shows the same selected fields, but in this figure the cumulative albedo is displayed against the cumulative growth degree days

A thick canopy cover, like sugarcane, challenges the performance of spectral indices. Baghdadi et al., 2009 found a similar outcome in the NDVI signal, where NDVI saturated after a height of 150cm. Saturation effects in spectral indices of sugarcane were also documented by Simões et al., 2009. Only in the case of significant differences, where non- or barely vegetated pixels are present, spatial heterogeneity is detectable. Such as at the last two stages in figure A.5 where there is a significant contrast between good and poor performing fields. Molijn et al., 2019 found high spatial resolution NDVI imagery best suitable to monitor sugarcane crop growth compared to different Synthetic Aperture Radar (SAR) products. Molijn et al., 2019 found saturation of NDVI around 80 tonnes/ha. This may explain the results presented in figure A.5 and table A.3 in Appendix A, where we are able to distinguish between poor and good performing fields based on the CV of NDVI and mean NDVI in the last two growth stages.

Additionally, Molijn et al., 2019 point out the inconsistencies when relating early crop growth imagery with later imagery. The NDVI in the first crop stages shows more variability between images in their analysis. The inconsistencies found by Molijn et al., 2019 in NDVI at the start of the growing period can explain partly the reason why the start of the growing season is not indicative of the biomass production or final yield. This corresponds with the results in figure A.5.

A.3.3. ACTUAL EVAPORATION

In the fields considered for analysis in group 1, mean actual evaporation per field ranged between 1390 and 1483 mm/season, with minimum values of 693 mm/season and maximum 1589 mm/season. There is a large difference between actual evaporation values within fields. To compare the actual evaporation estimates, we consult another actual evaporation product with a different methodology (FAO, 2018). For the year 2016 and 2017, yearly values between 1098 to 1505 mm/season and 1013 to 1513 mm/season were documented within WAPOR for the same area. These estimates are also in line with the reported industry standard sugarcane ET of 1365 mm/season in the sugarcane states in Swaziland that are located near the Mozambique border (Karimi et al., 2019).

Figure A.6 presents the accumulated difference between maximum crop evaporation and actual evaporation over the growing period within each pixel and field. Each pixel in figure 9 indicates accumulated stress. The three fields with a good performance, indicating 110.3, 93.5 and 92.5 tonnes/ha, show a small difference between maximum crop and actual evaporation. In these fields, the mean field difference is 91 mm/season, 93 mm/season, and 126 mm/season respectively. The fields with a yield of 50.4 and 44.0 tonnes/ha indicate a large difference between the maximum crop and actual evaporation. In these fields the mean field difference is 223 mm/season and 335 mm/season respectively. A large difference between maximum crop and actual evaporation indicates more stress.

Additionally, table A.2 shows the effect of harvest date on the difference between maximum crop and actual evaporation. In group 1 and 3 this difference is smaller than in group 2. Group 2 the difference between maximum crop evaporation and actual evaporation is 259 mm/season or more. The larger difference can be explained by the harvest date. The harvest dates of the fields in group 1 and 3 lie around June, whereas the harvest dates in group 2 are around the end of November. This is in line with expectation as the

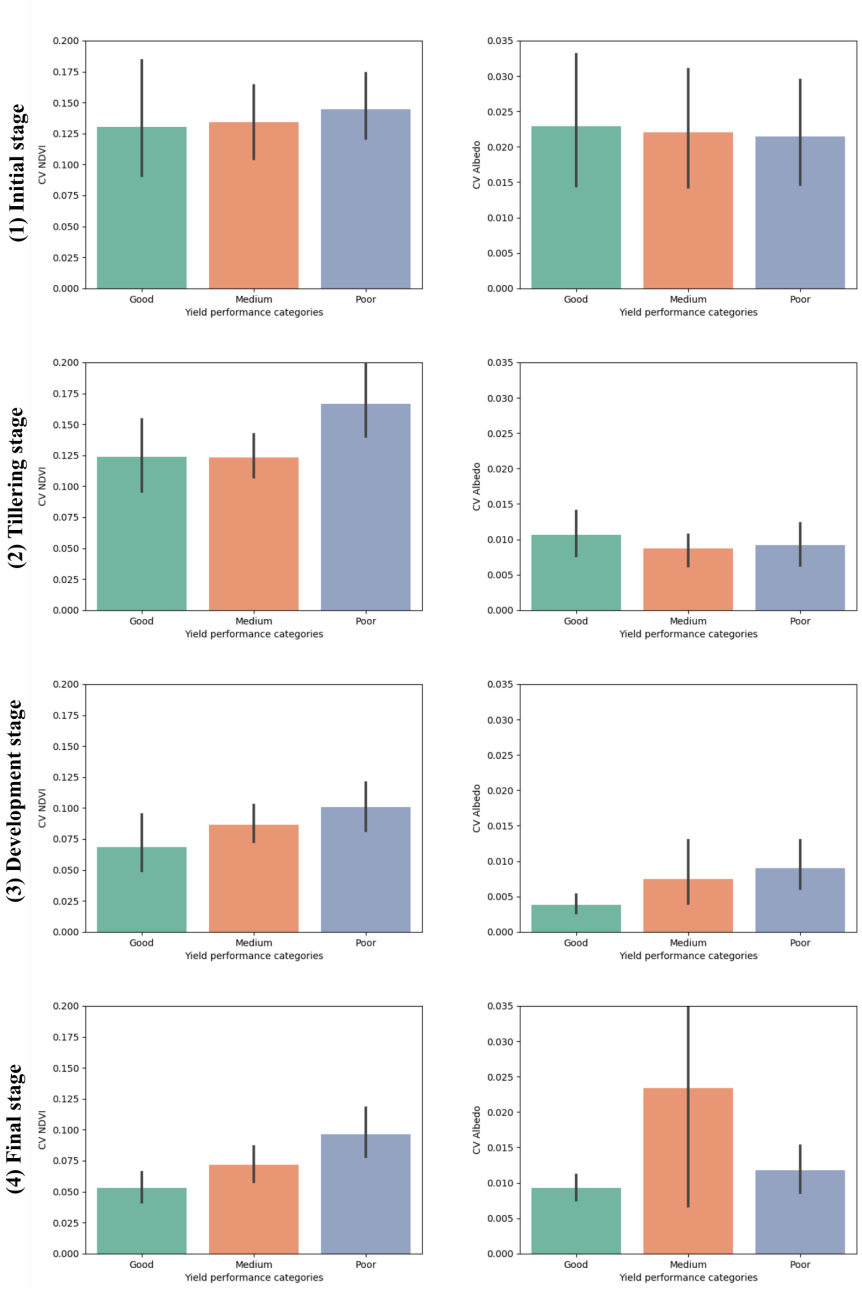

Figure A.5: The first and second column represent the NDVI and Albedo, respectively. The rows present the different growth stages of sugarcane and the relation of NDVI in the different performance categories.

yield decreases with harvest dates towards the end of the year. Fields with a harvest date at the end of a calendar year experience the rainy season at the start of their growing season. This is the period with the highest evaporation rates and largest difference between maximum crop and actual evaporation.

Using NDVI to incorporate stress in actual evaporation calculations it is possible to distinguish between differently performing fields. NDVI is indicative of the chlorophyll content in the crop or irregularities in sugarcane growth, which can be affected by several factors besides drought. To continue, NDVI can identify hampered growth due to soil nutrition deficits, poor drainage, or secondary salinity effects, amongst other factors. However, to assist irrigation the spatial evaporation estimates need to distinguish between drought-related stress and other crop stresses to prevent overirrigation. This pitfall in current satellite based evaporation algorithms is also identified by Jones, 2016. With regard to crop monitoring, the spatial information provided in figure A.6 can already identify problematic fields and in-field irregularities which can provide valuable information for on-site agronomists.

A.4. CONCLUSION

The objective of this study was to determine daily actual evaporation estimates at 20m resolution for a furrow irrigated site of a large sugarcane plantation in Xinavane, Mozambique, using a combination of satellite imagery and local weather data. A method is set up to apply the Priestley-Taylor methodology spatially and demonstrate the accompanied steps.

Creating a crop growth curve from NDVI as a function of CGDD, allowed the correction of the reference evaporation to the specific growth stage. This resulted in maximum crop evaporation estimates. Identifying stress with spectral indices on a daily scale and with the current resolution of the Sentinel-2 imagery is challenging. Analysis was done to compare the spectral indices of good, medium, and poor performing fields in different growth stages. Albedo estimates show little spatial variability. NDVI in different crop stages in different performance categories showed better results.

With crop yield data and NDVI images per observation from the plantation, different categories of differently performing fields were detected. Especially in the last crop stages the poor, medium, and good performing fields could be distinguished by NDVI observations. Therefore, NDVI shows potential to be used as an input for a crop stress adjustment factor. This adjustment factor can be used to incorporate crop stress in the maximum crop evaporation calculations to obtain actual evaporation estimates. Testing the consistency of the methodology should be part of future research with a larger database and preferably at different geographic locations. Additionally, the methodology can benefit from a comparison with in-situ field measurements.

In practice irrigation scheduling is often based on calculations which considers point-based meteorological data. Spatial visualization of the evaporation fluxes will give farmers and/ or plantations an overview of crop development and growth irregularities. However, in order to be of use to irrigation scheduling, the identified crop stress should be related to drought stress to prevent over-irrigation. The proposed methodology sets a first step in deriving an operational high spatial and temporal resolution of the actual evaporation flux.

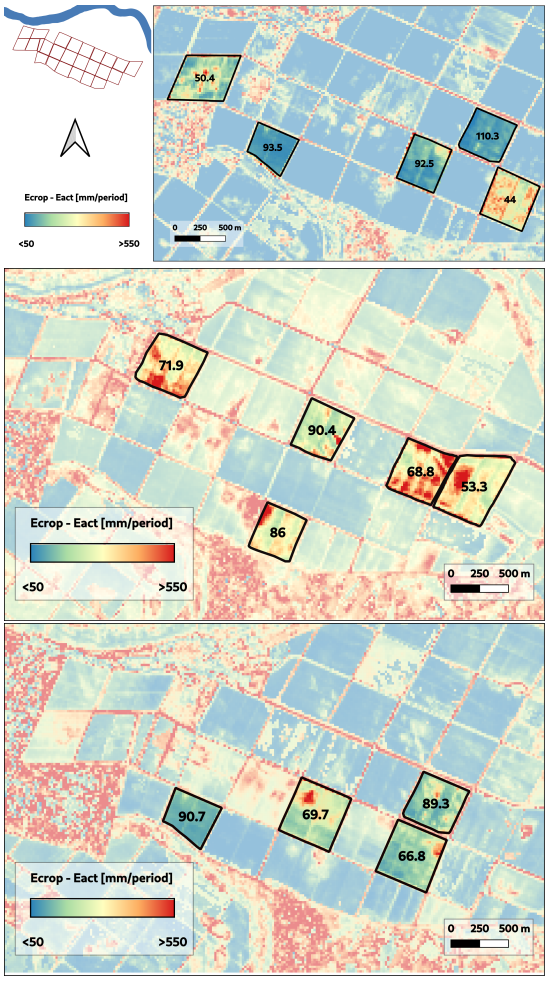

Figure A.6: The difference between maximum crop potential and actual evaporation is presented. Figure A, B, and C zoom in on different groups sugarcane fields with similar growing periods. The fields presented show simulations of the fields with their corresponding plant and harvest dates, as explained in the methodology. The numbers in each field indicate the yield in tonne/ha.

Acknowledgements: The authors want to thank the staff from the agricultural department at Tongaat Hulett Xinavane. Everybody at the department was very cooperative in providing data and thinking along. Also, we would like to thank Neil Lecler and Alisdair Harris from Tongaat Hulett headquarters in Durban for the support from the start of the project. Additionally, we would like to thank the Netherlands Enterprise Agency for subsidizing the work done in this study. The study was part of a bigger project, named IWACA-Tech (http://www.iwacatech.com/).

Table A.1: An overview of three groups of fields that were considered for analysis with a similar harvest date and length of growing season. The rows indicate the yield (tonne/ha), planting date, harvest date with the date of the nearest Sentinel overpass.

Group 1

	XNC18 (ratoon 5)	XNE22 (ratoon 4)	XND19 (ratoon 8)	MDD17 (ratoon 7)	XND24 (ratoon 8)
Yield 2017 (tonne/ha)	110.3	93.5	92.5	44.0	50.4
Planting date	5/28/2016	7/26/2016	7/22/2016	6/18/2016	5/28/2016
Harvest date (Overpass)	6/3/2017 (5/19/2017)	6/25/2017 (6/28/2017)	7/10/2017 (6/28/2017)	7/12/2017 (6/28/2017)	6/15/2017 (11/22/2017)

Group 2

	MDC17 (ratoon 7)	MDC16 (ratoon 7)	XNE19 (ratoon 4)	XNC19 (ratoon 6)	XNC22 (ratoon 5)
Yield 2017 (tonne/ha)	68.8	53.3	86	90.4	71.9
Planting date	11/14/2016	11/16/2016	11/26/2016	11/11/2016	12/8/2016
Harvest date (Overpass)	12/21/2017 (11/22/2017)	12/17/2017 (11/22/2017)	12/17/2017 (11/22/2017)	12/17/2017 (11/22/2017)	12/19/2017 (11/22/2017)

Group 3

	XNC18 (ratoon 6)	XNE22 (ratoon 5)	XND18 (ratoon 8)	XND20 (ratoon 9)	
Yield 2018 (tonne/ha)	89.3	90.7	66.8	69.7	
Planting date	6/3/2017	6/25/2017	6/16/2017	7/10/2017	
Harvest date (Overpass)	6/4/2018 (5/11/2018)	5/26/2018 (5/11/2018)	5/31/2018 (5/11/2018)	6/21/2018 (6/10/2018)	

A

Table A.2: An overview of three groups of fields that were considered for analysis with a similar harvest date and length of growing season.

Group 1

	XNC18 (ratoon 5)	XNE22 (ratoon 4)	XND19 (ratoon 8)	XND24 (ratoon 8)	MDD17 (ratoon 7)
Yield 2017 (tonne/ha)	110.3	93.5	92.5	50.4	44.0
Ecrop-Eact: mean (std)	91 (σ=23)	93 (σ=51)	126 (σ= 63)	223 (σ=95)	334 (σ=88)

Group 2

	XNC19 (ratoon 6)	XNE19 (ratoon 4)	XNC22 (ratoon 5)	MDC17 (ratoon 7)	MDC16 (ratoon 7)
Yield 2017 (tonne/ha)	90.4	86	71.9	68.8	53.3
Ecrop-Eact: mean (std)	259 (σ=84)	322 (σ=89)	361 (σ=93)	411 (σ=121)	345 (σ=113)

Group 3

	XNE22 (ratoon 5)	XNC18 (ratoon 6)	XND20 (ratoon 9)	XND18 (ratoon 8)	
Yield 2018 (tonne/ha)	90.7	89.3	69.7	66.8	
Ecrop-Eact: mean (std)	129 (σ=39)	187 (σ=67)	265 (σ=101)	193 (σ=77)	

Appendix A.1:

Table A.3: NDVI results. The results in this table present the outcome of the Mann-Whitney U test for mean NDVI in different crop stages.

	Good - Poor	Good - Medium	Medium - Poor
Stage 1	U-Statistic=353 P-value=0.27 Sample size - Good: 29 Sample size - Poor: 27	U-Statistic=151 P-value=0.16 Sample size - Good: 29 Sample size - Medium: 13	U-Statistic=159 P-value=0.32 Sample size - Medium: 13 Sample size -Poor: 27
Stage 2	U-Statistic=382 P-value=0.28 Sample size - Good: 30 Sample size - Poor: 28	U-Statistic=234 P-value=0.45 Sample size - Good: 30 Sample size - Medium: 16	U-Statistic=203 P-value=0.31 Sample size - Medium: 16 Sample size - Poor: 28
Stage 3	U-Statistic=1073 P-value=0.02 Sample size - Good: 42 Sample size - Poor: 67	U-Statistic=503 P-value=0.16 Sample size - Good: 42 Sample size - Medium: 28	U-Statistic=831 P-value=0.2 Sample size - Medium: 28 Sample size - Poor: 67
Stage 4	U-Statistic=337 P-value=3.44x10-7 Sample size - Good: 41 Sample size - Poor: 44	U-Statistic=260 P-value=0.003 Sample size - Good: 41 Sample size - Medium: 22	U-Statistic=339 P-value=0.02 Sample size - Medium: 22 Sample size - Poor: 44

A

Table A.4: Albedo results. The results in this table present the outcome of the Mann-Whitney U test for mean albedo in different crop stages.

	Good - Poor	Good - Medium	Medium - Poor
Stage 1	U-Statistic=382 P-value=0.44 Sample size - Good: 29 Sample size - Poor: 27	U-Statistic=169 P-value=0.3 Sample size - Good: 29 Sample size - Medium: 13	U-Statistic=151 P-value=0.24 Sample size - Medium: 13 Sample size - Poor: 27
Stage 2	U-Statistic=306 P-value=0.04 Sample size - Good: 30 Sample size - Poor: 28	U-Statistic=223 P-value=0.35 Sample size - Good: 30 Sample size - Medium: 16	U-Statistic=178 P-value=0.13 Sample size - Medium: 16 Sample size - Poor: 28
Stage 3	U-Statistic=1050 P-value=0.01 Sample size - Good: 42 Sample size - Poor: 67	U-Statistic=417 P-value=0.02 Sample size - Good: 42 Sample size - Medium: 28	U-Statistic=928 P-value=0.47 Sample size - Medium: 28 Sample size - Poor: 67
Stage 4	U-Statistic=480 P-value=0.0001 Sample size - Good: 41 Sample size - Poor: 44	U-Statistic=346 P-value=0.07 Sample size - Good: 41 Sample size - Medium: 22	U-Statistic=366 P-value=0.055 Sample size - Medium: 22 Sample size - Poor: 44

B

APPENDIX B

B

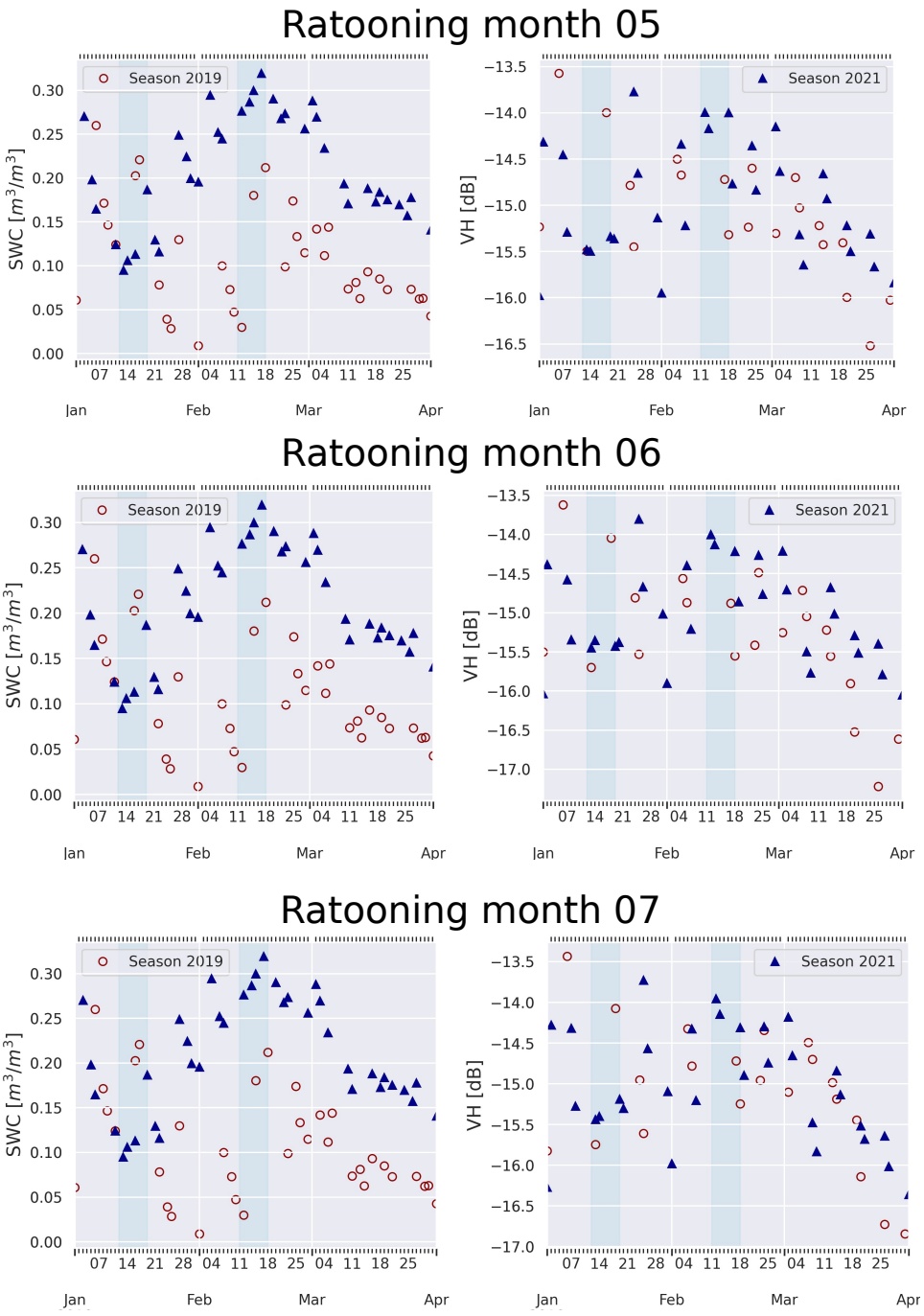

Figure B.1: Soil Water Content (SWC) and the VH Polarization in 2019 and 2021 for rattoning months May (05), June (06), and July (07).

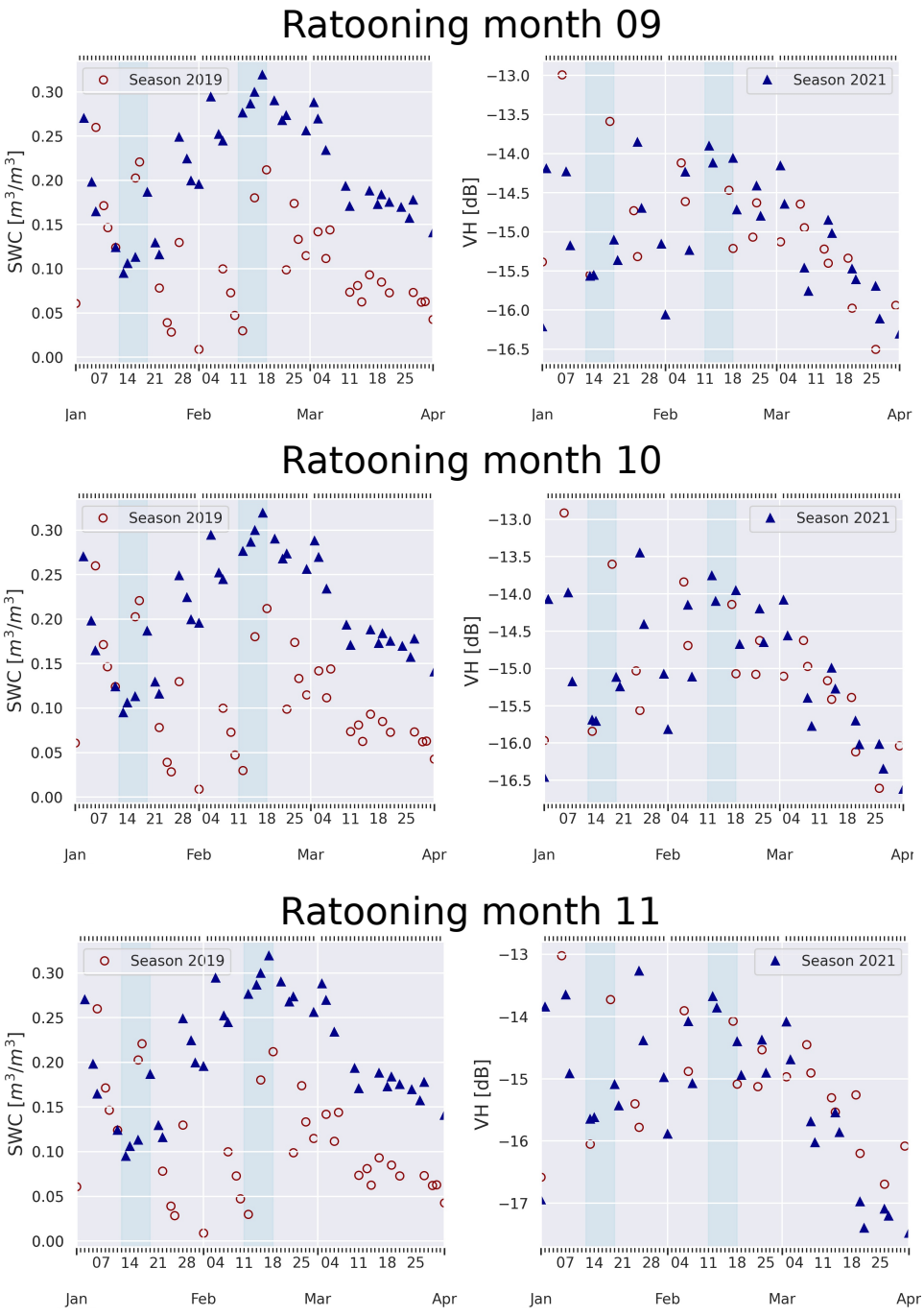

Figure B.2: Soil Water Content (SWC) and the VH Polarization in 2019 and 2021 for rattoning months September (09), October (10), and November (11).

BIBLIOGRAPHY

Abdel-Rahman, E., & Ahmed, F. B. (2008). The application of remote sensing techniques to sugarcane (saccharum spp. hybrid) production: A review of the literature. *International Journal of Remote Sensing*, *29*(13), 3753–3767.

Ač, A., Malenovskỳ, Z., Olejnıéčková, J., Gallé, A., Rascher, U., & Mohammed, G. (2015). Meta-analysis assessing potential of steady-state chlorophyll fluorescence for remote sensing detection of plant water, temperature and nitrogen stress. *Remote Sensing of Environment*, *168*, 420–436.

Achutuni, R. (1996). Global monitoring of large area flooding using the dmsp ssm/i soil wetness index. *annual meeting, Amer. Meteoro. Soc.*, 455–459.

Aires, F., Miolane, L., Prigent, C., Pham, B., Fluet-Chouinard, E., Lehner, B., & Papa, F. (2017). A global dynamic long-term inundation extent dataset at high spatial resolution derived through downscaling of satellite observations. *Journal of Hydrometeorology*, *18*(5), 1305–1325.

Aires, F., Papa, F., & Prigent, C. (2013). A long-term, high-resolution wetland dataset over the amazon basin, downscaled from a multiwavelength retrieval using sar data. *Journal of Hydrometeorology*, *14*(2), 594–607.

Allen, R. G., Pereira, L. S., Raes, D., Smith, M., et al. (1998). Crop evapotranspiration-guidelines for computing crop water requirements-fao irrigation and drainage paper 56. *Fao, Rome*, *300*(9), D05109.

Allen, R. G., Tasumi, M., & Trezza, R. (2007). Satellite-based energy balance for mapping evapotranspiration with internalized calibration (metric)—model. *Journal of irrigation and drainage engineering*, *133*(4), 380–394.

Alsdorf, D. E., Rodrıéguez, E., & Lettenmaier, D. P. (2007). Measuring surface water from space. *Reviews of Geophysics*, *45*(2).

Anderson, M. C., Norman, J. M., Mecikalski, J. R., Otkin, J. A., & Kustas, W. P. (2007). A climatological study of evapotranspiration and moisture stress across the continental united states based on thermal remote sensing: 1. model formulation. *Journal of Geophysical Research: Atmospheres*, *112*(D10).

Anderson, M., Kustas, W., Norman, J., Hain, C., Mecikalski, J., Schultz, L., González-Dugo, M., Cammalleri, C., d'Urso, G., Pimstein, A., et al. (2010). Mapping daily evapotranspiration at field to global scales using geostationary and polar orbiting satellite imagery. *Hydrol. Earth Syst. Sci. Discuss*, *7*, 5957–5990.

Apan, A., Held, A., Phinn, S., & Markley, J. (2004). Detecting sugarcane 'orange rust'disease using eo-1 hyperion hyperspectral imagery. *International journal of remote sensing*, *25*(2), 489–498.

Aragon, B., Ziliani, M. G., Houborg, R., Franz, T. E., & McCabe, M. F. (2021). Cubesats deliver new insights into agricultural water use at daily and 3 m resolutions. *Scientific Reports*, *11*(1), 1–12.

Arguello, M. N., Mason, R. E., Roberts, T. L., Subramanian, N., Acuna, A., Addison, C. K., Lozada, D. N., Miller, R. G., & Gbur, E. (2016). Performance of soft red winter wheat subjected to field soil waterlogging: Grain yield and yield components. *Field Crops Research*, *194*, 57–64.

Aroca, R. (2012). Plant responses to drought stress. *From Morphological to Molecular Features. Springer, Berlin Heidelberg*.

Atzberger, C. (2013). Advances in remote sensing of agriculture: Context description, existing operational monitoring systems and major information needs. *Remote sensing*, *5*(2), 949–981.

Avivi, S., Arini, S. F. M., Soeparjono, S., Restanto, D. P., Fanata, W. I. D., & Widjaya, K. A. (2020). Tolerance screening of sugarcane varieties toward waterlogging stress. *E3S Web of Conferences*, *142*, 03007.

Baghdadi, N., Boyer, N., Todoroff, P., El Hajj, M., & Bégué, A. (2009). Potential of sar sensors terrasar-x, asar/envisat and palsar/alos for monitoring sugarcane crops on reunion island. *Remote Sensing of Environment*, *113*(8), 1724–1738.

Barbagallo, S., Consoli, S., & Russo, A. (2009). A one-layer satellite surface energy balance for estimating evapotranspiration rates and crop water stress indexes. *Sensors*, *9*(1), 1–21.

Barker, J. B., Heeren, D. M., Neale, C. M., & Rudnick, D. R. (2018). Evaluation of variable rate irrigation using a remote-sensing-based model. *Agricultural Water Management*, *203*, 63–74.

Basist, A., Williams Jr, C., Ross, T. F., Menne, M. J., Grody, N., Ferraro, R., Shen, S., & Chang, A. T. (2001). Using the special sensor microwave imager to monitor surface wetness. *Journal of Hydrometeorology*, *2*(3), 297–308.

Bastiaanssen, W. G., Menenti, M., Feddes, R., & Holtslag, A. (1998). A remote sensing surface energy balance algorithm for land (sebal). 1. formulation. *Journal of hydrology*, *212*, 198–212.

Bastiaanssen, W. G., Molden, D. J., & Makin, I. W. (2000). Remote sensing for irrigated agriculture: Examples from research and possible applications. *Agricultural water management*, *46*(2), 137–155.

Bausch, W. C., & Neale, C. M. (1987). Crop coefficients derived from reflected canopy radiation: A concept. *Transactions of the ASAE*, *30*(3), 703–0709.

Bazzi, H., Baghdadi, N., Fayad, I., Charron, F., Zribi, M., & Belhouchette, H. (2020). Irrigation events detection over intensively irrigated grassland plots using sentinel-1 data. *Remote Sensing*, *12*(24). https://doi.org/10.3390/rs12244058

Bégué, A., Lebourgeois, V., Bappel, E., Todoroff, P., Pellegrino, A., Baillarin, F., & Siegmund, B. (2010). Spatio-temporal variability of sugarcane fields and recommendations for yield forecast using ndvi. *International Journal of Remote Sensing*, *31*(20), 5391–5407.

Bégué, A., Arvor, D., Bellon, B., Betbeder, J., De Abelleyra, D., P. D. Ferraz, R., Lebourgeois, V., Lelong, C., Simões, M., & R. Verón, S. (2018). Remote sensing and cropping practices: A review. *Remote Sensing*, *10*(1). https://doi.org/10.3390/rs10010099

Bellini, C., Pacurar, D. I., & Perrone, I. (2014). Adventitious roots and lateral roots: Similarities and differences. *Annual review of plant biology*, *65*, 639–666.

Berg, R., & Carter, D. L. (1980). Furrow erosion and sediment losses on irrigated cropland. *Journal of Soil and Water Conservation*, *35*(6), 267–270.

Bhaduri, A., Bogardi, J., Siddiqi, A., Voigt, H., Vörösmarty, C., Pahl-Wostl, C., Bunn, S. E., Shrivastava, P., Lawford, R., Foster, S., et al. (2016). Achieving sustainable development goals from a water perspective. *Frontiers in Environmental Science*, *4*, 64.

Bhatti, S., Heeren, D. M., Barker, J. B., Neale, C. M., Woldt, W. E., Maguire, M. S., & Rudnick, D. R. (2020). Site-specific irrigation management in a sub-humid climate using a spatial evapotranspiration model with satellite and airborne imagery. *Agricultural Water Management*, *230*, 105950. https://doi.org/https://doi.org/10.1016/j.agwat.2019.105950

Blatchford, M., M. Mannaerts, C., Zeng, Y., Nouri, H., & Karimi, P. (2020). Influence of spatial resolution on remote sensing-based irrigation performance assessment using wapor data. *Remote sensing*, *12*(18), 2949.

Bocca, F. F., Rodrigues, L. H. A., & Arraes, N. A. M. (2015). When do i want to know and why? different demands on sugarcane yield predictions. *Agricultural Systems*, *135*, 48–56.

Bordonal, R. d. O., Carvalho, J. L. N., Lal, R., de Figueiredo, E. B., de Oliveira, B. G., & La Scala, N. (2018). Sustainability of sugarcane production in brazil. a review. *Agronomy for Sustainable Development*, *38*(2), 1–23.

Butler, D. (2001). The performance of sugarcane varieties n23 and n25 on low yield potential soils in swaziland. *Proc S Afr Sug Technol Ass*, *75*, 165–170.

Calera, A., Campos, I., Osann, A., D'Urso, G., & Menenti, M. (2017). Remote sensing for crop water management: From et modelling to services for the end users. *Sensors*, *17*(5), 1104.

Cancela, J. J., González, X. P., Vilanova, M., & Mirás-Avalos, J. M. (2019). Water management using drones and satellites in agriculture. *Water*, *11*(5). https://www.mdpi.com/2073-4441/11/5/874

Cassidy, E. S., West, P. C., Gerber, J. S., & Foley, J. A. (2013). Redefining agricultural yields from tonnes to people nourished per hectare. *Environmental Research Letters*, *8*(3), 034015.

Chabot, R., Bouarfa, S., Zimmer, D., Chaumont, C., & Duprez, C. (2002). Sugarcane transpiration with shallow water-table: Sap flow measurements and modelling. *Agricultural water management*, *54*(1), 17–36.

Chaerle, L., Lenk, S., Leinonen, I., Jones, H. G., Van Der Straeten, D., & Buschmann, C. (2009). Multi-sensor plant imaging: Towards the development of a stress-catalogue. *Biotechnology Journal: Healthcare Nutrition Technology*, *4*(8), 1152–1167.

Chaubell, J., Yueh, S., Entekhabi, D., & Peng, J. (2016). Resolution enhancement of smap radiometer data using the backus gilbert optimum interpolation technique. *2016 IEEE International Geoscience and Remote Sensing Symposium (IGARSS)*, 284–287.

Chen, D., Huangfu, C., Liu, H., Wang, N., & Yang, D. (2013). Effects of water stress and fungicide on the growth and drought resistance of flaveria bidentis. *Acta Ecol Sin*, *33*(7), 2113–2120.

B

Chen, H., Zeng, W., Jin, Y., Zha, Y., Mi, B., & Zhang, S. (2020). Development of a waterlogging analysis system for paddy fields in irrigation districts. *Journal of Hydrology*, *591*, 125325.

Chen, Y., Xia, J., Liang, S., Feng, J., Fisher, J. B., Li, X., Li, X., Liu, S., Ma, Z., Miyata, A., et al. (2014). Comparison of satellite-based evapotranspiration models over terrestrial ecosystems in china. *Remote Sensing of Environment*, *140*, 279–293.

Choubey, V. (1997). Detection and delineation of waterlogging by remote sensing techniques. *Journal of the Indian Society of Remote Sensing*, *25*(2), 123–135.

Choudhury, B. J. (1989). Monitoring global land surface using nimbus-7 37 ghz data theory and examples. *International Journal of Remote Sensing*, *10*(10), 1579–1605.

Chowdary, V., Chandran, R. V., Neeti, N., Bothale, R., Srivastava, Y., Ingle, P., Ramakrishnan, D., Dutta, D., Jeyaram, A., Sharma, J., et al. (2008). Assessment of surface and sub-surface waterlogged areas in irrigation command areas of bihar state using remote sensing and gis. *Agricultural water management*, *95*(7), 754–766.

Christen, E. W., Ayars, J. E., & Hornbuckle, J. W. (2001). Subsurface drainage design and management in irrigated areas of australia. *Irrigation Science*, *21*(1), 35–43.

Chukalla, A. D., Mul, M. L., van der Zaag, P., van Halsema, G., Mubaya, E., Muchanga, E., den Besten, N., & Karimi, P. (2022). A framework for irrigation performance assessment using wapor data: The case of a sugarcane estate in mozambique. *Hydrology and Earth System Sciences*, *26*(10), 2759–2778. https://doi.org/10.5194/hess-26-2759-2022

Cock, J. (2001). Sugarcane growth and development. *SUGAR CANE INTERNATIONAL*, 5–15.

Cristea, N. C., Kampf, S. K., & Burges, S. J. (2012). Revised coefficients for priestley-taylor and makkink-hansen equations for estimating daily reference evapotranspiration. *Journal of Hydrologic Engineering*, *18*(10), 1289–1300.

Davidson, M., Chini, M., Dierking, W., Djavidnia, S., Haarpaintner, J., Hajduch, G., Laurin, G., Lavalle, M., López-Martıénez, C., Nagler, T., et al. (2019). Copernicus l-band sar mission requirements document.

De Roo, R. D., Du, Y., Ulaby, F. T., & Dobson, M. C. (2001). A semi-empirical backscattering model at l-band and c-band for a soybean canopy with soil moisture inversion. *IEEE Transactions on Geoscience and Remote Sensing*, *39*(4), 864–872.

den Besten, N., Steele Dunne, S., Mahmud, A., Jackson, D., Aouizerats, B., de Jeu, R., Burger, R., Houborg, R., McGlinchey, M., & van der Zaag, P. (2023). Understanding sentinel-1 backscatter response to sugarcane yield variability and waterlogging. *Remote Sensing of Environment*, *290*, 113555. https://doi.org/https://doi.org/10.1016/j.rse.2023.113555

den Besten, N., Kassing, R., Muchanga, E., Earnshaw, C., Jeu de, R., Karimi, P., & van der Zaag, P. (2020). A novel approach to the use of earth observation to estimate daily evaporation in a sugarcane plantation in xinavane, mozambique. *Physics and Chemistry of the Earth, Parts A/B/C*, 102940. https://doi.org/https://doi.org/10.1016/j.pce.2020.102940

den Besten, N., Schellekens, J., Jeu, R. d., & Van der Zaag, P. (2019). The influence of shallow groundwater on the actual transpiration flux of irrigated fields using

satellite observations. *Remote Sensing for Agriculture, Ecosystems, and Hydrology XXI, 11149*, 111490N.

den Besten, N., Steele-Dunne, S., Aouizerats, B., Zajdband, A., De Jeu, R., & Van Der Zaag, P. (2021). Observing sucrose accumulation with sentinel-1 backscatter. *Frontiers in Remote Sensing, 2*, 1–9.

den Besten, N., Steele-Dunne, S., de Jeu, R., & van der Zaag, P. (2021). Towards monitoring waterlogging with remote sensing for sustainable irrigated agriculture. *Remote Sensing, 13*(15), 2929.

Dennis, E. S., Dolferus, R., Ellis, M., Rahman, M., Wu, Y., Hoeren, F., Grover, A., Ismond, K., Good, A., & Peacock, W. (2000). Molecular strategies for improving waterlogging tolerance in plants. *Journal of experimental botany, 51*(342), 89–97.

Donaldson, R., Redshaw, K., Rhodes, R., Antwerpen, R. v., et al. (2008). Season effects on productivity of some commercial south african sugarcane cultivars, ii: Trash production. *Proceedings of the Annual Congress-South African Sugar Technologists' Association*, (81), 528–538.

Doorenbos, J., & Kassam, A. (1979). Yield response to water. *Irrigation and drainage paper, 33*, 257.

Doorenbos, J., & Pruitt, W. (1977). Crop water requirements, fao irrig. drain. pap., 24. *Food and Agriculture Organization, Rome*.

Dubb, A., Scoones, I., & Woodhouse, P. (2017). The political economy of sugar in southern africa–introduction.

Dwivedi, R., Ramana, K., & Sreenivas, K. (2007). Temporal behaviour of surface waterlogged areas using spaceborne multispectral multitemporal measurements. *Journal of the Indian Society of Remote Sensing, 35*(2), 173–184.

El Bastawesy, M., & Ali, R. R. (2013). The use of gis and remote sensing for the assessment of waterlogging in the dryland irrigated catchments of farafra oasis, egypt. *Hydrological processes, 27*(2), 206–216.

El Bastawesy, M., Ali, R. R., Deocampo, D. M., & Al Baroudi, M. S. (2012). Detection and assessment of the waterlogging in the dryland drainage basins using remote sensing and gis techniques. *IEEE journal of selected topics in applied earth observations and remote sensing, 5*(5), 1564–1571.

El Hajj, M., Baghdadi, N., Wigneron, J.-P., Zribi, M., Albergel, C., Calvet, J.-C., & Fayad, I. (2019). First vegetation optical depth mapping from sentinel-1 c-band sar data over crop fields. *Remote Sensing, 11*(23), 2769.

El-Rayes, M. A., & Ulaby, F. T. (1987). Microwave dielectric spectrum of vegetation-part i: Experimental observations. *IEEE Transactions on Geoscience and Remote Sensing*, (5), 541–549.

Emery, W., & Camps, A. (2017). *Introduction to satellite remote sensing: Atmosphere, ocean, land and cryosphere applications*. Elsevier.

Endres, L., Moura dos Santos, C., Verissimo de Souza, G., Menossi, M., Marcelino dos Santos, J. C., et al. (2018). Morphological changes recorded in different phenophases of sugarcane plants subjected to water stress in tropical field conditions. *Australian Journal of Crop Science, 12*(7), 1041.

ESA. (2021a). Sentinel-1 observation scenario [Accessed: 2021-07-07].

ESA. (2021b). Snap [Accessed: 2021-12-03].

B

Ezin, V., Pena, R. D. L., & Ahanchede, A. (2010). Flooding tolerance of tomato genotypes during vegetative and reproductive stages. *Brazilian Journal of Plant Physiology*, *22*(2), 131–142.

FAO. (2016a). Aquastat main database, food and agriculture organization of the united nations (fao) [Website accessed on (27.10.2019) http://www.fao.org/nr/water/aquastat/data/].

FAO. (2016b). Aquastat main database, food and agriculture organization of the united nations (fao) [Website accessed on (27.10.2019) http://www.fao.org/nr/water/aquastat/].

FAO. (2016c). Coping with water scarcity in agriculture a global framework for action in a changing climate.

FAO. (2018). *Wapor database methodology: Level 1. remote sensing for water productivity technical report: Methodology series*. FAO.

FAO. (2021a). Chapter 5. sugar [Accessed: 2021-07-07].

FAO. (2021b). Faostat [Accessed: 2021-07-07].

Fei, X., LI, Y.-z., Yun, D., Feng, L., Yi, Y., Qi, F., & Xuan, B. (2014). Monitoring perennial sub-surface waterlogged croplands based on modis in jianghan plain, middle reaches of the yangtze river. *Journal of Integrative Agriculture*, *13*(8), 1791–1801.

Ferguson, I. M., & Maxwell, R. M. (2012). Human impacts on terrestrial hydrology: Climate change versus pumping and irrigation. *Environmental Research Letters*, *7*(4), 044022.

Fernandes, J. L., Ebecken, N. F. F., & Esquerdo, J. C. D. M. (2017). Sugarcane yield prediction in brazil using ndvi time series and neural networks ensemble. *International Journal of Remote Sensing*, *38*(16), 4631–4644.

Ferreira, T. H., Tsunada, M. S., Bassi, D., Araujo, P., Mattiello, L., Guidelli, G. V., Righetto, G. L., Goncalves, V. R., Lakshmanan, P., & Menossi, M. (2017). Sugarcane water stress tolerance mechanisms and its implications on developing biotechnology solutions. *Frontiers in plant science*, *8*, 1077.

Fischer, G., Tubiello, F. N., Van Velthuizen, H., & Wiberg, D. A. (2007). Climate change impacts on irrigation water requirements: Effects of mitigation, 1990–2080. *Technological Forecasting and Social Change*, *74*(7), 1083–1107.

Fisher, J., Hook, S., Allen, R., Anderson, M., French, A., Hain, C., Hulley, G., & Wood, E. (2015). Ecostress: Nasa's next-generation mission to measure evapotranspiration from the international space station. *AGU Fall Meeting Abstracts*, 4–13.

Fisher, J. B., Tu, K. P., & Baldocchi, D. D. (2008). Global estimates of the land–atmosphere water flux based on monthly avhrr and islscp-ii data, validated at 16 fluxnet sites. *Remote Sensing of Environment*, *112*(3), 901–919.

Franke, J., & Menz, G. (2007). Multi-temporal wheat disease detection by multi-spectral remote sensing. *Precision Agriculture*, *8*(3), 161–172.

Frappart, F., Wigneron, J.-P., Li, X., Liu, X., Al-Yaari, A., Fan, L., Wang, M., Moisy, C., Le Masson, E., Aoulad Lafkih, Z., et al. (2020). Global monitoring of the vegetation dynamics from the vegetation optical depth (vod): A review. *Remote Sensing*, *12*(18), 2915.

French, A. N., Hunsaker, D. J., & Thorp, K. R. (2015). Remote sensing of evapotranspiration over cotton using the tseb and metric energy balance models. *Remote Sensing of Environment*, *158*, 281–294.

Fukao, T., Barrera-Figueroa, B. E., Juntawong, P., & Pena-Castro, J. M. (2019). Submergence and waterlogging stress in plants a review highlighting research opportunities and understudied aspects. https://doi.org/10.3389/fpls.2019.00340

Galantowicz, J. F. (2002). High-resolution flood mapping from low-resolution passive microwave data. *IEEE International Geoscience and Remote Sensing Symposium*, *3*, 1499–1502.

Galantowicz, J. F., Picton, J., & Root, B. (2017). Mapping daily and maximum flood extents at 90-m resolution during hurricanes harvey and irma using passive microwave remote sensing. *AGU Fall Meeting Abstracts*, *2017*, NH23E–2833.

Gelcer, E., Fraisse, C., Zotarelli, L., Perondi, D., Malia, H., Ecole, C., & Migliaccio, K. (2018). A smart irrigation tool to determine the effects of enso on water requirements for tomato production in mozambique. *Water*, *10*(12), 1820.

Giddings, L., & Choudhury, B. (1989). Observation of hydrological features with nimbus-7 37 ghz data, applied to south america. *International Journal of Remote Sensing*, *10*(10), 1673–1686.

Glaz, B., Morris, D. R., & Daroub, S. H. (2004). Sugarcane photosynthesis, transpiration, and stomatal conductance due to flooding and water table. *Crop Science*, *44*(5), 1633–1641.

Gomathi, R., Rao, P. G., Chandran, K., & Selvi, A. (2015). Adaptive responses of sugarcane to waterlogging stress an over view. *Sugar Tech*, *17*(4), 325–338.

Govender, M., Govender, P., Weiersbye, I., Witkowski, E., & Ahmed, F. (2009). Review of commonly used remote sensing and ground-based technologies to measure plant water stress. *Water Sa*, *35*(5).

Gowda, P., Chavez, J., Colaizzi, P., Evett, S., Howell, T., & Tolk, J. (2007). Remote sensing based energy balance algorithms for mapping et: Current status and future challenges. *Transactions of the ASABE*, *50*(5), 1639–1644.

Gowda, P., Senay, G., Howell, T., & Marek, T. (2009). Lysimetric evaluation of simplified surface energy balance approach in the texas high plains. *Applied engineering in agriculture*, *25*(5), 665–669.

Gowda, P. H., Chavez, J. L., Colaizzi, P. D., Evett, S. R., Howell, T. A., & Tolk, J. A. (2008). Et mapping for agricultural water management: Present status and challenges. *Irrigation science*, *26*(3), 223–237.

Gunarathna, M., Sakai, K., Nakandakari, T., Momii, K., Onodera, T., Kaneshiro, H., Uehara, H., & Wakasugi, K. (2018). Optimized subsurface irrigation system: The future of sugarcane irrigation. *Water*, *10*(3), 314.

Hamilton, S., Sippel, S., & Melack, J. (1996). Inundation patterns in the pantanal wetland of south america determined from passive microwave remote sensing. *Archiv für Hydrobiologie*, *137*(1), 1–23.

He, M., Kimball, J. S., Yi, Y., Running, S. W., Guan, K., Moreno, A., Wu, X., & Maneta, M. (2019). Satellite data-driven modeling of field scale evapotranspiration in croplands using the mod16 algorithm framework. *Remote Sensing of Environment*, *230*, 111201.

B

Holmes, T., De Jeu, R., Owe, M., & Dolman, A. (2009). Land surface temperature from ka band (37 ghz) passive microwave observations. *Journal of Geophysical Research: Atmospheres*, *114*(D4).

Hong, S.-h., Hendrickx, J. M., & Borchers, B. (2009). Up-scaling of sebal derived evapotranspiration maps from landsat (30 m) to modis (250 m) scale. *Journal of hydrology*, *370*(1-4), 122–138.

Houborg, R., & McCabe, M. F. (2018a). A cubesat enabled spatio-temporal enhancement method (cestem) utilizing planet, landsat and modis data. *Remote Sensing of Environment*, *209*, 211–226.

Houborg, R., & McCabe, M. F. (2018b). Daily retrieval of ndvi and lai at 3 m resolution via the fusion of cubesat, landsat, and modis data. *Remote Sensing*, *10*(6), 890.

Houk, E., Frasier, M., & Schuck, E. (2006). The agricultural impacts of irrigation induced waterlogging and soil salinity in the arkansas basin. *Agricultural water management*, *85*(1-2), 175–183.

Inman-Bamber, G. (2013). Sugarcane yields and yield-limiting processes. *Sugarcane: physiology, biochemistry, and functional biology*, 579–600.

Inman-Bamber, N., Bonnett, G., Spillman, M., Hewitt, M., & Xu, J. (2009). Source–sink differences in genotypes and water regimes influencing sucrose accumulation in sugarcane stalks. *Crop and Pasture Science*, *60*(4), 316–327.

Inman-Bamber, N., & McGlinchey, M. (2003). Crop coefficients and water-use estimates for sugarcane based on long-term bowen ratio energy balance measurements. *Field Crops Research*, *83*(2), 125–138.

Inman-Bamber, N., & Smith, D. (2005). Water relations in sugarcane and response to water deficits. *Field crops research*, *92*(2-3), 185–202.

Irfan, M., Hayat, S., Hayat, Q., Afroz, S., & Ahmad, A. (2010). Physiological and biochemical changes in plants under waterlogging. *Protoplasma*, *241*(1-4), 3–17.

Jackson, R. D. (1986). Remote sensing of biotic and abiotic plant stress. *Annual review of Phytopathology*, *24*(1), 265–287.

Jelsma, I., Bolding, A., & Slingerland, M. (2010). Smallholder sugarcane production systems in xinavane, mozambique: Report from the field. *Wageningen: Plant Production Systems, Plant Sciences Group, Wageningen University*.

Jensen, K., McDonald, K., Podest, E., Rodriguez-Alvarez, N., Horna, V., & Steiner, N. (2018). Assessing l-band gnss-reflectometry and imaging radar for detecting sub-canopy inundation dynamics in a tropical wetlands complex. *Remote Sensing*, *10*(9), 1431.

Jeu de, R. A. (2003). Retrieval of land surface parameters using passive microwave remote sensing. *PhD diss., Vrije Universiteit Amsterdam*.

Jiang, Z., Huete, A., Chen, J., Chen, Y., Li, J., Yan, G., & Zhang, X. (2006). Analysis of ndvi and scaled difference vegetation index retrievals of vegetation fraction. *Remote sensing of environment*, *101*(3), 366–378.

Joerg, H., Pardini, M., Hajnsek, I., & Papathanassiou, K. P. (2018). Sensitivity of sar tomography to the phenological cycle of agricultural crops at x-, c-, and l-band. *IEEE Journal of Selected Topics in Applied Earth Observations and Remote Sensing*, *11*(9), 3014–3029.

Jones, H. (2016). Opportunities and pitfalls in the use of thermal sensing for monitoring water stress and transpiration. *International Symposium on Sensing Plant Water Status-Methods and Applications in Horticultural Science 1197*, 31–44.

Jones, H. (2018). Opportunities and pitfalls in the use of thermal sensing for monitoring water stress and transpiration. *Acta horticulturae*.

Kamble, B., Kilic, A., & Hubbard, K. (2013). Estimating crop coefficients using remote sensing-based vegetation index. *Remote Sensing*, *5*(4), 1588–1602.

Karam, M. A., & Fung, A. K. (1989). Leaf-shape effects in electromagnetic wave scattering from vegetation.

Karimi, P., Bongani, B., Blatchford, M., & de Fraiture, C. (2019). Global satellite-based et products for the local level irrigation management: An application of irrigation performance assessment in the sugarbelt of swaziland. *Remote Sensing*, *11*(6), 705.

Kaur, G., Singh, G., Motavalli, P. P., Nelson, K. A., Orlowski, J. M., & Golden, B. R. (2020). Impacts and management strategies for crop production in waterlogged or flooded soils: A review. *Agronomy Journal*, *112*(3), 1475–1501.

Kaur, G., Zurweller, B. A., Nelson, K. A., Motavalli, P. P., & Dudenhoeffer, C. J. (2017). Soil waterlogging and nitrogen fertilizer management effects on corn and soybean yields. *Agronomy journal*, *109*(1), 97–106.

Kaushik, S., Dhote, P. R., Thakur, P. K., Nikam, B. R., & Aggarwal, S. P. (2019). An integrated approach for identification of waterlogged areas using rs and gis technique and groundwater modelling. *Sustainable Water Resources Management*, *5*(4), 1887–1901.

Khabbazan, S., Steele-Dunne, S., Vermunt, P., Judge, J., Vreugdenhil, M., & Gao, G. (2022). The influence of surface canopy water on the relationship between l-band backscatter and biophysical variables in agricultural monitoring. *Remote Sensing of Environment*, *268*, 112789.

Khabbazan, S., Vermunt, P., Steele-Dunne, S., Ratering Arntz, L., Marinetti, C., van der Valk, D., Iannini, L., Molijn, R., Westerdijk, K., & van der Sande, C. (2019). Crop monitoring using sentinel-1 data: A case study from the netherlands. *Remote Sensing*, *11*(16), 1887.

Khanal, S., Fulton, J., & Shearer, S. (2017). An overview of current and potential applications of thermal remote sensing in precision agriculture. *Computers and Electronics in Agriculture*, *139*, 22–32.

Khanal, S., Kc, K., Fulton, J. P., Shearer, S., & Ozkan, E. (2020). Remote sensing in agriculture—accomplishments, limitations, and opportunities. *Remote Sensing*, *12*(22), 3783.

Kustas, W. P., Norman, J. M., Anderson, M. C., & French, A. N. (2003). Estimating subpixel surface temperatures and energy fluxes from the vegetation index–radiometric temperature relationship. *Remote sensing of Environment*, *85*(4), 429–440.

Lang, M. W., Townsend, P. A., & Kasischke, E. S. (2008). Influence of incidence angle on detecting flooded forests using c-hh synthetic aperture radar data. *Remote Sensing of Environment*, *112*(10), 3898–3907.

Le Toan, T., Ribbes, F., Wang, L.-F., Floury, N., Ding, K.-H., Kong, J. A., Fujita, M., & Kurosu, T. (1997). Rice crop mapping and monitoring using ers-1 data based on experi-

B

ment and modeling results. *IEEE Transactions on Geoscience and Remote Sensing*, *35*(1), 41–56.

Lillesand, T., Kiefer, R. W., & Chipman, J. (2015). *Remote sensing and image interpretation*. John Wiley & Sons.

Linkemer, G., Board, J. E., & Musgrave, M. E. (1998). Waterlogging effects on growth and yield components in late-planted soybean. *Crop Science*, *38*(6), 1576–1584.

Liu, X., Wigneron, J.-P., Fan, L., Frappart, F., Ciais, P., Baghdadi, N., Zribi, M., Jagdhuber, T., Li, X., Wang, M., Bai, X., & Moisy, C. (2021). Ascat ib: A radar-based vegetation optical depth retrieved from the ascat scatterometer satellite. *Remote Sensing of Environment*, *264*, 112587. https://doi.org/https://doi.org/10.1016/j.rse.2021.112587

Lofton, J., Tubana, B. S., Kanke, Y., Teboh, J., Viator, H., & Dalen, M. (2012). Estimating sugarcane yield potential using an in-season determination of normalized difference vegetative index. *Sensors*, *12*(6), 7529–7547.

Louis, J., Debaecker, V., Pflug, B., Main-Knorn, M., Bieniarz, J., Mueller-Wilm, U., Cadau, E., & Gascon, F. (2016). Sentinel-2 sen2cor: L2a processor for users. *Proceedings of the Living Planet Symposium, Prague, Czech Republic*, 9–13.

Macelloni, G., Paloscia, S., Pampaloni, P., Marliani, F., & Gai, M. (2001). The relationship between the backscattering coefficient and the biomass of narrow and broad leaf crops. *IEEE Transactions on Geoscience and Remote Sensing*, *39*(4), 873–884.

Maes, W., & Steppe, K. (2012). Estimating evapotranspiration and drought stress with ground-based thermal remote sensing in agriculture: A review. *Journal of Experimental Botany*, *63*(13), 4671–4712.

Maestrini, B., & Basso, B. (2018). Drivers of within-field spatial and temporal variability of crop yield across the us midwest. *Scientific reports*, *8*(1), 1–9.

Maguire, M. S., Neale, C. M., Woldt, W. E., & Heeren, D. M. (2022). Managing spatial irrigation using remote-sensing-based evapotranspiration and soil water adaptive control model. *Agricultural Water Management*, *272*, 107838. https://doi.org/https://doi.org/10.1016/j.agwat.2022.107838

Mancini, A., Frontoni, E., & Zingaretti, P. (2019). Satellite and uav data for precision agriculture applications. *2019 International Conference on Unmanned Aircraft Systems (ICUAS)*, 491–497.

Mandal, A. K., & Sharma, R. (2011). Delineation and characterization of waterlogged salt affected soils in ignp using remote sensing and gis. *Journal of the Indian Society of Remote Sensing*, *39*(1), 39–50.

Mann, H. B., & Whitney, D. R. (1947). On a test of whether one of two random variables is stochastically larger than the other. *The annals of mathematical statistics*, 50–60.

Martens, B., de Jeu, R., Verhoest, N., Schuurmans, H., Kleijer, J., & Miralles, D. (2018). Towards estimating land evaporation at field scales using gleam. *Remote Sensing*, *10*(11), 1720.

Marti, J., Savin, R., & Slafer, G. (2015). Wheat yield as affected by length of exposure to waterlogging during stem elongation. *Journal of Agronomy and Crop Science*, *201*(6), 473–486.

Martinez, J.-M., & Le Toan, T. (2007). Mapping of flood dynamics and spatial distribution of vegetation in the amazon floodplain using multitemporal sar data. *Remote sensing of Environment*, *108*(3), 209–223.

Martinez-Feria, R. A., & Basso, B. (2020). Unstable crop yields reveal opportunities for site-specific adaptations to climate variability. *Scientific reports*, *10*(1), 1–10.

Martinis, S., & Rieke, C. (2015). Backscatter analysis using multi-temporal and multi-frequency sar data in the context of flood mapping at river saale, germany. *Remote Sensing*, *7*(6), 7732–7752.

Martins, M. T. B., de Souza, W. R., da Cunha, B. A. D. B., Basso, M. F., de Oliveira, N. G., Vinecky, F., Martins, P. K., de Oliveira, P. A., Arenque-Musa, B. C., de Souza, A. P., et al. (2016). Characterization of sugarcane (saccharum spp.) leaf senescence: Implications for biofuel production. *Biotechnology for biofuels*, *9*(1), 153.

Martıénez, M., Arata, A. F., Lázaro, L., Stenglein, S. A., & Dinolfo, M. I. (2019). Effects of waterlogging stress on plant-pathogen interaction between fusarium poae and wheat/barley. *Acta Scientiarum. Agronomy*, *41*.

Mashnik, D., Jacobus, H., Barghouth, A., Wang, E. J., Blanchard, J., & Shelby, R. (2017). Increasing productivity through irrigation: Problems and solutions implemented in africa and asia. *Sustainable Energy Technologies and Assessments*, *22*, 220–227.

McCabe, M. F., Houborg, R., & Lucieer, A. (2016). High-resolution sensing for precision agriculture: From earth-observing satellites to unmanned aerial vehicles. *Remote Sensing for Agriculture, Ecosystems, and Hydrology XVIII*, *9998*, 346–355.

McDonald, K. C., Zimmermann, R., & Kimball, J. S. (2002). Diurnal and spatial variation of xylem dielectric constant in norway spruce (picea abies [l.] karst.) as related to microclimate, xylem sap flow, and xylem chemistry. *IEEE Transactions on Geoscience and Remote Sensing*, *40*(9), 2063–2082.

McNairn, H., & Brisco, B. (2004). The application of c-band polarimetric sar for agriculture: A review. *Canadian Journal of Remote Sensing*, *30*(3), 525–542.

Meerdink, S., Hook, S., Abbott, E., & Roberts, D. (2018). The ecostress spectral library 1.0 [Website accessed on (accessed 9.1.18) https://speclib.jpl.nasa.gov/library]. *Accessed online*, *1*(03).

Meyer, T., Jagdhuber, T., Piles, M., Fink, A., Grant, J., Vereecken, H., & Jonard, F. (2019). Estimating gravimetric water content of a winter wheat field from l-band vegetation optical depth. *Remote sensing*, *11*(20), 2353.

Miralles, D., Holmes, T., De Jeu, R., Gash, J., Meesters, A., Dolman, A., et al. (2011). *Global land-surface evaporation estimated from satellite-based observations* (Doctoral dissertation). VU University Amsterdam.

Mohanty, A., Panda, R., Rout, G., Muduli, K., & Tripathy, P. (2020). Impact of short term water logging on flowering, fruit setting, yield and yield attributes in tomato (solanum lycopersicum l. mill). *Journal of Pharmacognosy and Phytochemistry*, *9*(4), 760–763.

Molijn, R. A., Iannini, L., Vieira Rocha, J., & Hanssen, R. F. (2019). Sugarcane productivity mapping through c-band and l-band sar and optical satellite imagery. *Remote Sensing*, *11*(9), 1109.

Mondal, D., & Pal, S. (2018). Monitoring dual-season hydrological dynamics of seasonally flooded wetlands in the lower reach of mayurakshi river, eastern india. *Geocarto international*, *33*(3), 225–239.

Moore, P. H., & Botha, F. C. (2013). *Sugarcane: Physiology, biochemistry and functional biology*. John Wiley & Sons.

Morel, J., Todoroff, P., Bégué, A., Bury, A., Martiné, J.-F., & Petit, M. (2014). Toward a satellite-based system of sugarcane yield estimation and forecasting in smallholder farming conditions: A case study on reunion island. *Remote Sensing*, *6*(7), 6620–6635.

Mourtzinis, S., Arriaga, F., Balkcom, K. S., & Price, A. J. (2015). Vertical distribution of corn biomass as influenced by cover crop and stover harvest. *Agronomy Journal*, *107*(1), 232–240.

Mu, Q., Heinsch, F. A., Zhao, M., & Running, S. W. (2007). Development of a global evapotranspiration algorithm based on modis and global meteorology data. *Remote sensing of Environment*, *111*(4), 519–536.

Muchow, R., Robertson, M., & Wood, A. (1996). Growth of sugarcane under high input conditions in tropical australia. ii. sucrose accumulation and commercial yield. *Field Crops Research*, *48*(1), 27–36.

Mueller, N. D., Gerber, J. S., Johnston, M., Ray, D. K., Ramankutty, N., & Foley, J. A. (2012). Closing yield gaps through nutrient and water management. *Nature*, *490*(7419), 254.

Mulla, D. J. (2013). Twenty five years of remote sensing in precision agriculture: Key advances and remaining knowledge gaps. *Biosystems engineering*, *114*(4), 358–371.

Mustafa, G., Joyia, F. A., Anwar, S., Parvaiz, A., & Khan, M. S. (2018). Biotechnological interventions for the improvement of sugarcane crop and sugar production. *Sugarcane-Technology and Research; IntechOpen: London, UK*, 113–138.

Neumann, K., Stehfest, E., Verburg, P. H., Siebert, S., Müller, C., & Veldkamp, T. (2011). Exploring global irrigation patterns: A multilevel modelling approach. *Agricultural Systems*, *104*(9), 703–713.

Norman, J. M., Kustas, W. P., & Humes, K. S. (1995). Source approach for estimating soil and vegetation energy fluxes in observations of directional radiometric surface temperature. *Agricultural and Forest Meteorology*, *77*(3-4), 263–293.

Olivier, F. C., & Singels, A. (2015). Increasing water use efficiency of irrigated sugarcane production in south africa through better agronomic practices. *Field Crops Research*, *176*, 87–98.

O'Shaughnessy, S. A., Evett, S. R., Colaizzi, P. D., Andrade, M. A., Marek, T. H., Heeren, D. M., Lamm, F. R., & LaRue, J. L. (2019). Identifying advantages and disadvantages of variable rate irrigation: An updated review. *Applied Engineering in Agriculture*, *35*(6), 837–852.

Owe, M., de Jeu, R., & Holmes, T. (2008). Multisensor historical climatology of satellite-derived global land surface moisture. *Journal of Geophysical Research: Earth Surface*, *113*(F1).

Pampana, S., Masoni, A., & Arduini, I. (2016). Grain yield of durum wheat as affected by waterlogging at tillering. *Cereal Research Communications*, *44*(4), 706–716.

Papa, F., Prigent, C., Aires, F., Jimenez, C., Rossow, W., & Matthews, E. (2010). Interannual variability of surface water extent at the global scale, 1993–2004. *Journal of Geophysical Research: Atmospheres*, *115*(D12).

Parent, C., Capelli, N., Berger, A., Crèvecoeur, M., Dat, J. F., et al. (2008). An overview of plant responses to soil waterlogging. *Plant stress*, *2*(1), 20–27.

Parrens, M., Al Bitar, A., Frappart, F., Paiva, R., Wongchuig, S., Papa, F., Yamasaki, D., & Kerr, Y. (2019). High resolution mapping of inundation area in the amazon basin from a combination of l-band passive microwave, optical and radar datasets. *International Journal of Applied Earth Observation and Geoinformation*, *81*, 58–71.

Parrens, M., Al Bitar, A., Frappart, F., Papa, F., Calmant, S., Crétaux, J.-F., Wigneron, J.-P., & Kerr, Y. (2017). Mapping dynamic water fraction under the tropical rain forests of the amazonian basin from smos brightness temperatures. *Water*, *9*(5), 350.

Pekel, J.-F., Cottam, A., Gorelick, N., & Belward, A. S. (2016). High-resolution mapping of global surface water and its long-term changes. *Nature*, *540*(7633), 418–422.

Pfister, S., Bayer, P., Koehler, A., & Hellweg, S. (2011). Projected water consumption in future global agriculture: Scenarios and related impacts. *Science of the total environment*, *409*(20), 4206–4216.

Philpot, W. D., & Philipson, W. R. (2012). Remote sensing fundamentals. *Chapter 10 passive microwave*. Cornell University.

Pierdicca, N., Pulvirenti, L., Boni, G., Squicciarino, G., & Chini, M. (2017). Mapping flooded vegetation using cosmo-skymed: Comparison with polarimetric and optical data over rice fields. *IEEE Journal of Selected Topics in Applied Earth Observations and Remote Sensing*, *10*(6), 2650–2662.

Pinheiro Lisboa, I., Melo Damian, J., Roberto Cherubin, M., Silva Barros, P. P., Ricardo Fiorio, P., Cerri, C. C., & Eduardo Pellegrino Cerri, C. (2018). Prediction of sugarcane yield based on ndvi and concentration of leaf-tissue nutrients in fields managed with straw removal. *Agronomy*, *8*(9), 196.

Planet. (2021). *Planet fusion monitoring - technical specification* (Version 1.0.0-beta.3). 654 Harrison St. Floor 4, San Francisco CA, 94107.

Plaut, Z., Meinzer, F. C., & Federman, E. (2000). Leaf development, transpiration and ion uptake and distribution in sugarcane cultivars grown under salinity. *Plant and Soil*, *218*(1-2), 59–69.

Poddar, R., Qureshi, M. E., & Syme, G. (2011). Comparing irrigation management reforms in australia and india–a special reference to participatory irrigation management. *Irrigation and drainage*, *60*(2), 139–150.

Price, J. C. (1982). Estimation of regional scale evapotranspiration through analysis of satellite thermal-infrared data. *IEEE Transactions on Geoscience and Remote Sensing*, (3), 286–292.

Priestley, C. H. B., & Taylor, R. (1972). On the assessment of surface heat flux and evaporation using large-scale parameters. *Monthly weather review*, *100*(2), 81–92.

Prigent, C., Jimenez, C., & Bousquet, P. (2020). Satellite-derived global surface water extent and dynamics over the last 25 years (giems-2). *Journal of Geophysical Research: Atmospheres*, *125*(3), e2019JD030711.

Prigent, C., Aires, F., Rossow, W., & Matthews, E. (2001). Joint characterization of vegetation by satellite observations from visible to microwave wavelengths: A sensitivity analysis. *Journal of Geophysical Research: Atmospheres*, *106*(D18), 20665–20685.

Prigent, C., Lettenmaier, D. P., Aires, F., & Papa, F. (2016). Toward a high-resolution monitoring of continental surface water extent and dynamics, at global scale: From giems (global inundation extent from multi-satellites) to swot (surface water ocean topography). *Remote sensing and water resources* (pp. 149–165). Springer.

Prigent, C., Papa, F., Aires, F., Rossow, W., & Matthews, E. (2007). Global inundation dynamics inferred from multiple satellite observations, 1993–2000. *Journal of Geophysical Research: Atmospheres*, *112*(D12).

Pulvirenti, L., Chini, M., Pierdicca, N., & Boni, G. (2015). Use of sar data for detecting floodwater in urban and agricultural areas: The role of the interferometric coherence. *IEEE Transactions on Geoscience and Remote Sensing*, *54*(3), 1532–1544.

Raine, S., & Bakker, D. (1996). Increased furrow irrigation efficiency through better design and management of cane fields. *Proceedings-australian Society of Sugar Cane Technologists*, 119–124.

Ren, B., Zhang, J., Dong, S., Liu, P., & Zhao, B. (2016). Root and shoot responses of summer maize to waterlogging at different stages. *Agronomy Journal*, *108*(3), 1060–1069.

Rhine, M. D., Stevens, G., Shannon, G., Wrather, A., & Sleper, D. (2010). Yield and nutritional responses to waterlogging of soybean cultivars. *Irrigation Science*, *28*(2), 135–142.

Richard de, J., Anne, D. N., & Michel, V. K. (2016). Method and system for improving the resolution of sensor data.

Rietz, D., & Haynes, R. (2002). Effect of irrigation-induced salinity and sodicity on sugarcane yield. *Proceeding South African Sugar Technology Association*, *76*, 173–185.

Ritzema, H. (2016). Drain for gain: Managing salinity in irrigated lands—a review. *Agricultural Water Management*, *176*, 18–28.

Ritzema, H., Satyanarayana, T., Raman, S., & Boonstra, J. (2008). Subsurface drainage to combat waterlogging and salinity in irrigated lands in india: Lessons learned in farmers' fields. *agricultural water management*, *95*(3), 179–189.

Rouse, J. W., Haas, R. H., Schell, J. A., Deering, D. W., et al. (1974). Monitoring vegetation systems in the great plains with erts. *NASA special publication*, *351*(1974), 309.

Sairam, R., Kumutha, D., Ezhilmathi, K., Deshmukh, P., & Srivastava, G. (2008). Physiology and biochemistry of waterlogging tolerance in plants. *Biologia plantarum*, *52*(3), 401.

Santillán-Fernández, A., Santoyo-Cortés, V., Garcıéa-Chávez, L., Covarrubias-Gutiérrez, I., & Merino, A. (2016). Influence of drought and irrigation on sugarcane yields in different agroecoregions in mexico. *Agricultural Systems*, *143*, 126–135.

Sasidharan, R., & Voesenek, L. A. (2015). Ethylene-mediated acclimations to flooding stress. *Plant Physiology*, *169*(1), 3–12.

Schaaf, C., & Wang, Z. (2015). Mcd43d60 modis/terra+aqua brdf/albedo white sky albedo nir daily l3 global 30arcsec cmg v006 nasa eosdis l. process. daac. [Website accessed on (accessed 4.17.19) https://doi.org/10.5067/MODIS/MCD43D60.006].

Schmugge, T., O'Neill, P. E., & Wang, J. R. (1986). Passive microwave soil moisture research. *IEEE Transactions on Geoscience and Remote Sensing*, (1), 12–22.

Schroeder, R., McDonald, K. C., Chapman, B. D., Jensen, K., Podest, E., Tessler, Z. D., Bohn, T. J., & Zimmermann, R. (2015). Development and evaluation of a multi-year fractional surface water data set derived from active/passive microwave remote sensing data. *Remote Sensing*, *7*(12), 16688–16732.

Schumann, G., & Moller, D. (2015). Microwave remote sensing of flood inundation. *Physics and Chemistry of the Earth, Parts a/b/c*, *83*, 84–95.

Schumann, G. J., & Bates, P. D. (2018). The need for a high-accuracy, open-access global dem. *Frontiers in Earth Science*, *6*, 225.

Scofield, R. A., & Achutuni, R. (1996). The satellite forecasting funnel approach for predicting flash floods. *Remote Sensing Reviews*, *14*(1-3), 251–282.

Senay, G. B., Budde, M., Verdin, J. P., & Melesse, A. M. (2007). A coupled remote sensing and simplified surface energy balance approach to estimate actual evapotranspiration from irrigated fields. *Sensors*, *7*(6), 979–1000.

Shabbir, R., Javed, T., Afzal, I., Sabagh, A. E., Ali, A., Vicente, O., & Chen, P. (2021). Modern biotechnologies: Innovative and sustainable approaches for the improvement of sugarcane tolerance to environmental stresses. *Agronomy*, *11*(6), 1042.

Shah, N. A., Srivastava, J. P., da Silva, J. A. T., & Shahi, J. P. (2012). Morphological and yield responses of maize (zea mays l.) genotypes subjected to root zone excess soil moisture stress. *Plant Stress*, *6*(1), 59–72.

Shang, H. (2017). *Applications of passive microwave data to monitor inundated areas and model stream flow* (Doctoral dissertation). Delft University of Technology.

Sharkov, E. A. (2003). *Passive microwave remote sensing of the earth: Physical foundations*. Springer Science & Business Media.

Shaw, R. E., Meyer, W. S., McNeill, A., & Tyerman, S. D. (2013). Waterlogging in australian agricultural landscapes: A review of plant responses and crop models. *Crop and Pasture Science*, *64*(6), 549–562.

Shendryk, Y., Davy, R., & Thorburn, P. (2021). Integrating satellite imagery and environmental data to predict field-level cane and sugar yields in australia using machine learning. *Field Crops Research*, *260*, 107984.

Silva, V., Garcêz, S., Silva, B. d., Albuquerque, M. d., & Almeida, R. (2015). Métodos de estimativa da evapotranspiração da cultura da cana-de-açúcar em condições de sequeiro. *Revista Brasileira de Engenharia Agrıécola e Ambiental*, *19*(5), 411–417.

Simões, M. d. S., Rocha, J. V., & Lamparelli, R. A. C. (2009). Orbital spectral variables, growth analysis and sugarcane yield. *Scientia Agricola*, *66*(4), 451–461.

Singels, A., Kennedy, A., & Bezuidenhout, C. (1998). Irricane: A simple computerised irrigation scheduling method for sugarcane. *Proc S Afr Sug Technol Ass*, *72*, 117–122.

Singh, A. (2016). Hydrological problems of water resources in irrigated agriculture: A management perspective. *Journal of Hydrology*, *541*, 1430–1440.

Singh, A., Kumari, V., Gupta, R., Singh, P., & Solomon, S. (2018). Efficient irrigation water management in sugarcane through alteration of field application parameters under subtropical india. *Sugar Tech*, *20*(1), 21–28.

B

Singh, S. K., & Pandey, A. (2014). Geomorphology and the controls of geohydrology on waterlogging in gangetic plains, north bihar, india. *Environmental earth sciences*, *71*(4), 1561–1579.

Sippe, S., Hamilton, S., Melack, J., & Novo, E. (1998). Passive microwave observations of inundation area and the area/stage relation in the amazon river floodplain. *International Journal of Remote Sensing*, *19*(16), 3055–3074.

Sippel, S. J., Hamilton, S. K., Melack, J. M., & Choudhury, B. J. (1994). Determination of inundation area in the amazon river floodplain using the smmr 37 ghz polarization difference. *Remote Sensing of Environment*, *48*(1), 70–76.

Som-ard, J., Atzberger, C., Izquierdo-Verdiguier, E., Vuolo, F., & Immitzer, M. (2021). Remote sensing applications in sugarcane cultivation: A review. *Remote Sensing*, *13*(20). https://www.mdpi.com/2072-4292/13/20/4040

Steduto, P., Hoogeveen, J., Winpenny, J., Burke, J., et al. (2017). *Coping with water scarcity: An action framework for agriculture and food security*. Food; Agriculture Organization of the United Nations Rome, Italy.

Steele-Dunne, S. C., McNairn, H., Monsivais-Huertero, A., Judge, J., Liu, P.-W., & Papathanassiou, K. (2017). Radar remote sensing of agricultural canopies: A review. *IEEE Journal of Selected Topics in Applied Earth Observations and Remote Sensing*, *10*(5), 2249–2273.

Sullivan, M., VanToai, T., Fausey, N., Beuerlein, J., Parkinson, R., & Soboyejo, A. (2001). Evaluating on-farm flooding impacts on soybean. *Crop Science*, *41*(1), 93–100.

Sumranbumrung, R., Khunkitti, P., Siritaratiwat, A., & Kruesubthaworn, A. (2021). Characterization model of dielectric properties of cane sugar solution over 0.5–14 ghz. *IEEE Transactions on Instrumentation and Measurement*, *70*, 1–8.

Surendran, U., Ramesh, V., Jayakumar, M., Marimuthu, S., & Sridevi, G. (2016). Improved sugarcane productivity with tillage and trash management practices in semi arid tropical agro ecosystem in india. *Soil and Tillage Research*, *158*, 10–21.

Tareq, M. Z., Sarker, M. S. A., Sarker, M. D. H., Moniruzzaman, M., Hasibuzzaman, A. S. M., & Islam, S. N. (2020). Waterlogging stress adversely affects growth and development of tomato. *Asian Journal of Crop*, *2*(01), 44–50.

Tomkwok. (2022). Calendar heatmaps from pandas time series data.

Torres, R., Snoeij, P., Geudtner, D., Bibby, D., Davidson, M., Attema, E., Potin, P., Rommen, B., Floury, N., Brown, M., et al. (2012). Gmes sentinel-1 mission. *Remote Sensing of Environment*, *120*, 9–24.

Townsend, P. A., & Walsh, S. J. (1998). Modeling floodplain inundation using an integrated gis with radar and optical remote sensing. *Geomorphology*, *21*(3-4), 295–312.

Tsyganskaya, V., Martinis, S., Marzahn, P., & Ludwig, R. (2018a). Detection of temporary flooded vegetation using sentinel-1 time series data. *Remote Sensing*, *10*(8), 1286.

Tsyganskaya, V., Martinis, S., Marzahn, P., & Ludwig, R. (2018b). Sar-based detection of flooded vegetation–a review of characteristics and approaches. *International Journal of Remote Sensing*, *39*(8), 2255–2293.

Twele, A., Cao, W., Plank, S., & Martinis, S. (2016). Sentinel-1-based flood mapping: A fully automated processing chain. *International Journal of Remote Sensing*, *37*(13), 2990–3004.

Ulaby, F. T., Moore, R., & Fung, A. (1982). Microwave remote sensing: Active and passive. volume 2-radar remote sensing and surface scattering and emission theory.

Ulaby, F. T., Moore, R. K., & Fung, A. K. (1981). *Microwave remote sensing: Active and passive. volume 1 - microwave remote sensing fundamentals and radiometry*. Artech House.

Ulaby, F. T., & El-Rayes, M. A. (1987). Microwave dielectric spectrum of vegetation-part ii: Dual-dispersion model. *IEEE Transactions on Geoscience and Remote Sensing*, (5), 550–557.

Ulaby, F. T., & Jedlicka, R. (1984). Microwave dielectric properties of plant materials. *IEEE Transactions on Geoscience and Remote Sensing*, (4), 406–415.

Ulaby, F. T., Long, D. G., Blackwell, W. J., Elachi, C., Fung, A. K., Ruf, C., Sarabandi, K., Zebker, H. A., & Van Zyl, J. (2014). *Microwave radar and radiometric remote sensing* (Vol. 4). University of Michigan Press Ann Arbor, MI, USA.

Valipour, M. (2014). Drainage, waterlogging, and salinity. *Archives of Agronomy and Soil Science*, *60*(12), 1625–1640. https://doi.org/10.1080/03650340.2014.905676

van der Schalie, R., de Jeu, R. A., Kerr, Y., Wigneron, J.-P., Rodrıéguez-Fernández, N. J., Al-Yaari, A., Parinussa, R. M., Mecklenburg, S., & Drusch, M. (2017). The merging of radiative transfer based surface soil moisture data from smos and amsr-e. *Remote Sensing of Environment*, *189*, 180–193.

Van Leeuwen, B., Tobak, Z., & Kovács, F. (2020). Sentinel-1 and-2 based near real time inland excess water mapping for optimized water management. *Sustainability*, *12*(7), 2854.

van Heerden, P. D., Donaldson, R. A., Watt, D. A., & Singels, A. (2010). Biomass accumulation in sugarcane: Unravelling the factors underpinning reduced growth phenomena. *Journal of experimental botany*, *61*(11), 2877–2887.

Vanino, S., Nino, P., De Michele, C., Bolognesi, S. F., & Pulighe, G. (2015). Earth observation for improving irrigation water management: A case-study from apulia region in italy. *Agriculture and agricultural science procedia*, *4*, 99–107.

Vanino, S., Nino, P., De Michele, C., Bolognesi, S. F., D'Urso, G., Di Bene, C., Pennelli, B., Vuolo, F., Farina, R., Pulighe, G., et al. (2018). Capability of sentinel-2 data for estimating maximum evapotranspiration and irrigation requirements for tomato crop in central italy. *Remote sensing of environment*, *215*, 452–470.

Veloso, A., Mermoz, S., Bouvet, A., Le Toan, T., Planells, M., Dejoux, J.-F., & Ceschia, E. (2017). Understanding the temporal behavior of crops using sentinel-1 and sentinel-2-like data for agricultural applications. *Remote sensing of environment*, *199*, 415–426.

Vermunt, P. C., Khabbazan, S., Steele-Dunne, S. C., Judge, J., Monsivais-Huertero, A., Guerriero, L., & Liu, P.-W. (2020). Response of subdaily l-band backscatter to internal and surface canopy water dynamics. *IEEE Transactions on Geoscience and Remote Sensing*, *59*(9), 7322–7337.

Vermunt, P. C., Steele-Dunne, S. C., Khabbazan, S., Kumar, V., & Judge, J. (2022). Towards understanding the influence of vertical water distribution on radar backscatter

from vegetation using a multi-layer water cloud model. *Remote Sensing*, *14*(16), 3867.

Vilanculos, M., & Mafalacusser, J. (2012). *Soil survey report of acucareira de xinavane, sa* (tech. rep.). Instituto de Investigacao Agraria de Mocambique.

Viswanadham, Y., Silva Filho, V., & Andre, R. (1991). The priestley-taylor parameter α for the amazon forest. *Forest Ecology and Management*, *38*(3-4), 211–225.

Vreugdenhil, M., Wagner, W., Bauer-Marschallinger, B., Pfeil, I., Teubner, I., Rüdiger, C., & Strauss, P. (2018). Sensitivity of sentinel-1 backscatter to vegetation dynamics: An austrian case study. *Remote Sensing*, *10*(9), 1396.

Vuolo, F., D'Urso, G., De Michele, C., Bianchi, B., & Cutting, M. (2015). Satellite-based irrigation advisory services: A common tool for different experiences from europe to australia. *Agricultural water management*, *147*, 82–95.

Wallender, W. W., Tanji, K. K. et al. (2011). *Agricultural salinity assessment and management*. American Society of Civil Engineers (ASCE).

Wan, Z., Hook, S., & Hulley, G. (2015). Mod11a1 modis/terra land surface temperature/emissivity daily l3 global 1km sin grid v006. [Website accessed on (accessed 9.9.18) https://doi.org/10.5067/MODIS/MOD11A1.006].

Wang, J., Nayak, S., Koch, K., & Ming, R. (2013). Carbon partitioning in sugarcane (saccharum species). *Frontiers in plant science*, *4*, 201.

Wang, R., Zhang, M., Mujumdar, A. S., & Jiang, H. (2011). Effect of salt and sucrose content on dielectric properties and microwave freeze drying behavior of re-structured potato slices. *Journal of Food Engineering*, *106*(4), 290–297. https://doi.org/https://doi.org/10.1016/j.jfoodeng.2011.05.015

Wang, S., & Davidson, A. (2007). Impact of climate variations on surface albedo of a temperate grassland. *Agricultural and Forest Meteorology*, *142*(2-4), 133–142.

Wang, S., Davidson, A., & Latifovic, R. (2004). Impact of drought on land surface albedo. *AGU Spring Meeting Abstracts*, 85.

Wang, Z., Wang, K., Liu, K., Cheng, L., Wang, L., & Ye, A. (2019). Interactions between lake-level fluctuations and waterlogging disasters around a large-scale shallow lake: An empirical analysis from china. *Water*, *11*(2), 318.

Ward, P., Dunin, F., & Micin, S. (2002). Water use and root growth by annual and perennial pastures and subsequent crops in a phase rotation. *Agricultural Water Management*, *53*(1-3), 83–97.

Warrence, N. J., Bauder, J. W., & Pearson, K. E. (2002). Basics of salinity and sodicity effects on soil physical properties. *Departement of Land Resources and Environmental Sciences, Montana State University-Bozeman, MT*, *129*.

Weiss, M., Jacob, F., & Duveiller, G. (2020). Remote sensing for agricultural applications: A meta-review. *Remote Sensing of Environment*, *236*, 111402.

Yadav, R., Shukla, S., Suman, A., & Singh, P. (2009). Trichoderma inoculation and trash management effects on soil microbial biomass, soil respiration, nutrient uptake and yield of ratoon sugarcane under subtropical conditions. *Biology and Fertility of soils*, *45*(5), 461–468.

You, L., Ringler, C., Wood-Sichra, U., Robertson, R., Wood, S., Zhu, T., Nelson, G., Guo, Z., & Sun, Y. (2011). What is the irrigation potential for africa? a combined biophysical and socioeconomic approach. *Food Policy*, *36*(6), 770–782.

Zaag van der, P., & Carmo Vaz, Á. (2003). Sharing the incomati waters: Cooperation and competition in the balance. *Water Policy, 5*(4), 349–368.

Zhou, W., Chen, F., Meng, Y., Chandrasekaran, U., Luo, X., Yang, W., & Shu, K. (2020). Plant waterlogging/flooding stress responses: From seed germination to maturation. *Plant Physiology and Biochemistry, 148*, 228–236.